Macro to Micro Legacies of Landuse at the Calhoun Critical Zone Observatory

by

Zachary S. Brecheisen

Environment
Duke University

Date:_____
Approved:

_____
Daniel deB. Richter, Supervisor

_____
Patrick N. Halpin

_____
Mac A. Callaham, Jr.

_____
Sari Palmroth

Dissertation submitted in partial fulfillment of
the requirements for the degree of Doctor of Philosophy
in Environment in the Graduate School of
Duke University

2018

ABSTRACT

Macro to Micro Legacies of Landuse at the Calhoun Critical Zone Observatory

by

Zachary S. Brecheisen

Environment
Duke University

Date:_____
Approved:

_____
Daniel deB. Richter, Supervisor

_____
Patrick N. Halpin

_____
Mac A. Callaham, Jr.

_____
Sari Palmroth

An abstract of a dissertation submitted in partial fulfillment of
the requirements for the degree of Doctor of Philosophy
in Environment in the Graduate School of
Duke University

2018

Abstract

In this dissertation, human-critical zone (CZ) dynamics are explored at the Calhoun Critical Zone Observatory (CCZO). The 190km^2 CCZO is part of a broader landscape in the southeastern US which was subjected to extensive agricultural degradation for approximately two hundred years before cultivation was abandoned sixty or more years ago. The physical and functional dynamics of land abandonment were explored at three spatial scales herein: 1) landscape geomorphology and spatial patterns of CZ processes, 2) microtopographic roughness of hillslopes being diagnostic of landuse history and, 3) plot-based soil investigations of three landuse histories approximating the temporal succession from pre-disturbance forested landcover into deforested agricultural management and finally into secondary old-field mixed pine forests which typify the post-agricultural landscape of the Southeastern US.

In the second dissertation chapter it was observed that most of the landscape consists of interfluves and accompanying hillslopes and that quantifying the spatial patterns and connections of hillslopes is important for understanding landscape function and evolution. This work aims to describe and quantify upland terrain structure, which is a residual formation of interfluves and hillslopes formed over geologic time as the landscape has weathered and eroded. Landscape network structure was described and quantified with demonstration of how it drives the landscape

processes of soil erosion, bedrock weathering, and landcover. In this work, interfluve (hilltop) networks were ordered according to Hortonian methodology at the CCZO in South Carolina with corresponding "hillsheds" delineated and bounded at the base by floodplains and stream channels. At the CCZO, low-order interfluves are narrow, abundant, small, and steep with low elevation, while high-order interfluves are fewer, broad, and relatively flat with high elevation. We estimated that geologic erosion rates of 1st order interfluves were two orders of magnitude higher than on those of 4th or 5th orders, bedrock weathering is modeled to be deepest and most spatially variable on 1st order interfluves with depth and depth-variability decreasing as interfluve-order increases. It is further shown that agriculture has persisted to the greatest extent on high-order interfluves where human-accelerated erosion has been far less serious than on more highly gullied low-order interfluves. We conclude with an assertion that land-management and many fields of environmental research can benefit from ordered-interfluve networks and corresponding hillsheds much as they have benefited from the concepts of stream-orders and watersheds.

Chapter three focuses on terrain microtopography and erosive gullying at the Calhoun CZO. The CCZO in the Piedmont region of South Carolina is an ancient, highly weathered landscape which was transformed by historic agricultural erosion. Following the conversion of hardwood forests to cultivated fields and pastures for ~200 years, excess runoff from fields led to extreme sheet, rill, and gully erosion across the

landscape. Roads, terraces, and a variety of other human disturbances also increased the landscape's surface roughness. By the 1950s, cultivation-based agriculture had been abandoned in most of the Southern Piedmont due to soil erosion, declining agricultural productivity, and shifting agricultural markets. Forests dominated by loblolly and shortleaf pine species, have since reforested much of the landscape. There are, however, isolated hardwood forest stands and even entire small watersheds dotting the landscape which are believed to have never been clear-cut or plowed. These rare forests are expected to have special aesthetic and scientific research value as a Piedmont pre-disturbance reference condition. Hardwood reference forests may be of interest to hydrologists, environmental historians, biogeochemists, geomorphologists, geologists, pedologists, and others interested in understanding the legacy of landuse history in this severely altered environment. In this work we demonstrated how Light Detection And Ranging (LiDAR) digital elevation model (DEM) data and microtopographic terrain roughness analysis (MTRA) of fine scale variation in terrain slope was used in concert with historic aerial photography, contemporary remote sensing data, and field ecological interpretation to identify low human-impact, minimally eroded, reference hardwood stands, hillslopes, and even small watersheds for study and conservation.

Following the identification and selection of reference hardwood forests as a landuse history treatment for intensive study in chapter three, novel method development was needed in order to study the belowground dynamics of these forests

and other landuse histories of interest. One of the analytical tools necessary for this was the development of effective and reliable Field-Portable Gas Analysis tools (FPGA) and is outlined in chapter four. FPGAs have been developed at the Calhoun Critical Zone Observatory for the measurement and monitoring of soil O_2 and CO_2 in ecosystems with contrasting landuse histories. The tools and methodology developed and presented here are extremely cost-effective, are physically very light, compact, and robust for field deployment and reliable soil gas monitoring. The FPGA platform integrates off-the-shelf components including Vaisala™ non-dispersive infrared (NDIR) CO_2 probes and electro-chemical Apogee™ O_2 meters for flow-through gas analyses of soil gas using a Cole-Parmer™ vacuum-pressure pump. More than 1600 soil gas measurements have been made using these devices over more than 2 years of observations. Measurement accuracy of the FPGA is very consistent compared with conventional bench-top gas chromatography and time series representations of paired CO_2 and O_2 measurement under hardwood forests at the CCZO indicate the ability to observe and track seasonal and climatic patterns and events with this technology. Further, the ability to analyze the apparent respiratory quotient, the ratio of apparent CO_2 accumulation divided by apparent O_2 consumption relative to the aboveground atmosphere, indicates a high degree of sophisticated analyses are made possible with the FPGA platform. The accuracy and reliability of the FPGA platform for soil gas monitoring allows for temporally extensive and spatially expansive studies of soil respiration.

With the development of the FPGA in chapter four, plot-based field investigations were undertaken to determine how different critical zone measurements are able to quantify the vertical propagation of forest regeneration downward into soil profiles in chapter five. The below-ground effects of 60-80 years of old-field forest succession in the CCZO were explored via a space-for-time substitution with replication of ecosystems, also called a chronosequence approach (Richter and Markewitz 2001). Chronosequence plots consist of reference hardwood forests, plowed agricultural fields, and old-field secondary pine forests. In this framework, reference hardwood soil profiles are minimally degraded in terms of erosion, soil structure, and soil biogeochemistry while currently cultivated agricultural plots are maximally impacted. Old-field secondary pine forests are considered to be intermediate and and are somewhat regenerated in terms of soil structure and function as reforestation has occurred and proceeded for decades, though the degree of regeneration was uncertain. Following characterization of the aboveground forest vegetation, each landuse history comparison plot was studied and soil structural regeneration of bulk density, macropores (>0.075mm dia.) via X-ray Computed Tomography, and soil aggregate stability in the top 15cm of soil. Deeper monitoring of soil CO_2 and O_2 using FPGAs characterized belowground forest functioning down to 5m soil depth.

Hardwood forest soils have been observed to have higher CO_2 concentrations and lower O_2 below 2m soil depth, below the soil B-horizon, than either agricultural

plots or old-field pine forests. Results indicate that while there has been a high degree of soil regeneration above the B-horizon in old-field secondary forest soils in terms of forest aboveground vegetation, rooting, respiration dynamics, and soil structure, deep CZ processes below 2m remain significantly altered under old-field pine forests. This suggests that there may be a lag in below-ground regeneration relative to surficial soil regeneration. This appears to be due the hindering of root and macropore regeneration by a thick, low permeability, B_t-horizon. Abiotic CZ processes like storms which affected all treatments were also investigated as rapid declines in CO_2 concentrations were observed deep in soil profiles during periods of intense precipitation. This is presumably due to CO_2 dissolution and export into groundwater and indicates great potential to advance the fundamental understanding of the linkages between upland management and landcover, aerobic respiration, and deep critical zone processes like mineral weathering and the export of terrestrially-derived CO_2 to streams.

Dedication

This work is dedicated to those that have nurtured and supported me on this adventure thus far, a list too long for full entry here. To my dad who instilled a deep-seated mechanistic curiosity of the world around me and a grounded view of how one should live their life. To my mom who instilled a fierce, and sometimes irrational, determination to persevere without regard for the opinions of other people. To my wife whom I have never stopped learning from, a constant source of joy, support, and motivation to be the best person I can be, to finally let the world back in. To my big sister, the only person who has ridden the same roller coaster of life, crashing and smashing through the bullshit to come out stronger and smarter for it each and every day. You are all a constant source of inspiration. I wouldn't be where I am without you.

Contents

List of Tables

List of Figures

Acknowledgements

The amount of support I've received in the completion of this dissertation research is truly remarkable and far from the normal experiences of PhD graduate students. The network of researchers I have benefitted from and become a part of through the Calhoun Critical Zone Observatory, and the broader NSF Critical Zone Observatory program, have simultaneously broadened and focused my research endeavors. I've had the opportunity to work with and learn from researchers in closely allied disciplines with soil sciences like geology, hydrology, and geomorphology, but to also have my research enriched by environmental historians, archaeologists, and even one French philosopher of science. The first and greatest thanks are due to Dan Richter, my primary advisor and mentor in the pursuit of my PhD. I'm not sure what potential he saw in a student applicant who'd never had any formal coursework in soil science, but I am grateful beyond words that he took the leap in bringing me into Richter-research family and network of scientists. He allowed me the freedom to generate and test my own ideas without fear of my own initial naivete of Earth Sciences. He instead encouraged and helped me to bridge the gaps in my knowledge. Much of this occurred whilst wandering and wondering in the forests of the CCZO with Dan before NSF awarded the Calhoun funding and status as a CZO. Those early days were especially valuable for me and I thank you for them.

Many thanks are also due to my PhD advisory committee. Pat Halpin was the first to sign on after Dan when I had little more than a half-baked idea about topographic networks. Your feedback and guidance over the years on framing manuscripts and your conceptualization of the "landshed" was crucial for that work to mature beyond an interesting network of lines on a map. My appreciation of field work and my conceptualization of the living soil system would not be what they are without Mac Callaham. Mac has shared a wealth of knowledge in forest ecology which, paired with his practical and genuine perspective on science and research, have helped me to maintain a genuine curiosity of how human-forest-CZ systems function. Brian McGlynn taught me most of what I know about hydrology. Though he wasn't able to remain on my committee, his data-driven and mechanistic conceptualization of the Calhoun system and his feedback and advice on every dissertation research chapter have helped me greatly. Lastly, much appreciation is due to Sari Palmroth. Her thoughts on forest phenology, tree physiology, and soil gas dynamics have encouraged me experiment with and approach my data in insightful ways I wouldn't have otherwise.

Great thanks are also due to other Richter-researchers including professors Sharon Billings, Daniel Markewitz, and Allan Bacon who have all contributed to the development of my ideas about the critical zone and my development as a researcher over the last 5 years. Those deserving of thanks for help in the generation and testing of research ideas in the lab, in the field, and around campfires include Paul Heine, Will

Cook, Jay Austin, Mark River, John Mallard, Anna Wade, Junmo Ryang, Justin Gladman, Todd Smith, and Greg Chapman. Special thanks are also due to Brad Tomasek who fielded dozens of statistics and R questions over the years. I encourage readers to befriend members of the Clark lab, it can only help you greatly!

Supplementing Dan's expert training in soils fieldwork, special thanks are due to Alex Cherkinsky. If you need to auger through rock, learn from a Russian! Lastly, to all the other Calzones who've boosted me in my efforts to understand the Earth from "tree-top to bedrock" including Paul Schroeder, Michael Coughlan, Allan James, Jim Giesen, Christoph Lehmeier, Mukesh Kumar, Aaron Thompson, Steve Holbrook, Greg Hancock, and many others. This research was also greatly advanced through funding via the NSF IGERT WiSENet fellowship, a grant from the Duke Shared Materials Infrastructure Facility (SMIF), the Forest History Society's F.K.W. fellowship, and a Duke Incubation Fund grant.

Finally, I must thank my family for their support over the last 5 years. My wife Tory has given me more support and understanding than I could have ever hoped for. She's my partner in life and the #1 VIP in TeamHoney. I love you more every day and can't wait to see where else this crazy adventure takes us. My sister, Jennifer, the only person who can see the world through the same eyes as me. You kept me alive and sane in a time that was dark for both of us, and then make me happy as hell as we've both gone on to be awesome. You're the best sister I could ever hope for and I know mom

and dad would be just as proud of you as I am. Finally, there is a fleet of 4-legged (and 2-winged) creatures that have been a constant source of comfort and adventure during the course of my PhD: Cat, Mendelynn, Panda, Sanford, Luna, Slytherin, Ravenclaw, Hufflepuff, Gryffindor, and Lola.

1. Introduction

1.1 Scope of inquiry

The Earth's critical zone (CZ) spans the physical environment from the atmosphere down to the deepest weathering fronts of bedrock (Richter and Billings 2015). This "tree-top to bedrock" perspective links interactions between the physical environment and the processes within it as an expanded ecosystem. This dissertation, *Macro to Micro Legacies of Landuse at the Calhoun Critical Zone Observatory*, seeks to describe the patterning and effects of linked human-CZ processes in a post-agricultural environment (Richter and Markewitz 2001). Investigations in this dissertation occur at three spatial scales ranging from landscape (Chapter 2), to watershed hillslope (Chapter 3), and lastly soil-profile scales (Chapters 4 and 5).

Regional-scale CZ processes require landscape investigations to capture the patterns and temporal trajectories of large areas. In this case, the 190 km^2 CCZO is studied as part of the broader >100,000 km^2 Southern Piedmont region. CZ processes of landscape-scale interest are influenced by geomorphology and include historic land management on soil erosion (Dialynas, Bastola et al. 2016), forest succession and the spatial distribution of landuse/landcover (LULC) change (Hightower, Butterfield et al. 2014, Stahl 2015), and deep CZ structure and the depth to bedrock weathering fronts below the soil (Bacon, Richter et al. 2012, Rempe and Dietrich 2014, St Clair, Moon et al. 2015, Moon, Perron et al. 2017).

In this dissertation, study of human-CZ dynamics necessitated making specific LULC contrasts at the CCZO. The identification of research areas for targeted study required a reduction in spatial scale targeting individual watersheds, catenas, and hillslopes. LiDAR and other forms of remote sensing were employed to isolate and characterize Earth surface features and environments, both human-influenced and "reference" or minimally-impacted areas (Londoño 2008, Maxwell and Strager 2013, Hightower, Butterfield et al. 2014, Stahl 2015). The potential for LiDAR to highlight minimally eroded reference areas in contrast to those disturbed by human agricultural forcings is explored (James, Watson et al. 2007, Pike, Mueller et al. 2012) and could be of great value to researchers and conservationists.

Following the identification of reference research watersheds and forest stands, field instrumentation for the measurement and sampling of the CZ constitutes a final shift in scale and structural framework. This is particularly true in the hydro-biogeosciences when it is often experimentally impractical to sample or study an entire catchment or forest stand and thus research plots must be established. Here the structure of the soil profile as influenced by LULC histories and legacies as well as the natural environment is a central concern for CZ researchers studying erosion and altered hydrologic and biogeochemical regimes. In order to investigate Calhoun CZ processes, I pose three research questions spanning CZ structural scales of: landscape, small watersheds and forest stands, and the soil-weathering profile (Figure 1.1):

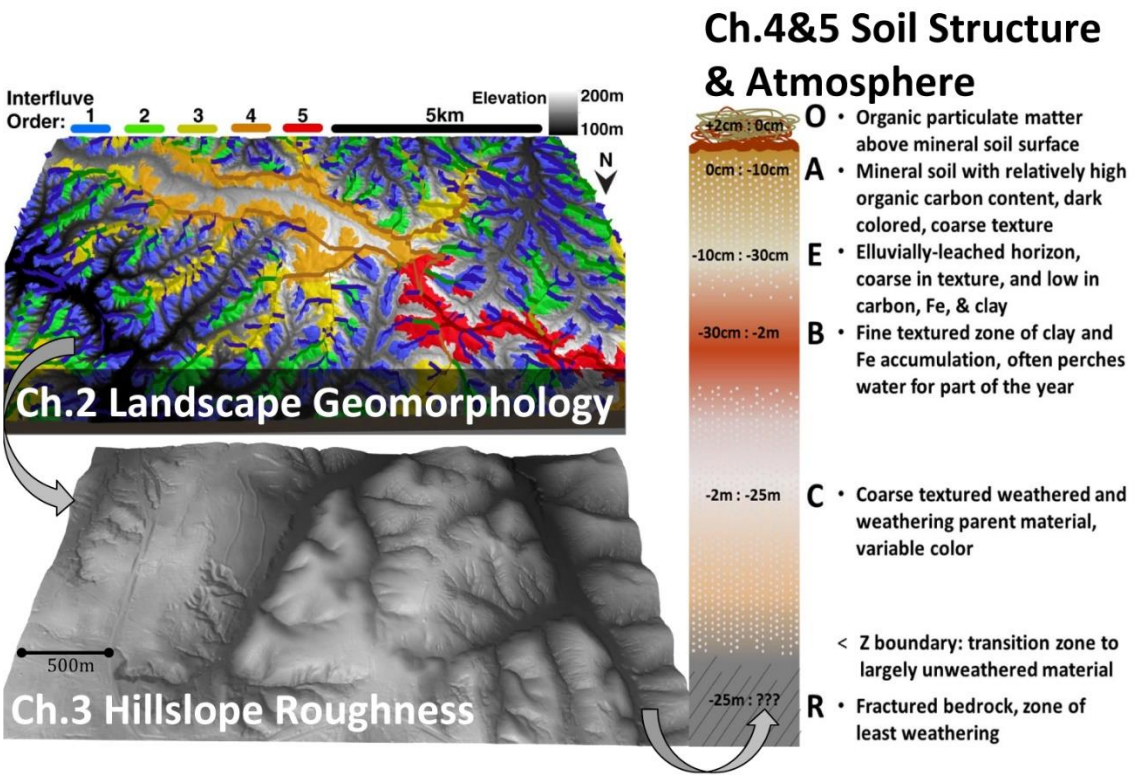

Figure 1.1: Dissertation spatial scales of inquiry by chapter

1.2 Research questions

Chapter 2. *How is landscape geomorphic structure reflected in the history of upland land cover, soil erosion potential, and geochemical weathering depth?* The manuscript produced from this work was written with Zach Brecheisen, Dan Richter, Suelgi Moon, and Pat Halpin as authors. Seulgi Moon, in addition to manuscript revision and editing, contributed a geophysical modeling dataset for analysis across interfluve orders.

Chapter 3. *How can LiDAR & microtopographic terrain structure derivatives be combined with historic and contemporary remote sensing data to identify reference hardwood stands and watersheds whose soils, land surface, and hillslopes are minimally impacted by*

historic anthropogenic land uses? The manuscript produced from this work was written with Zach Brecheisen and Dan Richter as authors.

Chapters 4 & 5. Chapter 4 details the development of a novel analytical apparatus for soil atmosphere monitoring and sampling. The methodology developed in Chapter 4 is currently in preparation for submission with Zach Brecheisen, Will Cook, Paul Heine, Junmo Ryang, and Dan Richter as authors. Will Cook collected approximately half of the field data presented in the paper and Paul Heine and Junmo Ryang conducted laboratory QAQC of the CO_2 data and also integrated lab and field measurement datasets. Chapter 5 investigates: *How have CZ systems evolved in old-field pine forests post abandonment and to what degree has the soil profile regenerated in terms of soil structure and the metabolic gasses that flow through them, relative to reference hardwood forest and continuously cultivated soils?* The manuscript for Chapter 5 is currently under development but will have the same authorship as the manuscript for Chapter 4 with the addition of Jay Austin and John Mallard who collected soil moisture and precipitation data, respectively.

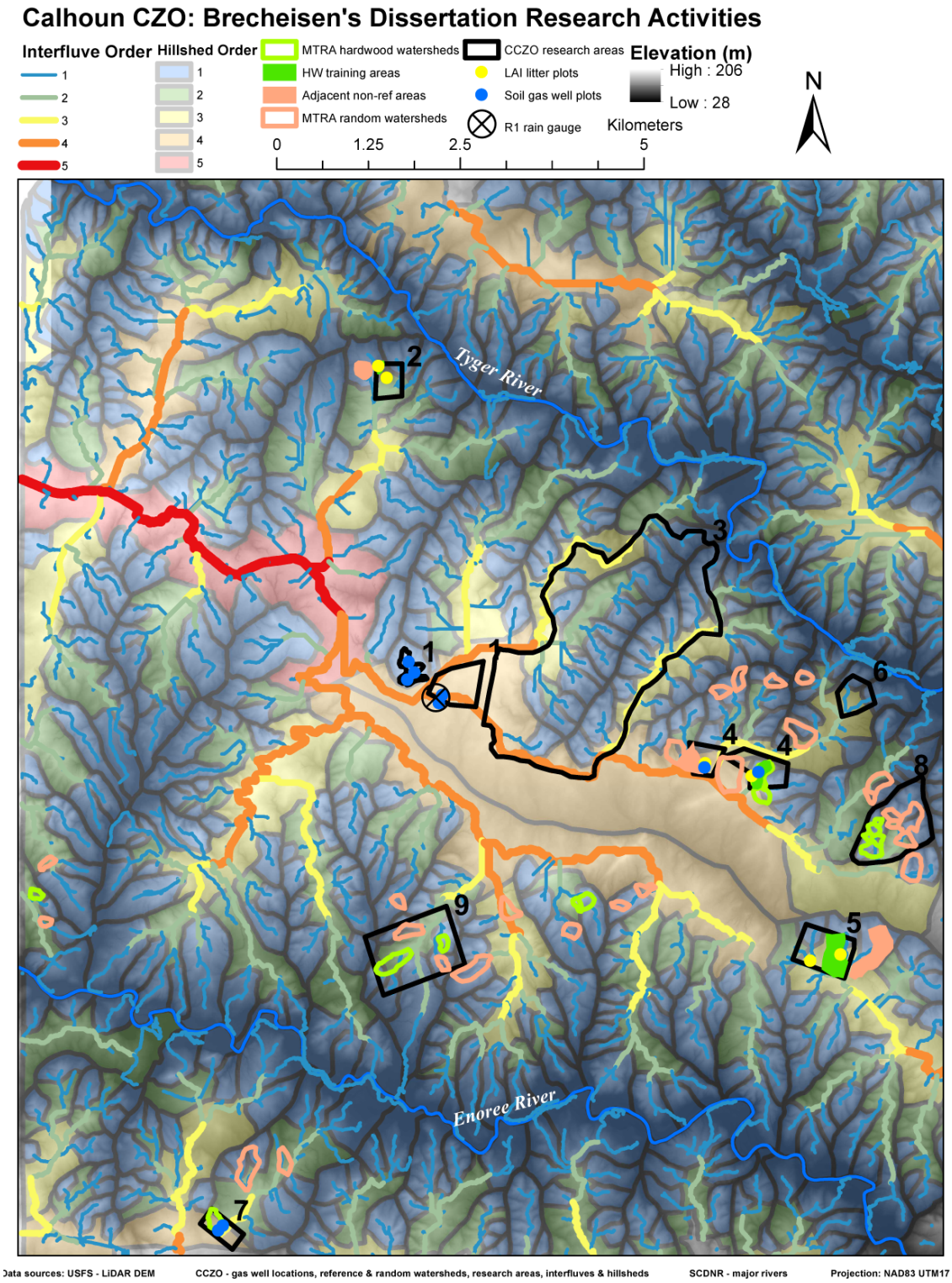

Figure 1.2: Map of dissertation research activities at the Calhoun CZO.

2. Quantitative analysis of hillshed geomorphology and critical zone function

2.1 Introduction

Interfluve networks, the geomorphic features that divide watersheds, and their topology (Werner 1972, Werner 1988) have a long history of attention and research (Horton 1945, Warntz 1975, Wilcox and Moellering 1995, Schneider 2005). We are, however, lacking a hierarchical interfluve-based corollary to ordered stream networks and the watershed. The need for improved systematic landform description and measurement is recognized within geomorphology (Evans 2012). Here we present a hierarchical ordering of landscape topology with discrete "hillshed" (Maxwell 1870, Meerveld and Weiler 2008, Evans 2012) landforms to further landscape geomorphometry and to link landform terrain directly to real-world critical zone (CZ) processes. The CZ is an expanded ecosystem within which researchers study the structure and functioning of the human-natural world spanning the lower atmosphere around tree-tops and the Earth's surface down into soils, groundwater, and finally bedrock (Brantley, Goldhaber et al. 2007, Richter and Billings 2015, Brantley, DiBiase et al. 2016).

Dendritic interfluve networks were ranked using Horton-Strahler (Horton 1945, Strahler 1957) stream ordering rules and corresponding hillsheds were delineated for each interfluve bounded by valleys and streams. First order interfluves, if not situated as isolated hills, lead to 2nd, 3rd, 4th etc… order interfluves in the uphill direction (Figure

1.2). Interfluves and their hillsheds are residual dissipative landforms (Bos 1971, Dietrich, Wilson et al. 1992) composed of the Earth's CZ that has not yet been eroded or dissolved away (Horton 1945, Ruhe, Daniels et al. 1967, Perron, Kirchner et al. 2009). As such, ordered interfluves and their hillsheds are considered as connected yet discrete components of larger "geomorphic dendrites" (Figure 2.1). Much as a tree's twigs, branches, and trunk are distinct yet also connected, interfluves exist as separate but connected branches and trunks of landscape geomorphology that interact with each other throughout their evolution.

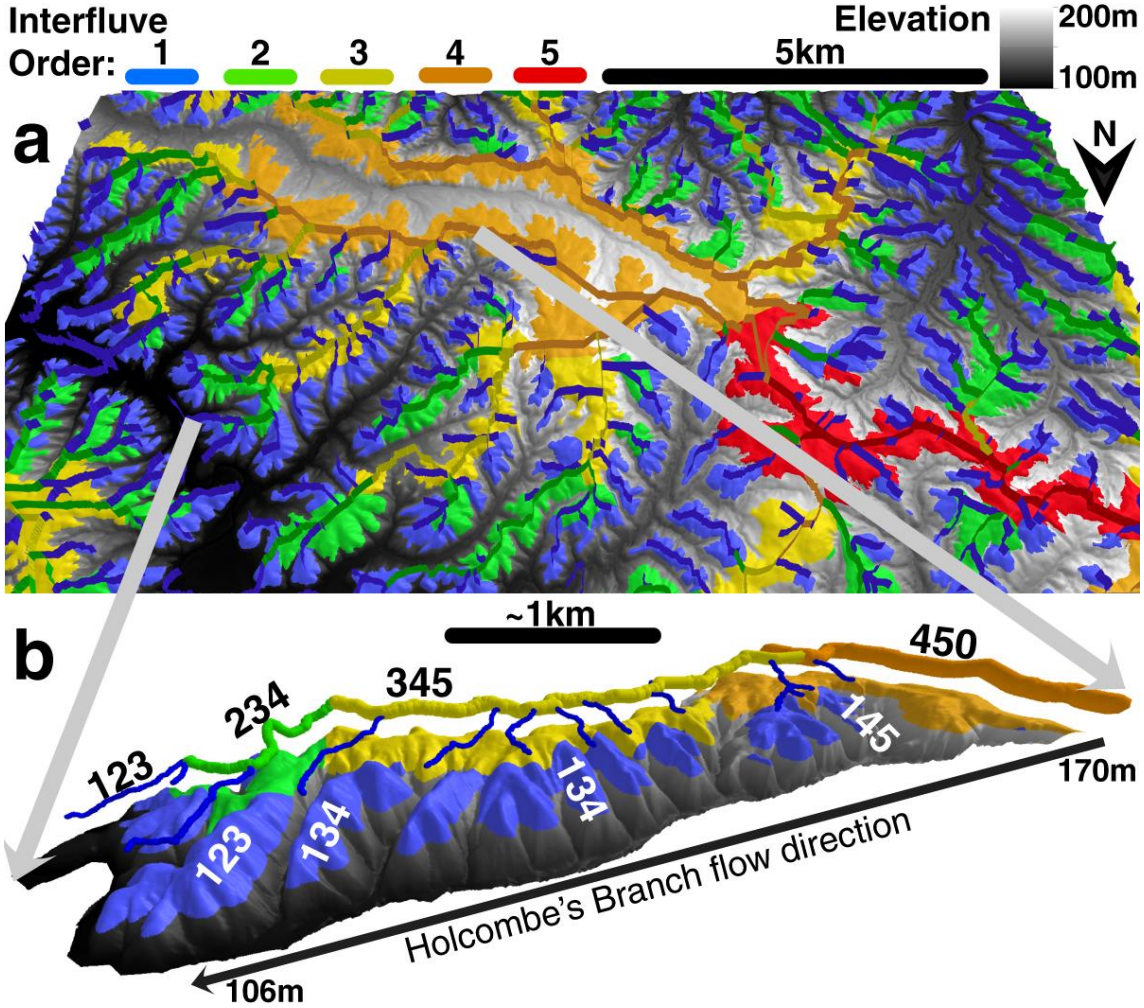

Figure 2.1: 3D representation of ordered interfluve networks a) across the CCZO landscape and b) zoomed in on the eastern half of Holcombe's Branch watershed illustrating how the orders of interfluve connections and topology can be captured via multi-digit interfluve

In the same way that twigs grow from branches and trunks, the branching sequences of primary, secondary, or tertiary interfluves are likely important to CZ structure and process. For example, terrain slope and elevation of hillsheds is influenced by the interfluve order of the hillshed from which they branch. Figure 1b illustrates branching sequences of 1st order interfluves joining 2nd, 3rd, or 4th order interfluves from

left to right, designated by a 3-digit interfluve ordering scheme along the Calhoun's eastern Holcombe's Branch watershed. Single-digit interfluve orders denote the interfluve order of a given hillshed while three-digit interfluve orders denote the interfluve order of the hillshed (in digit 1) as well as the interfluve orders of the first and second uphill junctions (in digits 2 and 3). This ordering scheme condenses hierarchical landscape topology information about the geomorphic neighborhood of each landform.

The ordered interfluve hillshed approach was developed and applied at the CCZO explicitly under the CZ science "tree top to bedrock" concept (Richter and Billings 2015, Brantley, DiBiase et al. 2016). We first quantitatively relate interfluve order to hillshed counts, junctions, areas, elevations, and slopes and then we apply the hierarchical ordering system to patterns in three important CZ processes of the CCZO: geological soil erosion potential using the Unit Stream Power Erosion-Deposition (USPED) model (Warren, Mitasova et al. 2005, Mitasova, Barton et al. 2013), spatially modeled geophysical weathering front depth (St Clair, Moon et al. 2015, Moon, Perron et al. 2017), and historic and contemporary landcover (Brecheisen, Cook et al. 2015). Geological erosion, bedrock weathering, and changes in landcover are complex CZ processes affected by natural, and even social and economic forcings, and are shown to vary with interfluve order as a function of their geomorphology. We hypothesize that interfluve ordering can be usefully related to the management and study of structure and function of many landscapes.

2.2 Methods

2.2.1 Derivation of ordered-interfluve networks and their hillsheds

Landscapes with appreciable ridgeline relief can be examined by inverting DEMs to generate interfluve networks using the same hydrologic GIS tools used to delineate stream networks. In this inverted-terrain framework, interfluves are transformed into flow-accumulating valleys and bottomlands. Geospatial analyses, models, and figures were generated and conducted using ArcGIS(ESRI 2014), Whitebox GIS(Lindsay 2014), and QGIS(Akagi 2015, QGIS Development Team 2016). The CCZO raster DEM (NCALM 2014) was inverted by summing the minimum and maximum values of the DEM and then subtracting each DEM raster cell value from this sum resulting in a DEM with positive elevation values and the same minimum and maximum elevation values as the original DEM on an inverted terrain surface, following equation (1):

$$DEM_{inv} = (DEM_{max} + DEM_{min}) - DEM_{landscape} \qquad (1)$$

Horton-Strahler (Horton 1945) network ordering was used to assign interfluve orders across the 190 km^2 Calhoun CZO in ArcGIS 10.2.2. Moving window DEM averaging was used to smooth gentle saddles and isolated rises within a 200m X 200m neighborhood, allowing flow direction and subsequent flow accumulation analyses to succeed. Resampling the DEM at coarser resolution rather than averaging could likely achieve a similar result and greatly decrease processing time.

Interfluve network delineation was accomplished with stepwise-flow accumulation "burn-in" (Callow, Van Niel et al. 2007). An initial high flow accumulation area threshold of 100ha was set and 10m elevation was subtracted from the inverted DEM for each elevation cell having a flow accumulation equal to or greater than 100ha, followed by a second flow accumulation analysis and second 10m burn-in at a 5ha threshold. At each step the decreasing flow accumulation thresholds serve to concentrate the modeled flow accumulation in increasingly incised, but more extensive, interfluve-channel networks.

This novel approach for the delineation of upland ridge-networks mimics a simplified process of initial channel incision and deepening on inverted terrain. A flow accumulation analysis was used to delineate the resulting interfluve ridge network (Figure 2.1) with a relatively low flow 1st order interfluve inverted DEM flow accumulation threshold of 3ha based on a heuristic interpretation of the DEM, derived slope maps and contours, and field experience of the CCZO landscape. The inverted DEM flow accumulation threshold values needed for 1st order interfluve identification are geomorphically dependent. For example, a second DEM from the 660 km^2 Boulder Creek CZO (BCCZO) near Boulder, Colorado, U.S.A (BCCZO 2010, Anderson, Anderson et al. 2012) was resampled from 1m to 30m spatial resolution and was analyzed to generate an illustrative interfluve network with a final 1st order interfluve threshold of 9ha (Appendix A). Contrasts in relief (100-200m elevation at CCZO vs. 1630-4070m at

the BCCZO), climate, and drainage density are contributing factors to the differing 1st order thresholds between the two research areas and will vary among geologic and climatic forcings elsewhere (Tucker and Bras 1998).

While flow accumulation thresholding of the final network may raise concerns, there should be tolerable threshold range within which interfluve lines and their junction nodes will be generated between drainages such that the great majority of 1st order interfluve-hillshed features can be delineated across a landscape. Within this range, the only thing to change significantly should be how long and how far down the hillslope 1st order interfluve lines are drawn. As long as interfluves are represented by nodes on the topographic network, their downslope hillshed landforms can be delineated. For all interfluves, hillshed boundaries were delineated manually using contour lines, slope maps, stream features, and valley bottoms for their bordering. This process is laborious but ensures geomorphic accuracy of the landforms. This was particularly necessary due to the 200m focal window averaging which, in addition to correcting flow-direction raster computation enabling Strahler-Horton ordering, blurs smaller scale terrain features, necessitating manual quality control of the network and resulting hillsheds.

2.2.2 Three applications of interfluve ordering

Three CZ processes are investigated from an ordered-interfluve perspective: rates of geologic pre-anthropogenic erosion, weathering front depth, and landcover and landcover trajectories.

2.2.2.1 Pre-anthropogenic geologic soil-erosion modeling

Soil erosion across interfluve orders was investigated using the Unit Stream Power Erosion-Deposition (USPED) model (Warren, Mitasova et al. 2005, Mitasova, Barton et al. 2013, Mitasova, Petrasova et al. 2014) at 30m spatial raster resolution to simulate landscape evolution erosion rates under hypothetical continuous forest cover (pre-human) across the CCZO landscape. USPED is formulated in equation (2):

$$T = R \times K \times C \times P \times LST \qquad (2)$$

Where T is the annual sediment transport capacity in Mg×m/ha×yr, R is the rainfall erosivity factor obtained from USDA isoerodent maps (USDA 1972) and is considered uniform across the landscape at 4680 MJ×mm/h×ha×year. K is the soil erodibility factor ranging from 0-0.04 Mg×ha×h/ha×MJ×mm. K factor data were obtained from the SSURGO GIS soils database (ESRI 2014) for the Enoree (HU 03050108) and Tyger (HU 03050107) basins. R and K factors were originally in non-metric units and were converted to metric units using conversion factors provided by Chang et al. (2016). C is the unitless cover management factor and represents the impact of landcover on erosion potential and was set to equal 0.0005 for permanent forest cover (Franzmeier,

Steinhardt et al. 2009). *P* is the practice factor and represents the impact of potential engineering practices that can reduce erosion potential such as terracing plowing practices and was set to 1 across the CCZO landscape under pre-anthropogenic conditions. *LST* is the combined slope-length and steepness factor of sediment transport capacity for overland water flow such that $LST = U^m \times (\sin\beta)^n$ where *U* is the upslope flow accumulation in m^2/m and β is the terrain slope in degrees (Warren, Mitasova et al. 2005, Mitasova, Barton et al. 2013, Mitasova, Petrasova et al. 2014). Exponents *m* and *n* adjust the interaction of water flow and terrain slope terms under sheet and rill runoff conditions. The exponents were set such that $m=n=1$ reflecting a combination of both rill and sheet erosion over long time periods with many large and small erosional flow events.

Following the calculation of *T* (net erosion and deposition), *D* (eroded soil loss) in Mg/ha×year was then calculated as a function of sediment flow along an elevation gradient as outlined by Mitasova et. al (Warren, Mitasova et al. 2005, Mitasova, Barton et al. 2013, Mitasova, Petrasova et al. 2014) in equation (3):

$$D = \partial(T \cos \alpha)/\partial x + \partial(T \sin \alpha)/\partial y \qquad (3)$$

where α is terrain aspect in degrees. For implementation in ArcGIS 10.2.2, *D* was calculated according to the relationship between the partial derivatives and surface slope (β) and aspect (α) in equation (4):

$$D = \partial T/\partial x + \partial T/\partial y \qquad (4)$$

where $\partial T/\partial x = (T \times tan\beta) \times (T \times cos\ \alpha)$ and $\partial T/\partial y = (T \times tan\beta) \times (T \times sin\ \alpha)$.

Subsequent calculations and conversions based on interfluve order aggregate median erosion values from Mg/ha-year to vertical soil loss denudation rates assume a soil bulk density of 1.25 g/cm^3 (Bacon, Richter et al. 2012). Lastly, sediment erosion : deposition ratios were estimated by successively subsetting the landscape by interfluve order and summing the values of negative USPED raster cells (erosional areas), then dividing by the sum of positive USPED raster cells (depositional areas) within each interfluve order.

2.2.2.2 Generation of bedrock weathering front depth dataset

Recent research on the patterns of bedrock weathering depth, both theoretical (Rempe and Dietrich 2014) and geophysical (Anderson 2015, St Clair, Moon et al. 2015), indicate that the depth to the bedrock weathering front (z-boundary (Rempe and Dietrich 2014)) may be highly variable in space and linked to patterns in topography. Bedrock weathering front depth investigations partition 3D topographic stress model results (St Clair, Moon et al. 2015) across interfluve orders in order to understand spatial patterns in the magnitude and variation of weathering front depth.

Following the methodology used by St.Clair et al. (2015) and Moon et al. (Moon, Perron et al. 2017), 3D topographic stress models were generated in the CCZO using poly3D (Thomas 1993). Due to computational limitations in generating least compressive stress models, four areas in close proximity within Holcombe's Branch

watershed totaling ~350ha spanning 1st, 2nd, 3rd, and 4th order interfluves were selected for modeling with ~9m resolution. The bedrock weathering front depth was calculated from the ground surface to the least compressive stress volume of 0.5MPa(Moon, Perron et al. 2017). Least compressive stress model values of 0.5MPa correspond closely to ~4 km/s *P*-wave velocities measured in the field (St Clair, Moon et al. 2015). These values are thought to represent and approximate the transition zone between fractured weathering parent material to un-weathered bedrock.

2.2.2.3 Landcover datasets

The second application of interfluve ordering involved landcover analysis focused on 1933 and 2014 land management. Landcover is classified as forest, grass/shrub, or bare earth in 1933 using mosaicked and georectified aerial photography (Brecheisen, Cook et al. 2015). For 2014 landcover was classified using $1m^2$ resolution canopy height derived from a July 2014 LiDAR flight (NCALM 2014) partitioned into: 0-1m considered to be hay field or pasture, 1m-5m interpreted as recently harvested forest and young tree regeneration, and >5m canopy height classified as intact forest. The contemporary landscape was also partitioned into privately and publicly owned USFS land (USFS 2016). A landcover transition matrix was then analyzed with possible transitions being from either forested (F) or non-forested (NF) in 1933 to forested (F) or non-forested (NF) in 2014 with a total of four possible outcomes: F-F, F-NF, NF-NF, NF-

F. This matrix was used to explore land cover changes over time whether continually-forested, net deforested, net reforested, or continually non-forested.

To create a historic landcover dataset classified as forest, shrub/grassland, and bare agricultural fields, 89 black and white photographs taken during an aerial survey in 1933 were scanned at 1200dpi resolution, georectified, color balanced, seamlined, and mosaicked in ArcGIS 10.2.2 at ~0.5m spatial resolution (Brecheisen, Cook et al. 2015). This raster layer was resampled to 30m resolution using "majority" pixel landcover assignment whereby each new coarser pixel value is equal to that of the most abundant landcover type within the original finer resolution raster. Given the three landcover classes for 1933, a comparable method was employed to classify the 2014 LiDAR canopy height into landcover categories of pasture or hayfield (0-1m), recently harvested young forest (1-5m), and intermediate or mature forest (>5m). The canopy height raster was generated by subtracting the LiDAR ground-return raster DEM (NCALM 2014) from the highest return LiDAR raster DEM (NCALM 2014) and resampling the resulting canopy height raster to 30m using bilinear interpolation in ArcGIS 10.2.2 (ESRI 2014). An additional dataset of the CCZO landscape within the boundaries of the 2014 LiDAR (NCALM 2014) was generated as either publicly or privately owned in 2014 by converting USFS vector data (USFS 2016) into 30m binary raster format. In 1933, all of this landscape was privately owned. Most of the USFS purchases were made later in the 1930s.

2.2.3 Statistical analyses of terrain and CZ processes

Across the southern Piedmont, floodplains have been loaded with sediments eroded from uplands and are a product of, or have at least been strongly impacted by, a very different anthropogenic-erosion regime than that which formed the dendritic interfluve network in geologic time (Richter and Markewitz 2001, James 2013). Because of this, we seek to remove the elementary form(Evans 2012) of the floodplain from statistical analysis, a multi-criterion task. Statistical analyses were conducted on hillshed raster data, which were masked to isolate hilltop-to-footslope terrain excluding major floodplains. Floodplains at the CCZO are generally characterized as being: low elevation (below 160m), below mid-slope as calculated via the Topographic Position Index (TPI) (Wilson and Gallant 2000), and having low topographic roughness (elevation range <9m within 0.18ha). The TPI step to mask floodplain data entailed 1km^2 focal window averaging of the 1m^2 LiDAR ground DEM (NCALM 2014) generating an average-elevation raster, which was then subtracted from the original LiDAR DEM. The raster generated from this subtraction was then thresholded, with values greater than zero being greater than average or mid-elevation (TPI=0 at mid-slope) within the window, equation (5) below:

$$Mask_{uplands} = DEM - DEM_{1km\ avg} > 0 \qquad (5)$$

These criteria were used to isolate floodplain terrain in the 190km^2 CCZO.

Statistical analyses in this paper partition the CCZO landscape into ordered interfluve hillsheds using 1 or 3 digits. The value of any digit can range from 1 to 5 in the 190km^2 CCZO and sequential digits can skip orders (e.g. hillsheds with 245 or 135 interfluve orders), though each sequential digit must be greater than the preceding digit. Thus, a 231 interfluve is nonsensical as the 3rd-to-1st transition is downhill and is not possible in inverted terrain Horton-Strahler ordered DEM flow-analysis. If either the first or second uphill junctions for a given a hillshed were outside the DEM, a 0 value was entered for partitioning later analyses. The terminal 5th order interfluve and all connections to it were retained for analysis and denoted as 500, #50, and ##5 in 3-digit ordering with "#" representing sequential integers less than 5.

The ordered-hillshed is the basic unit of study in this work. Analyses of central tendencies drawing upon individual ordered-hillsheds include the calculation and comparison of: area, median elevation, median slope, and mean USPED pre-anthropogenic soil erosion. The 727 delineated hillshed shapefiles were converted to raster formats using a unique ID ranging from 0-726, such that they were aligned with, and matched the resolution of, the various terrain or CZ application datasets and excluded floodplain areas. This was accomplished using the "raster" package in R (Hijmans 2015, R Core Team 2016). Areas, means, and medians for these datasets were calculated across the CCZO landscape for each of the 727 delineated hillsheds and were tabulated and appended to the original ordered-hillshed shapefile attribute table.

Hillsheds were partitioned for 1-way ANOVA analyses according to their 1- and 3- digit interfluve orders for landscape patterns of hillshed: ln(area) (ha), slope (°), and elevation (m) using the stats package in R(R Core Team 2016). In this way, each hillshed served as an individual data point with hillsheds grouped by interfluve order for terrain analyses. Median elevation for each ordered interfluve hillshed was further analyzed as a function of median hillshed slope values, natural log-transformed hillshed area, and the second interfluve junction order to investigate landscape evolution using multiple regression without interaction terms in R using the "stats" package (R Core Team 2016).

Aggregate and cumulative landscape analyses entailed subsetting the CCZO landscape by interfluve order for the calculation of total area per interfluve-order and interfluve-order landcover percent area analyses for: 1933, 2014, 1933 to 2014 landcover transitions, and public vs. private hillshed land area in 2015 using the "raster" (mask function) and "SDMTools" (ClassStat function) packages in R (VanDerWal, Falconi et al. 2014, Hijmans 2015, R Core Team 2016). In this way, the data for the entire portion of the CCZO landscape occupied by 1st, 2nd, 3rd, 4th, and then 5th order hillsheds were aggregated. Weathering front depth analyses, because they were spatially limited, were carried out by pooling all of the modeled geospatial raster values within corresponding hillshed orders for analysis.

2.3 Results

2.3.1 Terrain analyses of ordered interfluve hillsheds

Terrain analyses were conducted across upland terrain (~85% of the CCZO landscape) excluding floodplain bottomlands (~15% of the landscape) filled with meters of agriculturally eroded sediments (Richter and Markewitz 2001, Trimble 2008). Terrain analysis of individual hillsheds (Figure 2.2a), indicates that 81% of all hillsheds are 1st order, 14% are 2nd order, 3% are 3rd order, 0.6% are 4th order, and 0.1% are 5th order. This exponential distribution of interfluve-hillsheds matches hydrologic stream order distributions (Tarboton 1996) where order is typically strongly and negatively correlated to their abundance. Conversely, interfluve order is positively related to individual hillshed area as average area increases exponentially from 13.6 ha for 1st order hillsheds to 536.3 ha for 4th and 5th order hillsheds (Figure 2.2b). Total upland area in each hillshed order across the 190-km^2 CCZO landscape is the product of these two patterns and is characterized by a nearly linear trend of cumulative area (ha) across interfluve orders (Figure 2.2c). First order interfluves total about 8042.4ha whereas 4th and 5th order interfluves total 2476ha. First order interfluves thus cover about 48.8% of the non-floodplain CCZO, 2nd orders about 22.5%, 3rd orders 13.6%, 4th orders 11.8%, and 5th orders 3.3%.

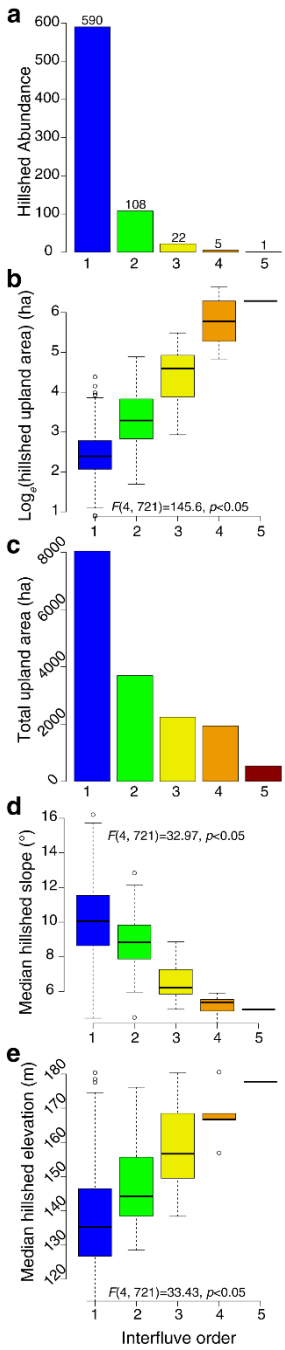

Figure 2.2: ordered interfluve terrain analyses of hillshed: a) abundance, b) area, c) cumulative area, and d) median slope, median elevation. The number of interfluves in each order is above each bar in the top abundance panel and ANOVA F-test results within ln(area), slope, and elevation plots.

Median hillshed slope is strongly and negatively related to interfluve order with the steepest average slopes on 1st order interfluves (mean=10.05°) and with interfluves becoming flatter uphill as interfluve order increases (Figure 2.2d). First to 5th order hillsheds had median elevations of 135.2, 144.2, 156.7, 166.7, and 177.7m (Figure 2.2e), likely the result of geologic erodibility of respective interfluves as a function of their slope, and breadth. Figure 2.3 integrates these variables of interfluve-hillshed order, area, number, slope, and elevation for the CCZO landscape as a whole.

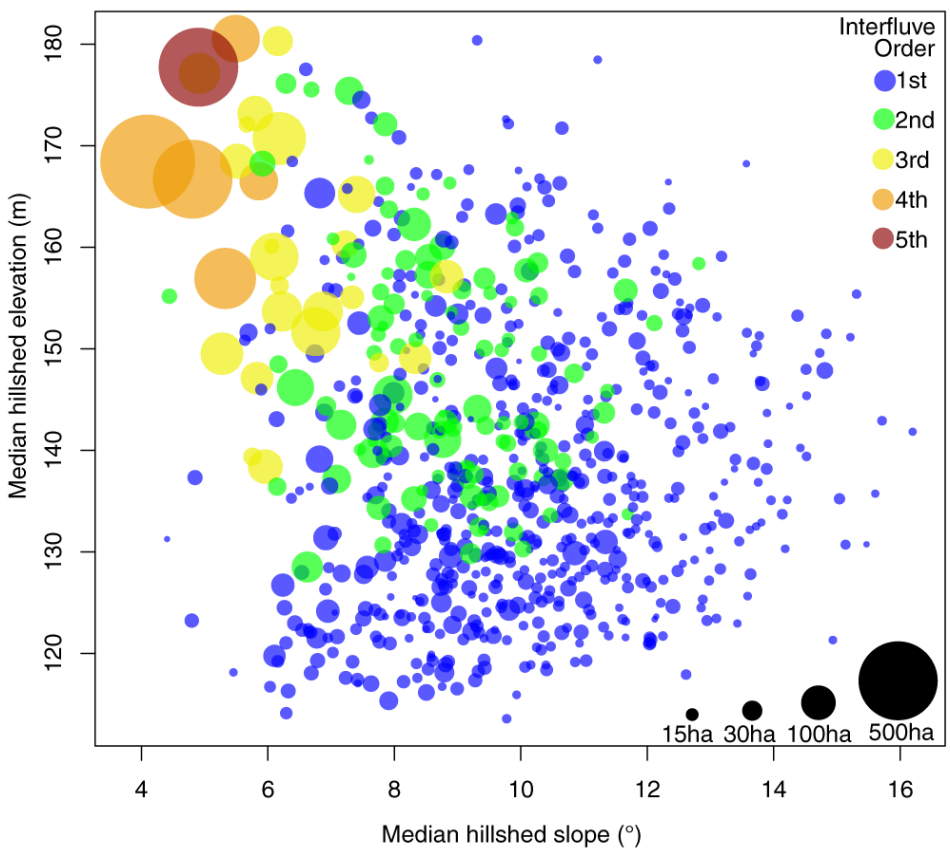

Figure 2.3: Terrain scatterplot of interfluve-ordered hillshed median elevation and median slope. The size of points corresponds geometrically to individual hillshed areas.

Terrain analyses demonstrate that the characteristics of interfluves often depend on the order of the interfluve order with which they are connected. Our interfluve ordering approach can thus be used to examine, for example, how a 1st order interfluve's geomorphology varies according to whether it joins a 2nd, 3rd, 4th, or 5th order interfluve (Figure 2.4a-4e). Most remarkable are relationships of slope and elevation with their three-digit order classifications (Figure 2.4e). Considered together, 3-digit hillshed slope and elevation reflect long-term landscape evolution with steeper and narrower interfluves eroding more rapidly being furthest from the geomorphic trunk of the landscape experiencing the greatest denudation. A terrain multiple regression analysis modeling median hillshed elevation as a function of median hillshed slope and log hillshed area not addressing the branching patterns of interfluves yields a very weak predictive model of elevation: $F(5, 557) = 26.85$, adj $R^2=0.08$, $p<0.05$). The same analysis, however, factoring in the second interfluve junction-order of each hillshed ($F(5, 554) = 120.2$, adj $R^2=0.52$, $p<0.05$)) demonstrates the driving importance of the connectedness of interfluves as drivers of landscape structure. Interfluves that are two junctions downhill from either 5th, 4th, or 3rd order interfluves are 11m, 28m, or 38m lower in elevation on average compared to interfluves which are 5th order or immediately branch from a 5th order interfluve (Figures 2.1 and 2.4e).

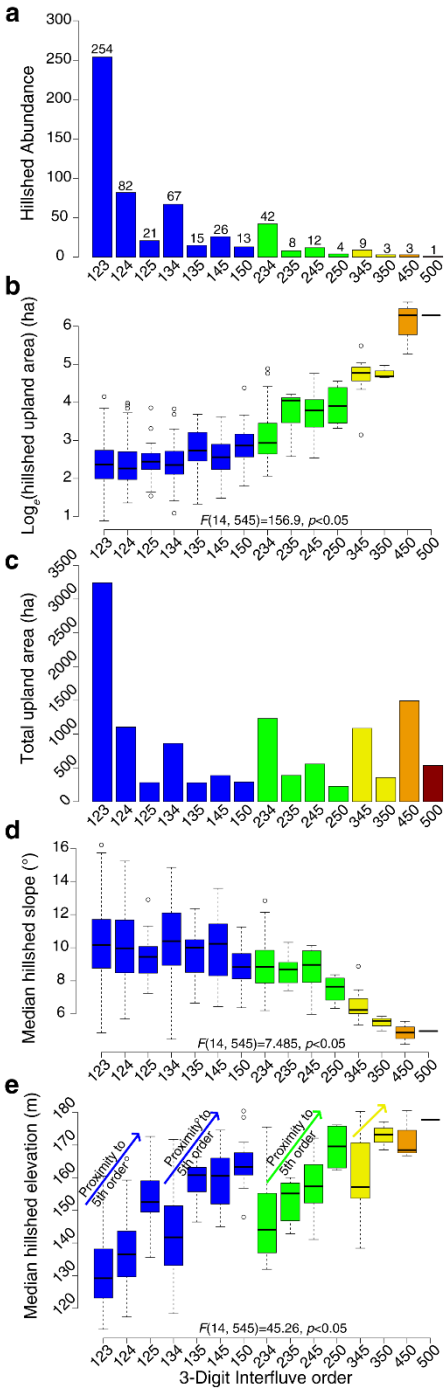

Figure 2.4: 3-digit ordered interfluve terrain analyses of hillshed: abundance, area, cumulative area, and median slope, median elevation with number of interfluves in each order above each bar in the top panel and ANOVA results at the bottom of loge(area), slope, and elevation plots.

2.3.2 USPED geological erosion as a function of interfluve order

The first application of interfluve and hillshed ordering was made with estimates of geological erosion across the CCZO landscape. The broadest interfluves of the CCZO landscape in the Southern Piedmont are biogeomorphically stable over geologic time, with erosion rates between 0.35m/Myr and 3m/Myr prior to colonial settlement (Bacon, Richter et al. 2012). On such interfluves, CCZO soils and saprolite are deep, extremely weathered, with soils having minimum 2 million year residence times and 10s of meters of depth above un-weathered granitic gneiss bedrock (Bacon, Richter et al. 2012). USPED modeling of geologic erosion (Warren, Mitasova et al. 2005, Mitasova, Barton et al. 2013) indicate that 1st order interfluve-hillsheds have about 30 times higher average (0.2 Mg/ha-yr) erosion rates as either 4th or 5th order interfluves (0.006 Mg/ha-yr) (Figure 2.5a). Assuming a bulk density (BD) of 1.25 g/cm^3 (Bacon, Richter et al. 2012), these erosion rates correspond to average denudation rates of ~16 m/My on 1st order interfluves declining to ~0.5 m/My on 4th and 5th order interfluves. This 30-fold increase from high- to low-order interfluves supports inferences made regarding the interaction of interfluve order and slope as drivers of landscape elevation evolution.

USPED, being a sediment transport capacity model, yields both net erosion and deposition. Aggregating these data across the CCZO according to interfluve order provided an estimate of mobilized soil net erosion vs. re-deposition ratios. This analysis indicated that 1st order interfluves have 1.56 times more net erosional loss from

hillsheds than is re-deposited. In contrast, 4th and 5th order interfluves have only 1.13 and 1.09 times more net erosional loss than would be redeposited, reflecting the broad and level terrain found on high-order interfluves.

2.3.3 Weathering front depth as a function of interfluve order

A second application of interfluve ordering was made with models of weathering front depth (Rempe and Dietrich 2014, St Clair, Moon et al. 2015, Moon, Perron et al. 2017). Here, we modeled weathering front depths by least compressive stress to locate the 0.5MPa boundary (Figure 2.5b), estimated empirically to correspond with a transition to highly competent bedrock (St Clair, Moon et al. 2015). Results clearly indicate that 1st order interfluves have both the greatest maximum depth (~53m) and the highest spatial variability in depth to modeled weathering front (Figure 2.5c). The depth to modeled weathering front at 0.5MPa becomes relatively shallower and much less variable as interfluve order increases (Figure 2.5b and 2.5c), a function of the characteristic slopes and breadths of interfluve and hillshed orders. This relationship is expected considering steep slopes and high curvatures of relatively narrow 1st order interfluves, which can perturb subsurface stress fields and produce a spatially variable weathering depth front which mirrors "pinched topography" across these hillsheds (Anderson 2015, St Clair, Moon et al. 2015, Moon, Perron et al. 2017). Considered as a three-dimensional volume, modeled 1st order interfluve hillshed areas have ~2740m^3/ha of weathered material with this volume decreasing slightly as interfluve order increases

to 4th order (~2540m^3/ha). Given these results and those of interfluve-dependent geologic erosion rates, weathering rates (Gilbert 1887) must also be interfluve order dependent and much higher at lower order interfluves of the CCZO. We suggest that this may well result from both more rapid rates of drainage (Rempe and Dietrich 2014) as well as more variable bedrock stress fields (Anderson 2015, St Clair, Moon et al. 2015, Moon, Perron et al. 2017) of the steeper, narrower low order interfluves compared with those of higher order.

2.3.4 Landcover changes as a function of interfluve order

The Calhoun Critical Zone has been subjected to some of the most severe agricultural erosion in the USA, a common condition of much of the Southern Piedmont. The deep soils and hillslopes are deeply incised by gullies and large quantities of soil eroded downslope over up to two centuries of agriculture as forests were cleared for cultivation, grazing, and wood products across even the most marginal areas (Hansen 1991, Richter and Markewitz 2001, Trimble 2008, Coughlan, Nelson et al. 2017). Low-order interfluves were so seriously eroded and gullied by farming that the USFS targeted farms with degraded lands for "retirement" and purchase in the 1930s as many debt-ridden farmers defaulted on taxes. Farms were sold to the federal government and the Enoree district of the Sumter National Forest was established (Metz 1958, Hansen 1991) with other National Forests in the region established similarly. The land ownership changes from private to public led to land management changes as

reforestation expanded across the not only the Sumter National Forest but the entire Southern Piedmont.

Connections between interfluve order, area, slope, and geologic erosion rates indicate that the history of land-use change at the CCZO maps well onto an ordered-interfluve landscape. Historic 1933 landcover patterns of percent bare cropland, grass/shrubland, and forest are strongly related to interfluve order (Figure 2.5d). Contemporary landcover patterns also map well onto interfluve orders with percent private land, public land, and distribution of non-forested vs. forested lands all strongly associated with interfluve orders (Figure 2.5d). Landcover on low order interfluves is more likely to have remained forested between 1933 and 2014 compared with forests on higher order interfluves (Figure 2.5d, F-F) (Coughlan, Nelson et al. 2017). Similarly, percent landcover which has remained non-forested from 1933 to 2014 (Figure 2.5d, NF-NF) is also positively related to interfluve order, with nearly all of this land on high order interfluves being privately owned (Figure2. 5d). New net-deforestation (F-NF), and prolonged non-forestation (NF-NF) appears concentrated on high order interfluves. The 5th order interfluve has 12% new deforestation compared to 1st through 4th order interfluves (4-5% average). Similarly, 5th order interfluves also have less net-reforestation (Figure 2.5d NF-F) (average 29.5%) than 1st-4th order interfluves (36.9%).

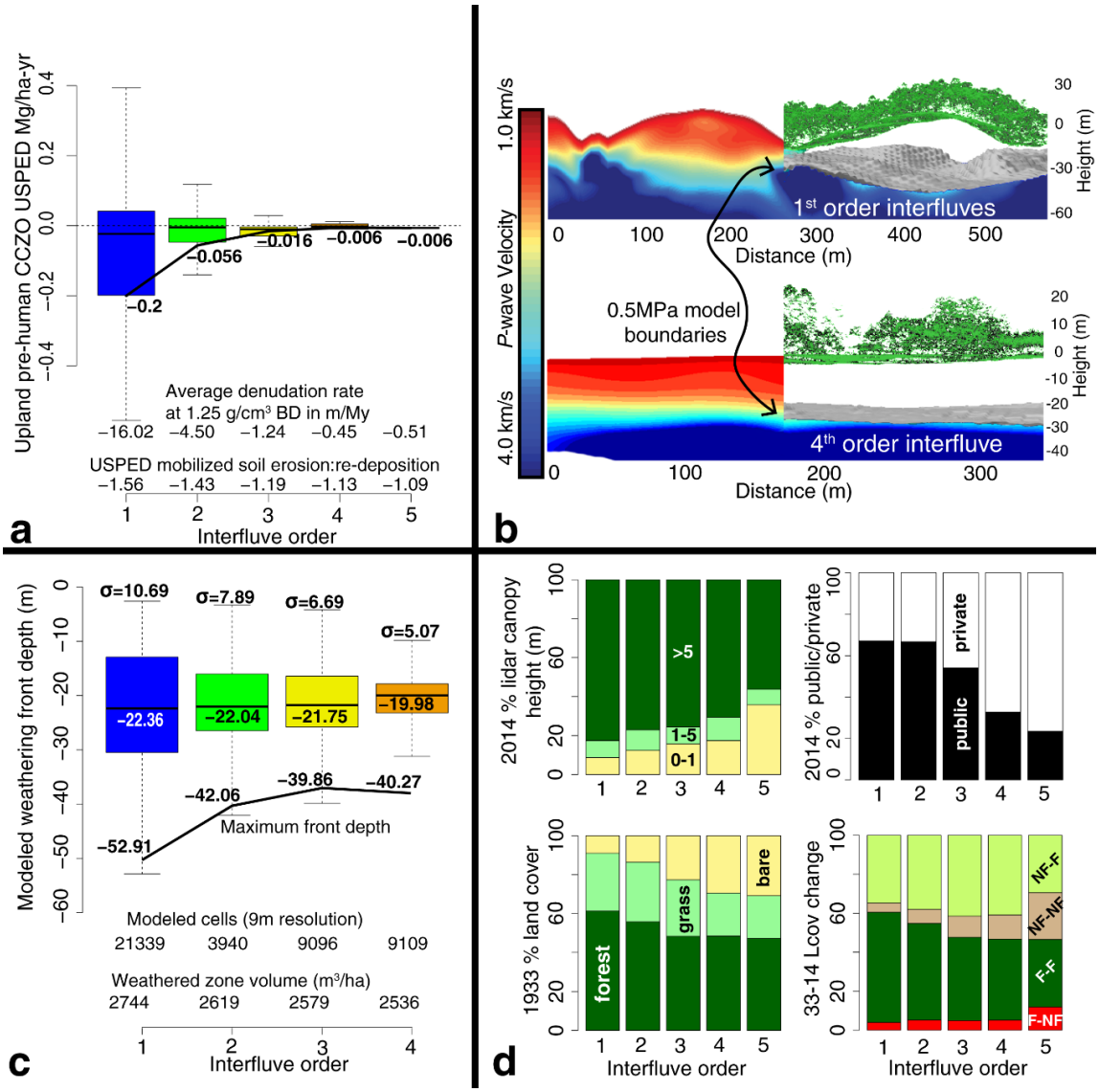

Figure 2.5: CZ application process graphs and diagrams of a) pre-anthropogenic geologic erosion model results with solid line and numbers equal to arithmetic average hillshed erosion rates, b) 3D weathering front surface (grey) modeled as least compressive stress at 0.5MPa from Moon et. al, 2017 corresponding to 2D cross sections ~4 km/s p-wave velocity (modified from St. Clair et. al, 2015) below green colored LiDAR point cloud highlighting vegetation and ground surface on 1st (top) and 4th (bottom) order interfluves, c) depth distribution of modeled depth to weathering front across interfluve orders, and d) land cover, landcover change, and land ownership. In panel d) "F" and "NF" refer to land cover states being "forested" or "non-forested" respectively.

2.4 Discussion

The interfluve ordering approach presented constitutes a geomorphic landform framework that can advance analyses of landscape connectivity by pairing hierarchical interfluve-ordering with hillshed landforms. This is accomplished in a manner not possible via grid-cell examinations or models of landscapes according slope, elevation, or curvature. Ranked hillsheds and interfluve orders capture important patterns and connections in landscape structure. Understanding the distribution of these landforms' areas, elevations, and slopes enhances our ability to link landscape structure to CZ function. This is illustrated in three applications of spatial and temporal patterns of soil erosion, geophysical weathering, and landcover change. Many other processes such as soil formation, groundwater storage and yields, catchment hydrologic responses, biologic productivity, management sustainability, and even fire behavior are likely correlated with the physical attributes of interfluve ordered hillsheds. These processes span the disciplines of geomorphology, environmental history and anthropology, biogeochemistry, geophysics, hydrology, remote sensing, soil science, ecology, and land and water management. Interfluve ordering provides a geomorphic organization that spans spatial and temporal scales in parallel with those of the critical zone.

Terrestrial environments are often characterized as having rolling hills or topographies with uplands dissected by drainage networks (Perron, Kirchner et al. 2009). Examples of similar topography include the Interior and Appalachian Plateaus of

North America, the Andean Piedmont and Amazon basin (Stahl 2015) in South America, and the Congo and Yangtze basins of Africa and China. The topographies of these regions are not a random occurrence of hills and dales (Maxwell 1870), but have organized patterns that result from landform evolution over multi-millennia, shaped by weathering, erosion, and conditioned by underlying bedrock, biota, and climate (Gilbert 1887, Jenny 1994, Perron, Kirchner et al. 2009). Future terrain analyses of interfluve orders will examine landscapes that contrast with those at the ancient, deeply weathered Calhoun CZO to further explore the connectedness and functions of interfluve networks. Mountainous landscapes, eroding canyon landscapes, those of loessal deposition, and other Piedmont landscapes should have landform organization amenable to interfluve ordering and will no doubt yield results that contrast with the structure and function of the CCZO Southern Piedmont.

3. Micro-Topographic Roughness Analysis (MTRA) highlights minimally eroded watersheds in an ancient landscape impacted by historic agriculture

3.1 Introduction

Light Detection And Ranging (LiDAR) and other remote sensing approaches can find, extract, and characterize fine-scale anthropogenic and natural earth surface features and environments for many disciplines (James, Watson et al. 2007, Listopad, Drake et al. 2011, Pike, Mueller et al. 2012, Maxwell and Strager 2013, Barbosa, Melendez-Pastor et al. 2014, Vaglio Laurin, Chen et al. 2014). This frequently involves edge-detection or identification of discontinuities in the terrain surface via visual or computational means (Brubaker, Myers et al. 2013, Hightower, Butterfield et al. 2014, Han, Yang et al. 2016). Spatial variation in the local steepness of slopes has been interpreted to be a highly sensitive indicator of historic erosion at the Calhoun Critical Zone Observatory (CCZO) in the South Carolina Piedmont. Severe sheet, rill, and gully agricultural erosion disturb, roughen, and scour previously smooth terrain surfaces (James, Watson et al. 2007, Brubaker, Myers et al. 2013, Stenberg, Tuukkanen et al. 2016). Here we use LiDAR's ability to detect fine meter-scale structure across terrain to locate and isolate "reference watersheds" where anthropogenic agricultural disturbance has been minimal or absent (James, Watson et al. 2007, Pike, Mueller et al. 2012, Hightower, Butterfield et al. 2014).

We conduct this research at the Calhoun CZO, an ancient unglaciated landscape in the humid subtropics that has deep and highly weathered soils that were biogeomorphically stable and mainly under forest cover prior to the arrival of non-native peoples to North America (Richter and Markewitz 2001, Bacon, Richter et al. 2012). High hillslope stability, extensive rooting, deep soil profile formation, and forest vegetation have result in a landscape with multi-million-year soil residence times (Bacon, Richter et al. 2012). High soil stability coupled with a warm and moist climate favoring diffusive landform evolution (Gilbert 1887, Jenny 1994) resulted in a smooth terrain surface, even on the steepest hillslopes. Because the majority of the Southern Piedmont was severely eroded and gullied by agricultural land uses from the late 1700s to the 1930s (Metz 1958, Trimble 2008, Coughlan, Nelson et al. 2017), we attempt to remotely identify minimally eroded reference watersheds by locating contiguous areas where gullies and associated microtopographic roughness are absent (Brubaker, Myers et al. 2013). Minimally eroded reference watersheds and their hillslopes are understood to have retained a smooth microtopographic surface, which should be characterized by having low local variability in slope. Meter-scale variability in local slope steepness, rather than absolute steepness in hillslopes, is analyzed because the goal is to exclude gullies, gully-edges, old roads and trails, terraces, ruts, drainage ditches, and other microtopographic disturbances linked to anthropogenic land management, not just steep hillslopes. Local variation in slope is a practical metric for analyzing

microtopography (Dikau 1990, MacMillan and Shary 2009, Brubaker, Myers et al. 2013), and tools and coding functions are readily available for estimating both terrain slope as well as local raster statistics within user-defined variably-sized focal windows in GIS and statistical programs (ESRI 2014, Lindsay 2014, Hijmans 2015, Evans 2016, QGIS Development Team 2016, R Core Team 2016).

Though the CCZO landscape is today blanketed by forests, they are almost entirely secondary forests. Beneath these forests, areas with higher local variation in slope across several meters can be identified and are thought to reflect rougher terrain with evidence of erosive advective water runoff from historic fields. Alternately, low local variability in slope should be indicative of smooth, ungullied terrain. The resulting microtopographic roughness analysis (MTRA) is used to index the degree of human disturbance such that relatively low values of terrain watershed standard deviation of slope (measured in degrees) indicate relatively smooth surfaces primarily shaped primarily by diffusion processes that operate on geologic time scales.

3.2 Methods

3.2.1 Characterization and identification of minimally-eroded reference terrain

To identify minimally disturbed reference watersheds across hundreds to thousands of square kilometers, Micro-Topographic Roughness Analysis (MTRA) was employed using ArcGIS 10.2.2. The CCZO landscape terrain analysis did not include floodplains along major rivers and streams prior to MTRA analyses as these areas are

almost all filled with large volumes of legacy sediments deposited from the eroded uplands (Hansen 1991, Trimble 2008, James 2013). MTRA was used to calculate the standard deviation (SD) of LiDAR-derived terrain slope at $1m^2$ resolution within a 7m x 7m focal window moving across ~$117km^2$ of the publicly-owned CCZO (ESRI 2014, USFS 2016). The LiDAR data are publicly available at OpenTopography as a product of the Calhoun Critical Zone Observatory (NCALM 2014). The MTRA-derived SD(slope) analysis of the CCZO landscape varied across a continuum from highly eroded and gullied to minimally disturbed.

In order to characterize minimally-eroded reference terrain, three reference hardwood training areas in research areas 2, 4, and 5 (~24ha total) (Figure 1.2), previously identified over decades of research in and around the Calhoun Experimental Forest (Metz 1958, Richter and Markewitz 1995, Richter and Markewitz 2001, Richter and Billings 2015) were compared to adjacent non-reference areas (~34ha total). The SD(slope) values of these areas, which did not all encompass discrete geomorphic units of watersheds or hillsheds (Brecheisen, Richter et al. 2018), were compared between reference vs. non-reference terrain using $1m^2$ resolution within 7m x 7m focal windows (Figure 3.1). Based on pooled terrain data, the mean reference SD(slope) value (rounded to 2.25°) was used as a cutoff in the search for minimally-eroded reference terrain.

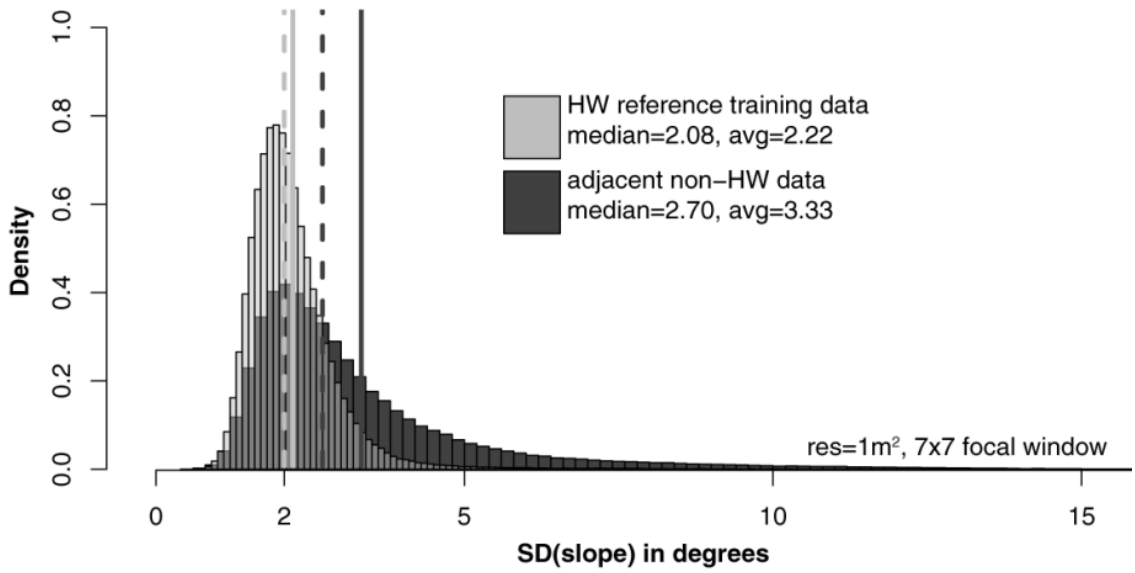

Figure 3.1: Pooled 1m² resolution raster SD(slope) histograms from 7x7 moving focal window data from three previously identified reference hardwood (HW) locations and adjacent non-reference areas in similar topographic settings. Reference HW data presented here was used as training data to determine a conservative cutoff by rounding up the HW reference mean value of 2.22°. In this way, across the ~190km² CCZO landscape, only terrain grid cells with SD(slope) < 2.25° were retained in the search for new minimally-eroded HW reference areas. The HW reference histogram is contrasted with pooled data from adjacent non-HW reference areas in similar geomorphic settings. Average values are indicated by solid lines and median values via dashed lines.

Potential reference watersheds and hillslopes can be identified by scanning the SD(slope)<2.25° raster overlain by contour lines to identify likely reference watersheds, or by employing sequential filtering to the SD(slope)<2.25° raster. Candidate areas that encompassed entire watersheds were then delineated. Even extremely smooth terrain will have greater local slope variation near valley bottoms and hilltops, where terrain curvature changes over relatively short distances. In cases where this occurred, these

areas were included in final watershed delineations even when SD(slope) was greater than 2.25°.

3.2.2 Reference vs random watershed comparisons

In order to describe the surface roughness of reference watersheds identified via MTRA, they were compared to 26 randomly delineated watersheds across the CCZO (Figure 1.2). Random watersheds are considered to represent average Southern Piedmont conditions of first-order catchments with more erosive land management over the last 200 years. Watershed analysis of SD(slope) as well as historic and contemporary landcover were contrasted between the reference vs. random watersheds. Further analyses were conducted to ensure that watershed area, slope, and elevation were not confounding factors. The randomly selected watersheds were delineated using contour and DEM maps across the CCZO landscape. Landcover validation datasets include georectified 1933 black and white aerial photography (Brecheisen, Cook et al. 2015), 1m^2 resolution 2014 LiDAR canopy height (NCALM 2014), and February 20th, 2015 LandSat 8 red-band data (scene ID: LC80170362015051LGN00) (USGS 2016).

For each of the individual reference and randomly selected watersheds, area (ha), median elevation (m), median slope (degrees), average 1933 image brightness, average 2014 canopy height (m), and average 2015 winter redness were estimated using the Raster package (Hijmans 2015) to read watershed shapefiles and SpatialEco (Evans 2016) (zonal.stats function) package in R (R Core Team 2016). Mann-Whitney-Wilcox rank-

sum tests (wilcox.test function in "stats" package) were then conducted in R (R Core Team 2016) to check for terrain and landcover differences between reference watersheds and randomly delineated watersheds.

3.2.3 Historic landcover data

In 1933 the U.S. Forest Service conducted aerial photographic surveys of the study area which was to become the Enoree District of the Sumter National Forest. This imagery, having been georectified and mosaiced previously (Brecheisen, Cook et al. 2015) black and white aerial photographs of the study area, forests and trees appear dark or black and so have lower pixel brightness values than areas with open canopies, sparse vegetative cover, or bare agricultural fields. Areas determined to be minimally eroded by farming via MTRA hypothetically have low 1933 aerial image brightness compared to randomly delineated watersheds as they are expected to have more intact forest canopies relative to other portions of the landscape. Present-day CCZO forests are typically pine or mixed deciduous-pine, with much of the post-agricultural forest dominated by loblolly pine, *Pinus taeda*. Reference watersheds identified via MTRA are expected to have more deciduous forest cover than randomly delineated watersheds. As such, randomly delineated watersheds should absorb more of the red portion of photosynthetically active radiation (PAR) in winter months than reference watersheds whose deciduous trees will have shed their leaves. Tree age is expected to be lower in

randomly delineated watersheds with shorter canopy heights, especially if there was timber harvest in the last several decades.

3.2.4 MTRA sensitivity to terrain raster resolution

Gully and rill erosion occur on the order of meters in breadth and depth (James, Watson et al. 2007) and so terrain raster data of this resolution should perform best for detecting these features. In order to evaluate the sensitivity of the MTRA technique to DEM raster resolution, the reference and randomly delineated watersheds were re-analyzed for MTRA SD(slope) at three coarser spatial resolutions: 1.52m, 5m, and 10m. Both the 5m and 10m datasets were generated by resampling the 2014 $1m^2$ LiDAR DEM using bilinear interpolation with slope calculated in degrees using ArcGIS 10.2.2 (ESRI 2014). These both underwent MTRA using 3x3 focal windows to capture the finest spatial resolution possible of slope variation at 5m and 10m resolutions. To demonstrate a robustness in our methods, we compared our analysis of the 2016 high resolution LiDAR data with a 1.52m resolution DEM, which was extracted from the statewide South Carolina 2008 LiDAR DEM and analyzed using a 5x5 raster cell focal window approximately equal in area (7.6m x 7.6m) to the 7x7 focal window used in the $1m^2$ resolution MTRA.

3.3 Results

3.3.1 Identification of minimally-eroded watersheds via MTRA

Though terrain microtopographic roughness falls along a spectrum from extremely rough to smooth, the mean SD(slope) cutoff value of 2.25° from the training dataset (Figure 3.1) effectively identified small, minimally disturbed reference watersheds amidst a much larger expanse of historically disturbed and gullied terrain (Figure 3.2). This was possible as we were able to preferentially exclude ~67% of non-reference terrain while retaining ~62% of potential reference terrain across the CCZO landscape (Figure 3.1). The remaining landscape terrain data, with SD(slope) values less than 2.25°, was then analyzed to identify areas encompassing entire watersheds for further consideration. Twelve new minimally eroded reference watersheds were identified and delineated within the public lands of the CCZO, totaling ~38ha out of a total 11,700ha analyzed. Reference watersheds are comparable with the randomly delineated watersheds in median elevation (156.7m SD±7m for reference, 148.0m SD±10.2m for randomly delineated) and median slope (Figure 3.2a). The MRTA-identified reference watersheds were smaller in area (average 2.9ha SD±2ha) but not significantly smaller compared to the randomly delineated watersheds (4.5ha SD±3.2ha).

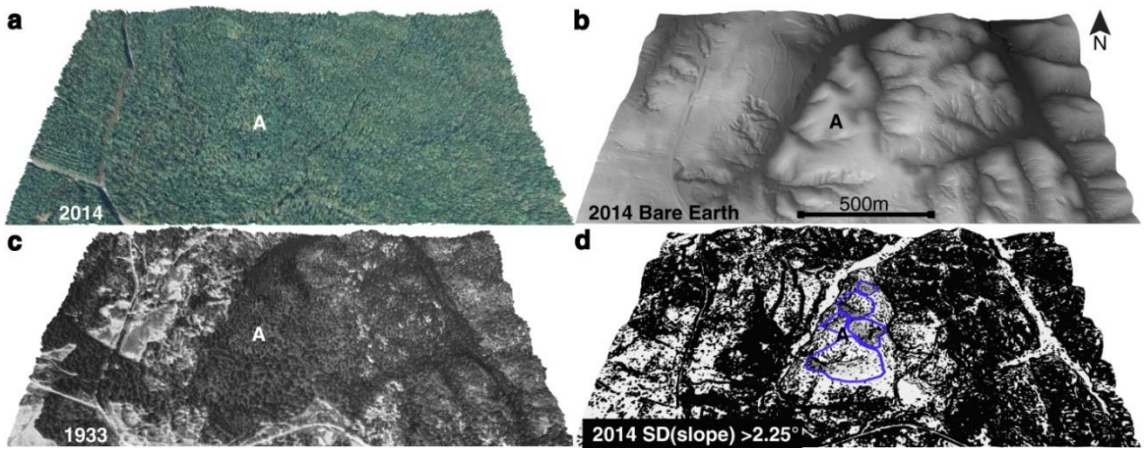

Figure 3.2: a) CCZO research area 8 identified at the CCZO via microtopographic roughness analysis: a) 2014 LiDAR canopy height terrain surface colored with National Agricultural Imagery Program (NAIP) landcover data, b) 2014 bare earth LiDAR terrain surface with elevation ranging from ~120-160m, c) 1933 aerial imagery terrain surface, d) standard deviation of slope at 1m2 resolution within a 7X7 window. 2014 SD(slope) >2.25° is black and SD(slope) <2.25° is white. A cluster of minimally impacted reference watersheds (A) are outlined in blue, with dense forest landcover in 1933, surrounded by rough gullied terrain visible in the bare earth surface and dark black areas in the SD(slope) panel. This is linked to historic agriculture and reduced soil-protecting vegetative cover in the past. These surrounding areas are now blanketed by mixed community forest cover dominated by loblolly pine, with increased microtopographic terrain roughness linked to LULC histories and a legacy of anthropogenic erosion.

3.3.2 Landcover analyses of reverence vs. random watersheds

Landcover analyses showed that MTRA-identified reference watersheds had significantly lower aerial image brightness in 1933 than randomly delineated watersheds (Figure 3.2c, Figure 3.3b), clearly demonstrating that reference watersheds had higher density and more intact deciduous tree canopies nearly 85 years in the past (W=52, $p < 0.05$). Considering that these deciduous stands would have likely been many decades old, this strongly suggests much more limited agricultural impacts based on history of

vegetation cover. Today, the average age of the reference hardwood stands is 108.5 years (n= 71 trees cored at breast height) while non-reference trees average 72.8 years (n=211 trees cored) (t= 6.73, df=89.39, p = 7.9e-10). Moreover, contemporary mean 2014 canopy height (W=299, $p < 0.05$) and mean 2015 winter redness values (W=328, $p < 0.05$) are both significantly higher for reference watersheds than the randomly delineated watersheds, indicating predominate deciduous hardwood cover over reference watersheds, with older and taller trees (Figure 3.3 c & d).

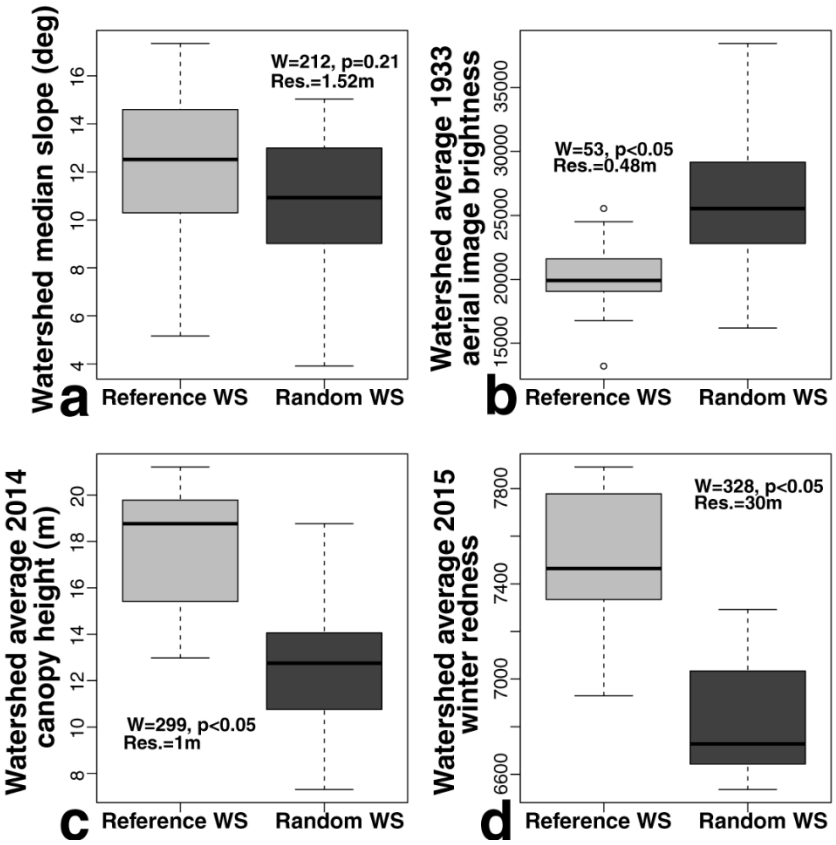

Figure 3.3: boxplots and Wilcox-tests of reference (n=13) vs. random watershed (n=26) comparison: a) median watershed slope, b) mean watershed 1933 image brightness (vegetation is dark, bare earth is bright), c) mean watershed 2014 canopy height, and d) mean watershed 2015 winter redness.

Plotted together, average canopy brightness of watersheds in 1933 aerial imagery and 2015 winter redness data show some overlap between MTRA-identified reference and randomly delineated watersheds as forest cover and human activity both vary in their nature and intensity (Figure 3.4). Nonetheless, there are statistically significant and readily interpretable differences between the historic and contemporary land covers of the reference watersheds and the randomly delineated watersheds representative of the broader Piedmont (Figure 3.4).

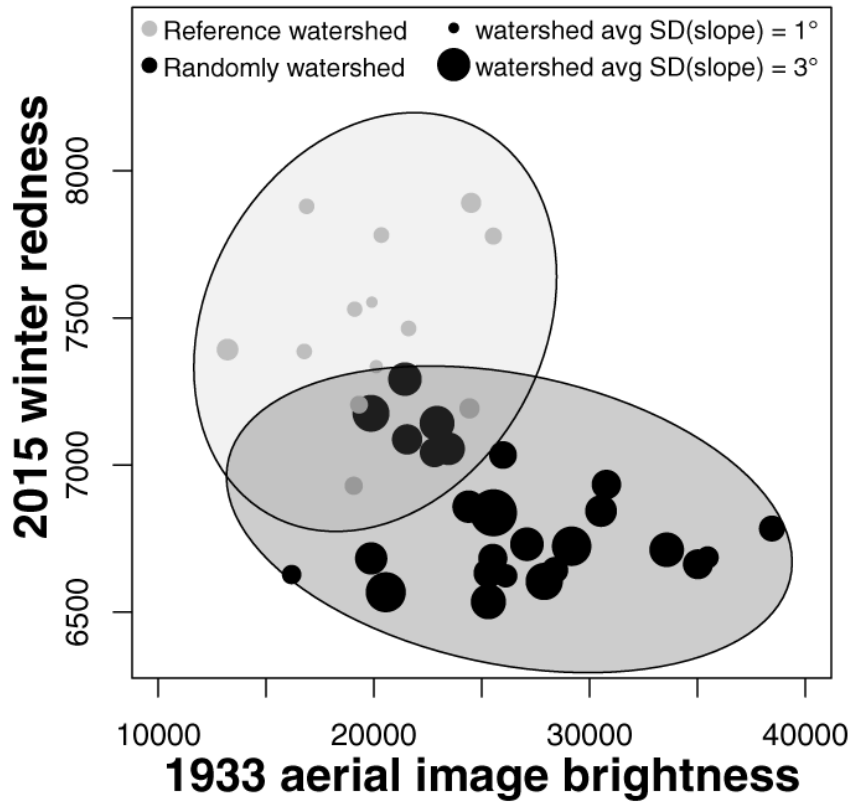

Figure 3.4: scatter plot of watershed average 1933 aerial imagery brightness and 2015 winter redness from Landsat TM8 with watershed points scaled to their 1.52m SD(slope) values with 95%CI ellipses for combined 1933 and 2015 landcover variables.

3.3.3 MTRA sensitivity to terrain raster resolution

MTRA DEM sensitivity analysis results indicate that both 1.52m and 5m resolution average watershed MTRA values are significantly different between reference vs. random watersheds (Figure 3.5). We attribute the ~1° decrease in SD(slope) when resolution drops from 1m to 1.5m to the 1.5m data losing smaller terrain irregularities. Additionally, even though the 1.52m resolution focal widow covers a similar spatial area, it has fewer raster cell data points (25 cells for 5x5 analysis) and so variation within the window is less than the 1m resolution MTRA results generated from the 49 cells for 7x7 analysis. This pattern repeats again with still lower SD(slope) values at 5m resolution, where reference watershed SD(slope) values are generally similar to randomly delineated watersheds (Figure 3.5). We attribute this pattern to reduced ability to capture features such as rills and gullies at 5m resolution. At 10m resolution, watershed-average SD(slope) values increased, likely due to the increasingly large area of the window (30m x 30m) that may capture larger-scale topographic changes in slope. These include transitions from hilltops, to nose slopes, to toe slopes, to valley bottoms and back uphill again in areas with many relatively small first-order interfluves and drainages (Brecheisen, Richter et al. 2018). These larger-scale terrain roughness patterns appear to be disconnected from erosive land use history, as reference watersheds were indistinguishable from random watersheds in the 10m resolution analysis (W=150,

p=0.59) (Figure 3.5). This indicates that microtopographic rill and gully terrain features are lost at this relatively coarse level of DEM resolution (James, Watson et al. 2007).

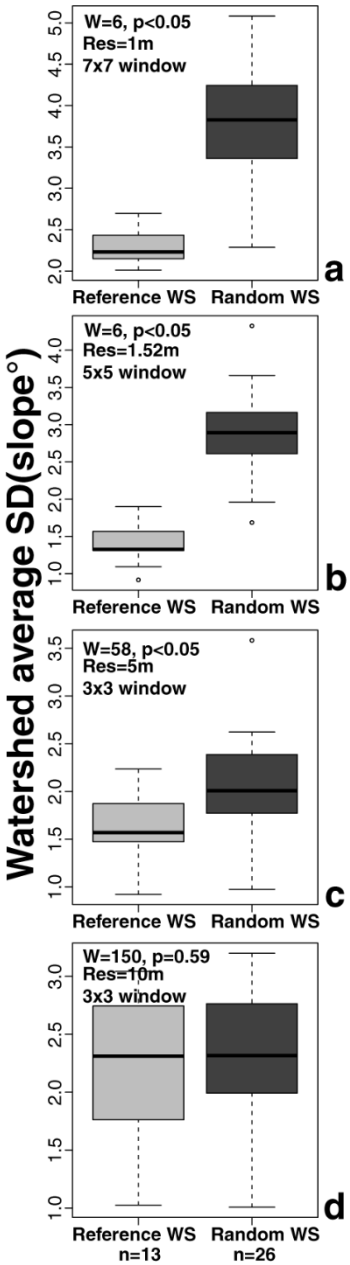

Figure 3.5: sensitivity analysis of reference watersheds vs. randomly delineated watersheds from: a) 2014 1m DEM, b) 1.52m 2008 DEM, c) 2014 5m DEM, and d) 2014 10m DEM comparing watershed-averaged SD(slope) values.

3.4 Discussion

Microtopographic Roughness Analysis (MTRA) conducted via meter-scale measurements of slope variability is sensitive to erosional and other disturbance characteristics left behind by historic land uses in the geomorphic surfaces of hillslopes. Reference watersheds and their hillslopes identified by MTRA not only had minimal anthropogenic disturbance, but also had Gaussian diffusion-mediated characteristic slope and local SD(slope) distributions (Figure 3.1). These smooth hilltops transition to slopes such that the shift from diffusive to advective flow paths near the base of hills is clear as flows accumulate into valleys (Dietrich, Wilson et al. 1992, Fernandes and Dietrich 1997). The majority of the CCZO landscape, however, was subjected to erosion-enhancing agricultural practices that concentrated water flowing off of fields and gullies cut towards the tops of hills in many places (Metz 1958, Montgomery and Dietrich 1992, Coughlan, Nelson et al. 2017). This resulted in a fundamental shift in microtopography, no longer Gaussian in the distribution of slope or local SD(slope) values, instead being strongly right-skewed, with a greater abundance of local terrain slope variability due to gully and rill erosion and other anthropogenic structures (Figures 3.1 and 3.2). There is a great potential to understand what magnitude of human impacts are required to shift previously stable hillslopes and hilltops by accelerated erosion and what timescales are required to regenerate Gaussian microtopographic structure. We suggest the surface of this landscape will remain altered for many centuries, possibly millennia.

The range and magnitude of SD(slope) values characteristic of minimal or highly impacted terrain in other landscapes will vary according to the intensity of human disturbance, the nature and distribution of the original terrain surface, and DEM resolution. Nonetheless, it can be readily calibrated using hillslope or watershed terrain training data or adjusted iteratively in exploratory MTRA. Further, MTRA DEM sensitivity analyses highlight the great utility of high resolution digital elevation data to characterize and quantify anthropogenic disturbance across large areas. Remarkably, 1m resolution MTRA analysis was best able to differentiate reference watersheds from random watersheds and resolutions of 5m or higher would likely be too low to have identified such watersheds *a priori*.

While historic erosion, 1933 canopy cover characteristics, current forest phenology and canopy height, and hardwood stand age all fall along a continuum from more to less impacted by human alteration, some areas fall far toward the minimally-impacted end of the metrics analyzed. The oldest reference hardwood trees date from the 18th and 19th centuries, with the average age being ~110yrs. Such reference forests and watersheds are incredibly rare across the Southern Piedmont of the USA. They occupy only ~0.3% of the public-owned CCZO landscape and are of high scientific and aesthetic value. The discovery of sites such as these and the broader characterization of human impact legacies in microtopography is valuable for study and conservation in the fields of environmental archeology (Hightower, Butterfield et al. 2014), geomorphology

(James, Watson et al. 2007), ecology (Barbosa, Melendez-Pastor et al. 2014), pedology (Dialynas, Bastola et al. 2016), and other critical zone sciences (Brecheisen, Richter et al. 2018) around the world.

4. Development and deployment of a field-portable O_2 and CO_2 gas analyzer and sampler

4.1 Introduction

Measurement of soil CO_2 fluxes from soil surfaces and, to a lesser extent, concentrations within soil profiles have been utilized for many years and the tools and methodologies for their measurement include field-based manual sampling and monitoring, to laboratory analyses, to real-time data-logging capabilities (Davidson and Trumbore 1995, Hall, McDowell et al. 2012, Hasenmueller, Jin et al. 2015, Richter and Billings 2015, Brantley, DiBiase et al. 2016). We are, however, beginning to recognize a great deficit in our understanding of soil respiration when only CO_2 is monitored and not O_2 as CO_2 is much more soluble in water than O_2, yet both gasses can be transported into and out of systems via groundwater and gas diffusion (Mayorga, Aufdenkampe et al. 2005, Johnson, Lehmann et al. 2008, Angert, Yakir et al. 2015). CO_2 further undergoes a series of equilibrium reactions that enhances its potential for storage and reactive transport in soil water (Brantley, Lebedeva et al. 2014, Angert, Yakir et al. 2015, Hasenmueller, Jin et al. 2015, Kim, Stinchcomb et al. 2017). Oxygen measurements are done infrequently in soil monitoring setups, except in the case where O_2 measurement probes are buried in the soil (Silver, Lugo et al. 1999, Liptzin, Silver et al. 2010, Hall, McDowell et al. 2012, Angert, Yakir et al. 2015). While there are products on the market targeted for portable field use that measure both CO_2 and O_2 via aspirated flow-through analysis, they are prohibitively expensive for many researchers, are often very heavy

precluding remote field use in excess of 15kg, and do not include an internal battery which may add an additional 10kg or more. Existing products infrequently offer the ability to collect of gas samples in the field for laboratory analyses. The field-portable gas sampler and analyzer (FPGA) platform described herein is less than 10kg including internal battery power, allows for sample collection, and can be constructed from materials totaling less than two thousand USD.

4.2 Materials & methods

4.2.1 Design and construction of the FPGA

The FPGA platform integrates several off-the-shelf components to form a robust and reliable system for field deployment inside a Pelican™ Model 1400 case (Figure 4.1). At the core are three products around which everything else operates: a Cole Parmer Air-Cadet™ vacuum-pressure pump (model EW-07532-25), Vaisala GMP 221 CO_2 probe with GMM220 transmitter module, and an Apogee MO220 O_2 meter (Figure 4.2). The Apogee MO220 meter can be ordered with a flow-through head directly, but a flow-through adapter must be ordered from Vaisala or manufactured by the user. Both approaches have worked well in our applications. A generic 7ah 12V battery is used to power the Cole-Parmer pump and Vaisala probe, each with dedicated power control switches and is generally able to last for a full day of sampling more than 50 gas wells (Figure 4.3) with a fully charged battery. The Apogee oxygen meter and digital voltmeter have internal battery power.

Figure 4.1: Frontal view of FPGA closed and ready for transport.

Masterflex™ Platinum Tubing (L/S® 24) is used for all connections inside the FPGA due to its tolerance for repeated long-duration bending and flexing without forming kinks. Water traps have been fashioned from a variety of vessels and should be configured such that inflow enters the bottom of the trap and outflow occurs towards the top. A water trap with a volume of 250ml or greater has been sufficient to give users ample warning and time to turn off the pump in the event that flooded or saturated soil conditions are encountered and water is pumped into the system out of the ground. A vacuum gauge with a range of -100 to 0 kPa should be used so that in the event of a clogged, kinked, or flooded input line, the user will be alerted to vacuum pressures dropping below -20kPa and can shut off power to the pump to avoid stress or damage to the pump and avoid overfilling the water trap if soils are saturated with water.

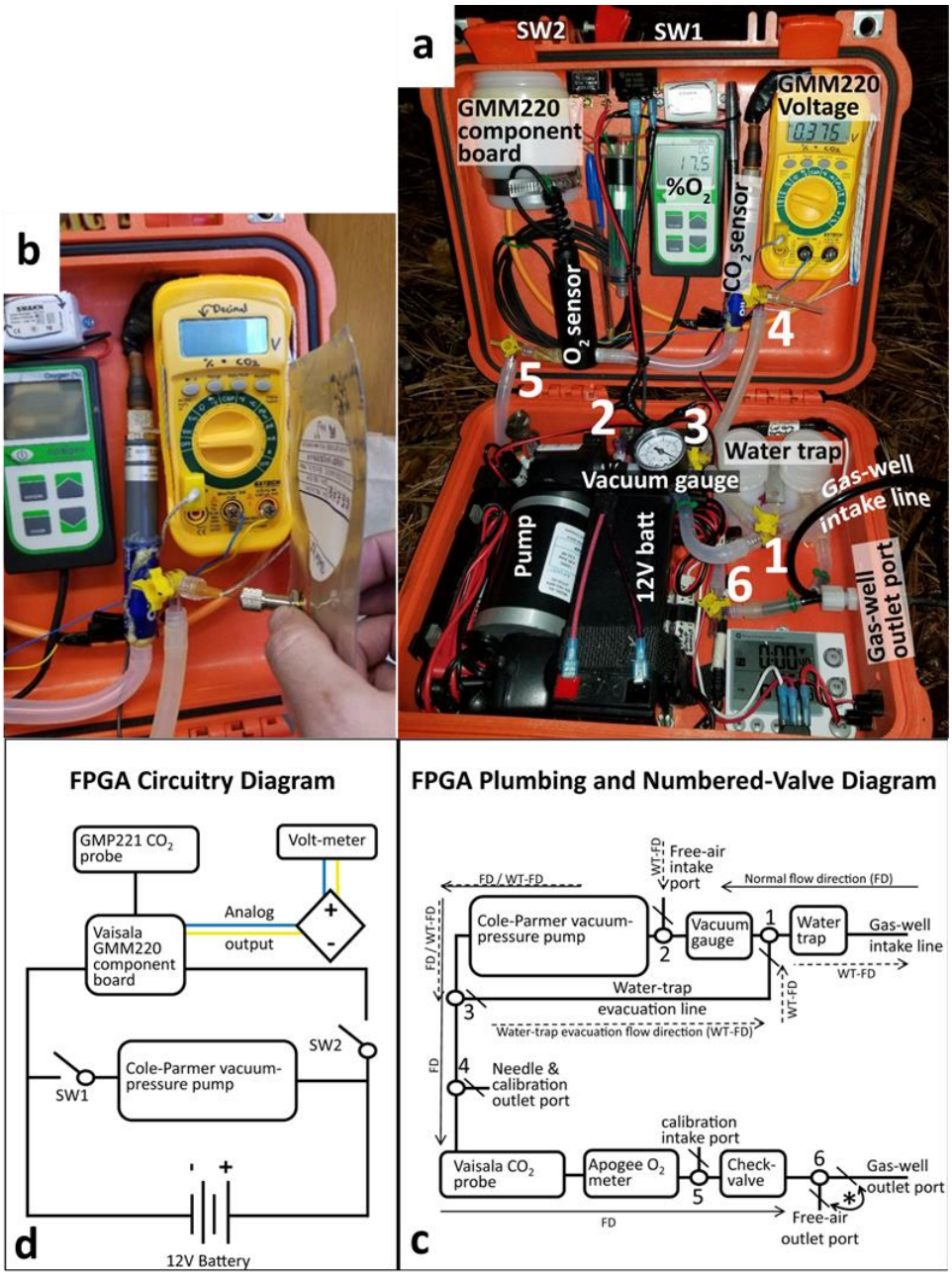

Figure 4.2: a) annotated FPGA components as seen during field deployment b) closeup view of hypodermic needle used to fill gas sample collection bags, c) plumbing diagram of the FPGA indicating flow directions through different components of the FPGA for regular use as well as water-trap evacuation. Numbered 3-way valves with "\" symbology indicate the closed line during normal use. d) Circuitry wiring diagram for the FPGA. See Appendix B for itemized parts list.

Upon flowing through and past the Vaisala and Apogee meters, gas passes through a 1-way check-valve to ensure that no backward flow or diffusion of aboveground air is possible during the flushing stage of analysis and sampling. Numbered 3-way valves are used to direct and control air flow pathways as necessary for flow-through gas analysis, circulating gas analysis, and sample collection via hypodermic 26ga needle. It is also possible to reverse the flow direction of pumped air in order to empty the water trap if water is drawn in during use (Figure 4.2b). A short segment of 6.35mm outer diameter bev-a-line™ tubing is inserted into the end of the Masterflex™ tubing after valve 6 and connected to a Jaco 6.35mm inner-diameter nylon bulk-head junction for connection to the gas-well outlet port. Though the particular design and installation of buried soil gas wells or other sampling points does not directly influence the design of the FPGA, we have found that 750ml volume PVC chambers open on the bottom and buried vertically in the soil with bev-a-line™ tubing entering from the top and running to the soil surface in a closed loop with plastic Jaco 6.35mm inner-diameter nylon union fittings function very well with this setup (Figure 4.3).

4.2.2 FPGA field deployment

Four FPGA's (Figure 4.1) have been constructed over the last 3 years and have been used to monitor soil O_2 and CO_2 dynamics in the Southern Piedmont of the US as well as the eastern foothills of the Pfälzerwald mountains located in southwestern

Germany. Most measurements are confined to the upper 5m of soil (Figure 4.3), though extend down to 8.5m in two US plot locations and further to 10m in one plot location in Germany which have been sampled successfully during periods when the groundwater table was below those depths. Gasses are sampled and analyzed from buried PVC soil gas wells with bev-a-line™ tubing running to the soil surface and connected to the FPGA using Jaco nylon unions (Figure 4.3). This procedure has worked well in a variety of remote field settings including agricultural fields, managed timber pine forests, natural hardwood forests, and vineyards.

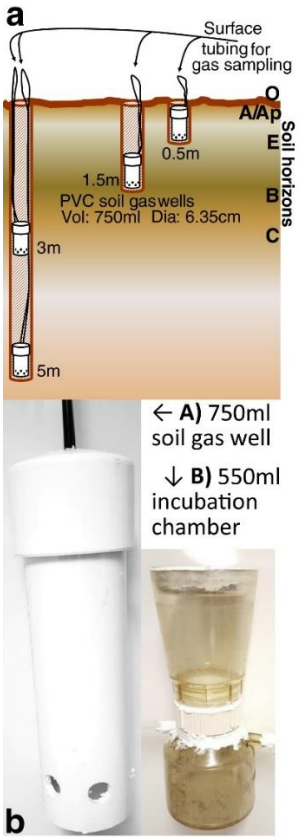

Figure 4.3: a) Field installation diagram of soil gas wells and b) PVC-constructed gas well (left) and soil incubation chamber (right).

Oxygen, carbon dioxide, and optional aboveground atmospheric temperature data are recorded manually using field notebooks and datasheets in the current FPGA platform and entered into spreadsheets upon return from the field. Field measurements of O_2 and CO_2 made by:

1) powering on the CO_2 and O_2 meters (switch 2) and running the pump (switch 1) for 30-45 seconds with nothing attached to the FPGA intake and outflow ports. This is done to calibrate the Apogee oxygen meter to ambient atmospheric conditions taken to be 20.95% O_2 (Figure 4.2a, 4.2c, 4.2d). Vaisala recommends a 1-minute warm-up period for the CO_2 sensor to stabilize. The CO_2 probe should return an analog voltage signal read via a voltmeter (Figure 4.2a, 4.2b, 4.2d) translating to approximately 0.04% CO_2. Exact analog voltage signals reported by the GMM220 series component board vary depending on the configuration ordered from Vaisala. Specific voltage multipliers (e.g. if 1V=2% CO_2, $\%CO_2=2*V_{analog}$) may be required depending on requested specifications. A direct 1V=1% CO_2 or 0.1V=1%CO_2 is a convenient configuration for data collection.

2) Connect the gas reservoir lines to the intake and outflow ports.

3) Flush the FPGA system with 1L or more of soil gas (~45 seconds) to saturate the entire system volume with soil atmosphere having valve 6 closed towards the gas-well outlet port and open to the free-air outlet port (Figure 4.2a, 4.2d).

4) Optionally collect a sample for laboratory analysis by turning valve 4 to needle outflow (valve 4 "off" should be pointing towards the CO_2 probe line) (Figure 4.2a, 4.2b, 4.2c).

5_1*) for non-circulating gas measurement, turn off power to the pump using switch 1 (Figure 4.2a, 4.2d) and record the maximum concentration value observed for both CO_2 and O_2 within 1 minute. There is a protective PTFE sleeve inside the outer shell of the GMP221 CO_2 probes which protects and shields the NDIR sensor, but it also slightly delays equilibration of pumped soil gas after flushing the system. Because of this, it is typical to observe a gradual increase in reported CO_2 concentration to a peak typically followed by a gradual decline in CO_2 concentration. This pattern assumes gas well sampling progresses from soils with lower CO_2 concentrations (e.g. shallow soil depth) to higher CO_2 concentrations (e.g. deeper soil depths).

5_2*) If it is necessary to evacuate a smaller volume of gas from the soil gas reservoir and surrounding soil volume (Figure 4.3a, 4.3b), the user may limit step 2 to flushing the system for a shorter period of time (at least 10 seconds is necessary to flush the water trap, pump, tubing, and probe volumes) and then close valve 6 towards the free-air outlet port and opening it towards the gas-well outlet port for circulatory gas analysis. We have observed an apparent dilution effect of up to 0.1-0.2% CO_2 decrease using this gas circulating methodology and so prefer the 5_1* procedure. Procedure 5_2* is

often necessary, however, when sampling low diffusivity saprolite or soils with high clay content when partially saturated with water.

6) Proceed to measuring/sampling the next gas well in the plot. It is not necessary to recalibrate the O_2 meter after every gas well measurement, but it should be recalibrated after every ~5th soil gas measurement. It is not necessary to flush the system with atmospheric air after each gas well measurement unless the user is using a very brief flushing period as in circulating analysis in *5[2], in which case it is advisable to flush with aboveground atmospheric air between samples to ensure there is no well-to-well measurement bias. An example of this would be if a gas well with high CO_2 (e.g. >5%) was measured immediately before a gas well with low CO_2 concentration (e.g. <0.5%). After the final measurement and sampling is complete at a site, and if the time until the next measurement will be taken is more than 10 minutes, it is recommended to turn off power to the Vaisala GMM220 (switch 2) until the next sampling as it will draw down battery power considerably if left turned on consistently.

In addition to on-site field gas analysis, the FPGA can collect samples in the field for laboratory gas chromatography analyses of gasses such as methane, nitrous oxide, and others as well as bench-top isotopic analyses (Figure 4.2b, 4.2c). This is accomplished with inflatable sample bags made of foil and plastic material or Tdelar™ with 100ml or more sample volume which have a septum punctured and inflated using a 26-gauge hypodermic needle on valve 4. For analyses or schedules requiring samples

to be stored for periods longer than a few days, it is recommended to transfer gas samples from sample bags into evacuated glass vials using a closeable syringe to minimize potential diffusion of sampled gases through sample bags. FPGA's have further been developed for bench-top laboratory applications for soil incubation experimental analyses targeting aerobic respiration rates (Figure 4.3b) using small circulating hand pumps widely available such as those offered by Mityvac™. Incubation experiments have been conducted on soils simulating terra-formation studies with Deep Space Ecology LLC as well as sediment carbon quality incubation experiments in the Duke University Wetland Center. FPGA measurements of soil gas concentration data from forests and agricultural fields as well as data generated from gas samples collected and analyzed for isotopes of ^{18}O in CO_2 and O_2 as well as ^{13}C and ^{14}C in CO_2 at the Calhoun CZO are in two manuscripts currently under review (Billings, Hirmas et al. 2018, Cherkinsky, Brecheisen et al. 2018).

4.2.3 Measurement validation, data plotting, and calculation of Apparent Respiratory Quotient (ARQ)

Data analysis and plotting outlined herein was conducted using R statistical software (R Core Team 2016) and the fields package (Nychka, Furrer et al. 2016). Comparison and data quality analyses were conducted via the collection of field samples for every belowground soil CO_2 measurement conducted over more than 2 years of analysis via laboratory GC analyses. Agreement between field CO_2 measurements and laboratory GC CO_2 measurements was accomplished via linear

regression in R (R Core Team 2016) whereby a very high R^2, a slope approximately equal to 1, and an intercept of approximately 0 indicate equivalence between measurement techniques. Both O_2 and CO_2 measurement accuracy of the FPGA were periodically tested using standard gasses in the lab. One Apogee MO120 meter was replaced in early 2016 when it was discovered that standard gasses below 15% O_2 were consistently reported lower than their true value. Because periodic testing of the FPGA caught this problem quickly and O_2 measurements below 15% are infrequent, this is not believed to have significantly affected data measurements from this period.

Timeseries datasets of gas concentrations measured across multiple depths can be plotted and interpreted using heatmap plots (Johnson, Lehmann et al. 2008, Richter and Billings 2015). There are many ways to accomplish this in statistical or mathematical software environments, those presented here are generated using the "fields" package in R (Nychka, Furrer et al. 2016, R Core Team 2016) using the Krig function (covariance= "Matern", theta=10, smoothness=1) for kriging interpolation of the Z-axis gas concentration values which are colored in the heatmaps. The Krig object can be plotted for quality assurance that the interpolated values are in agreement with the original data. Soil sampling depth is plotted on the y-axis and date is plotted along the x-axis. Date was converted to a consecutive integer format and scaled to be of similar range to values in the y and z axes (~0-10) prior to kriging. After kriging, the surface plotting

function was used with type="C" in order to plot contour lines in addition to colored heatmap plotting.

While both O_2 and CO_2 timeseries concentration data are very valuable individually, they can be integrated through the calculation of the Apparent Respiratory Quotient (ARQ) which is calculated as the increase in soil CO_2 concentrations above ambient atmospheric conditions (0.04%) divided by the reduction in soil O_2 below ambient atmospheric conditions (20.95%) and then multiplied by a diffusivity coefficient (0.76) (Angert, Yakir et al. 2015). The equation is thus:

$$ARQ_{soil} = 0.76*(\Delta CO_2/\Delta O_2)$$

The soil ARQ will tend to equal approximately 1 assuming a carbohydrate substrate for autotrophic and heterotrophic respiration (Masiello, Gallagher et al. 2008) and also assuming no other biotic or abiotic sources or sinks for either O_2 or CO_2 in the ecosystem. Both of these assumptions are frequently violated (Angert, Yakir et al. 2015) which makes the ARQ a valuable tool for linking soil gas dynamics to soil organic matter quality, soil moisture and infiltrating precipitation, and the nature of weatherable redox-active soil minerals.

4.3 Results and discussion

4.3.1 FPGA platform validation

Four FPGAs have been deployed to date requiring less than $2,000 each in materials. They have proven to be practical for field use in rugged terrain. Over 1600 gas

samples were measured by FPGA and by gas chromatograph in the laboratory and a linear regression of the CO_2 estimated in lab and field has a slope of 1.017, an intercept of -0.033, and an R^2 of 0.956. The range of CO_2 concentrations in the regression were from 0.25 to 7.75% CO_2.

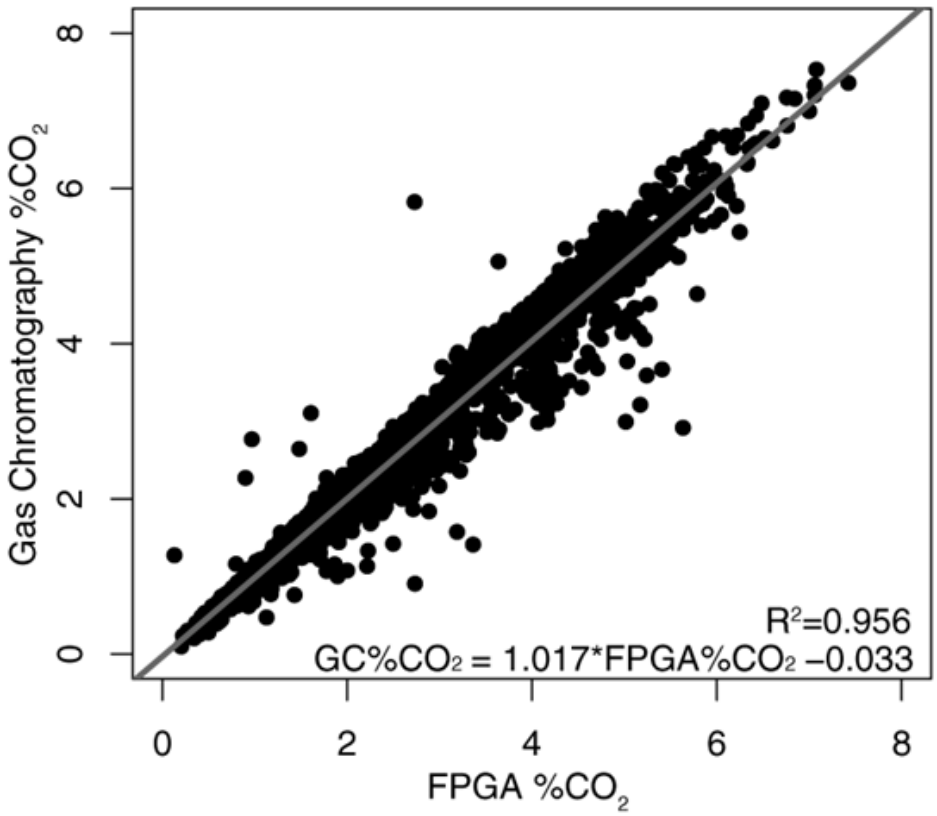

Figure 4.4: Carbon dioxide measurement comparison between FPGA and laboratory gas chromatography.

4.3.2 Temporal observations and ARQ

Plotted as a timeseries, seasonal dynamics of soil respiration are prominent under replicated hardwood forest soils in both the accumulation of CO_2 and the decline of O_2 during warmer spring and summer months with the pattern reversing in the fall

and winter (Figure 4.5). Apparent in the timeseries when plotted alongside publicly-available precipitation data is an apparent decline in soil CO_2 concentrations during high precipitation time periods which is not reflected by an increase in O_2. This deviation from a 1:1 tradeoff between the two gasses is presumably due to CO_2's greater solubility in water than O_2 and a subsequent series of chemical equilibrium reactions generating carbonic acid and bicarbonate (Mayorga, Aufdenkampe et al. 2005, Johnson, Lehmann et al. 2008, Angert, Yakir et al. 2015).

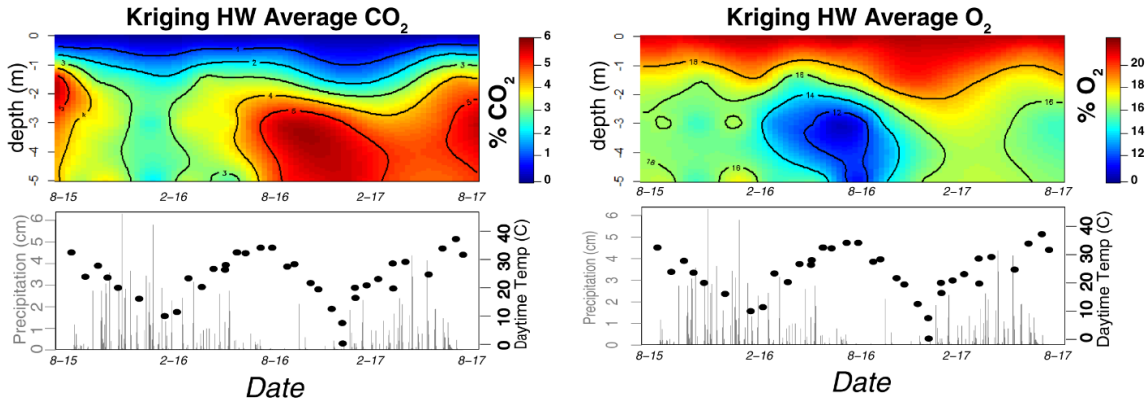

Figure 4.5: timeseries heatmap plotting of (top) FPGA-measured CO2 and O2 averaged across three replicate hardwood forests and (bottom) FPGA-measured aboveground temperature and NOAA precipitation. Precipitation data was generated at a local NOAA weather station in nearby Spartanburg, SC. Time is on the x-axis on all plots while redder colors indicate higher CO2 and O2 and bluer colors are lower for each. Black points correspond to mean daytime temperature during the course of sampling in the field and grey bars indicate total daily precipitation.

This deviation from the 1:1 gas ratio of CO_2 gain and O_2 loss can be quantified through the calculation of the ARQ which is used to color points in a scatterplot of observed CO_2 and O_2 data in Figure 4.6. This suggests that the FPGA has high potential to enhance field observations and monitoring of the consumption, production, and

transport of metabolic gasses. Because ARQ is a function of the deviation of measured soil atmosphere from ambient aboveground atmospheric concentrations of O_2=20.95% and CO_2=0.04%, ARQ calculations from gasses which are very close to ambient concentration in either CO_2 or O_2 can be easily skewed by small inaccuracies. A measurement error of ±0.1% CO_2 is proportionately much greater if the true concentration is 1.1% as compared to 5.1%. Because of this and for illustrative purposes, the plotted ARQ values in Figure 4.6 are plotted with ARQ values below the 2.5nd quartile and above the 97.5th quartile omitted.

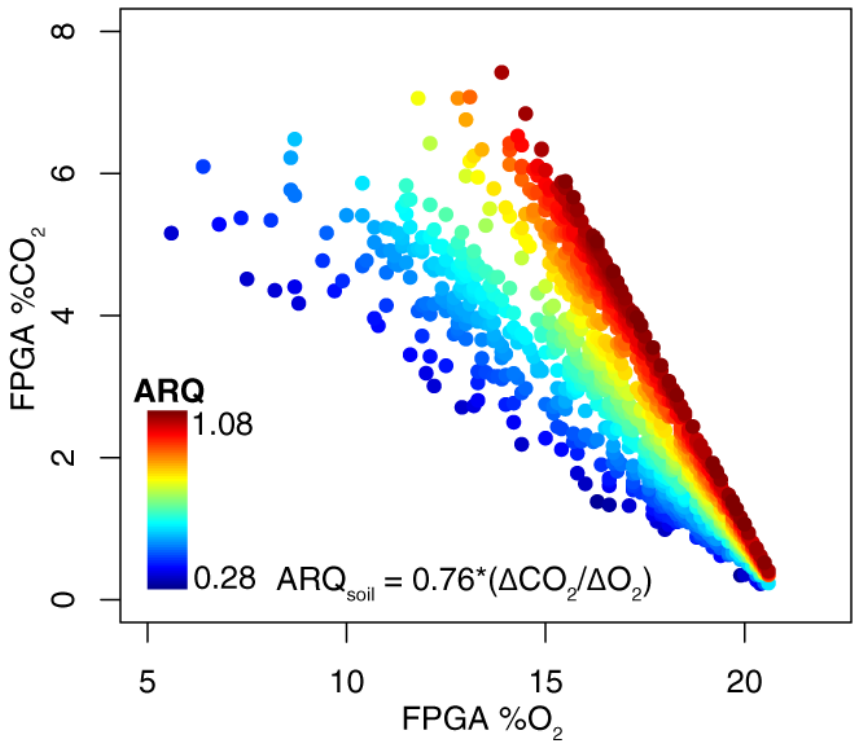

Figure 4.6: Scatterplot of FPGA-measured CO2 and O2 colored according to their Apparent Respiratory Quotient values. ARQ values indicate that the apparent consumption of O_2 is not always balanced 1:1 by observed CO_2 concentrations in soil

profiles. This indicates significant (a)biotic interactions for either or both of these gasses are present in the systems being monitored.

4.3.3 Potential for innovation, improvement, and future development of FPGA platform

While current FPGAs are robust and function reliably in their operation, they are unrefined in their use of separate screens for monitoring and data collection of O_2 and CO_2 data. Further, the use of a voltmeter for the monitoring of CO_2 analog data and data collection via manual writing of data measurements indicate a need for electronic data recording. We are currently developing means to directly interface CO_2 and O_2 probes with Raspberry pi™ microcomputers and touchscreen graphical user interface for on-demand recalibration and operation of the FPGA platform as well as automatic calculation of soil ARQ and data export to .csv file. An additional area of development is the configuration of the FPGA for use in measuring CO_2 fluxes from the soil surface. We are also committed to enhancing the expansibility and modularity of the FPGA platform and receiving feedback from the scientific community on how we can further develop and enhance the utility of these devices into the future.

5. Beneath a blanket of green: shallow and deep legacies of landuse in old-field secondary forests

5.1 Introduction

5.1.1 Overview of Southeastern Piedmont landuse history

This investigation seeks to quantify the below-ground effects of ~80 years of old-field succession at the Calhoun Critical Zone Observatory (CCZO) (Figure 5.1). The Calhoun Critical Zone Observatory (CCZO) is located in the Sumter National Forest in South Carolina, a region with deep and highly weathered Ultisol soils millions of years old (Bacon, Richter et al. 2012). It lies in one of the most highly degraded and impoverished regions of the US with the Southeastern Piedmont soils having lost much of their surface horizons to 200+ years of erosive ante- and post-bellum plantation agriculture (Richter and Markewitz 2001, Coughlan, Nelson et al. 2017). Hardwood forests were cleared from nearly all arable land, even expanding into marginal areas (Hansen 1991, Richter and Markewitz 2001). Farmers and workers expanded cultivation onto steeper slopes as fields eroded and lost fertility in the face of repeated plowing. This resulted in the destruction and alteration of many physical structural soil characteristics including the loss of macropores (soil pores >0.075mm dia.) (Schaetzl and Anderson 2005, Luo, Lin et al. 2010), reduced soil aggregate stability and enhanced erosivity in a region with high precipitation (Krishnaswamy and Richter 2002, Bin and Xin-Hua 2006, Duchicela, Sullivan et al. 2013, Devine, Markewitz et al. 2014), and

general soil compaction resulting in increased soil bulk density (Richter and Markewitz 2001, Krishnaswamy and Richter 2002, Strickland, Callaham et al. 2010).

Greatly accelerated erosion across the Southeastern Piedmont (Hansen 1991, Trimble 2008) forced debt-ridden farmers to sell their lands to the US Forest Service which was then establishing the Sumter National Forest in northern South Carolina. With the collapse of plantation agriculture, reforestation spread across the Sumter National Forest and, more generally, across the entire Southern Piedmont region of the United States. Planted and naturally-seeded forests dominated by loblolly pine (*Pinus taeda*) reclaimed the landscape. Many of these secondary forests are now on the order of 60-80 years old having reduced the rate of gross soil erosion (Richter and Markewitz 2001). Different measurements within the soil environment are explored to quantify the vertical propagation of forest regeneration fronts downward into soil profiles.

The soil profiles across landuse history replicates are of the Ultisol order with well-developed Bt-horizons enriched in clay content in upland environments (Figure 5.2). Soil texture (Figure 5.2) plotted from published data at the CCZO (Heine 2018) indicate greatest depth to maximum clay content under hardwood forest and the shallowest depth to peak clay content under cultivated agricultural fields with old-field pine forests being intermediate. This is presumably due to greater vertical topsoil erosion under the persistently cultivated field complex and a legacy of erosion in old-field pine forests.

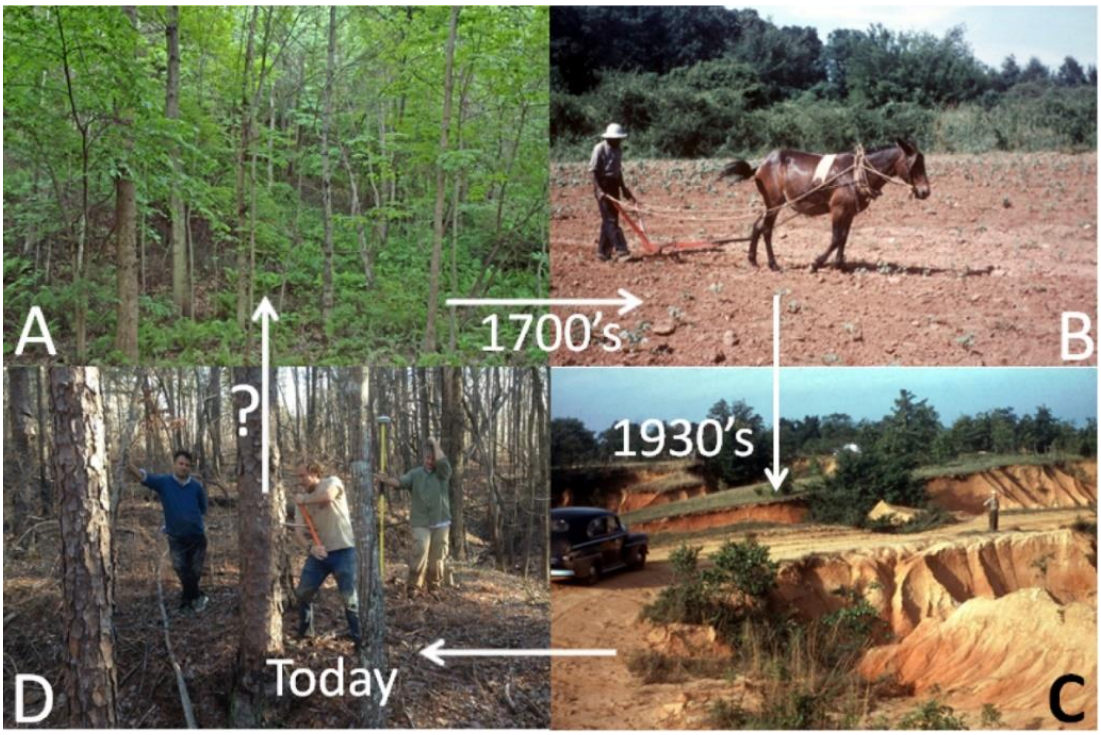

Figure 5.1: Overview of landuse and landcover transitions in the SE US A) pre-European contact hardwood (HW) forests which were converted to B) plowed agricultural plantations (CF) which were C) severely eroded before being D) abandoned and re-colonized by Loblolly Pine forests (OF).

5.1.2 Reference hardwood vs. old-field forest vegetation comparison

Old-field secondary forests are considered to be in a transition-stage with tall mature loblolly pine (*P. taeda*) forming the emergent canopy with an incipient hardwood understory developing (Figure 5.2) (Peet and Christensen 1980, Xi and Peet 2011, Christensen 2014). Reference hardwood forests, despite having had minimal anthropogenic erosive impacts as discussed in chapter 3, were not free of human landuse. These areas were frequently grazed and selectively logged for timber and firewood (Richter and Markewitz 2001). Nonetheless, the trees in these reference

hardwood forests are frequently over 100 years in age and are considered to be approaching a steady-state condition. Aboveground vegetation comparisons made between the two forest types include: stem density, basal area (BA), above ground biomass (AGB), and leaf-area index (LAI).

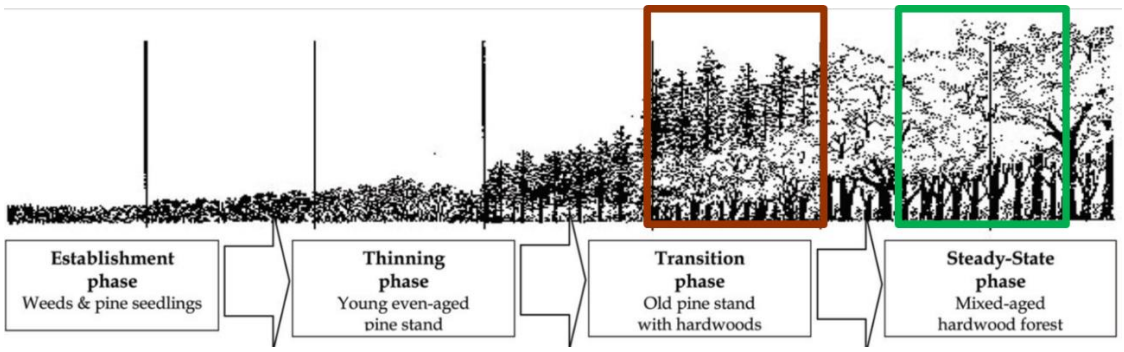

Figure 5.2: Old-field successionary progression diagram, adapted from Xi and Peet (2011). Approximate stages of old-field and reference hardwood treatments in this experimental design are indicated by the brown and green boxes respectively.

5.1.3 Ultisol soil profile description

Aerial photography indicates consistent plowed agricultural management in the CF agricultural field complex to at least the 1930's (Brecheisen, Cook et al. 2015) and likely for many decades or even centuries further into the past (Richter and Markewitz 2001, Coughlan, Nelson et al. 2017). Old-field pine forest plot locations are either under plowed agricultural management in 1930 or were very recently abandoned. Soil profiles are otherwise generally characterized as being coarse in texture near the surface A- and E-horizons. Depending on the magnitude of historic erosion, E and even A horizons may be absent. Texture is finer with soil permeability decreasing in the B-horizon and frequent perching of water on top B-horizon soils. Texture then becomes coarser again

with silt and then sand content increasing transitioning into the coarse C-horizon which remains unsaturated above the true groundwater table.

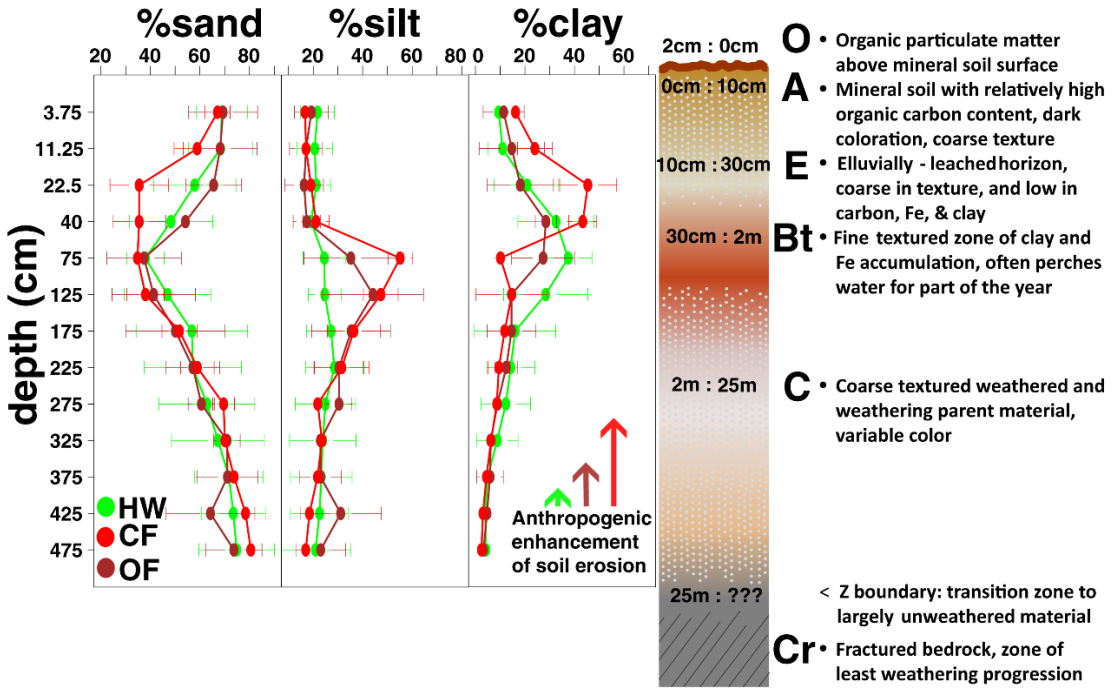

Figure 5.3: Left - observed soil profile textural characteristics for each of the three landuse history comparisons. HW corresponds to reference hardwood forest, CF corresponds to cultivated agricultural fields, and OF are old-field secondary pine forests. Right - Ultisol soil profile diagram and description.

5.1.4 Hypotheses regarding above- and belowground regeneration through old-field succession

Following agricultural abandonment, bare agricultural fields were reclaimed by increasingly woody vegetation progressing from grasses, forbs, and shrubs to dense pine sampling thickets which then self-thinned and have now matured to mixed pine-hardwood communities (Figure 5.2). It is hypothesized that stem density >6″ diameter at

breast height (DBH) and BA per unit area may remain higher in the old-field treatment than the reference hardwood condition as the process of self-thinning and selection for shade-tolerant trees is still underway in old-field forests, but should be greatly advanced in hardwood-dominant communities (Billings 1938). Reciprocally, AGB has been shown to be highly concentrated in large mature individual trees in some forest ecosystems (Slik, Paoli et al. 2013) and so AGB is expected to be higher in reference hardwood forests than in old-field forests. Lastly, LAI is hypothesized to be similar between the two forest types as both vegetative communities work to optimize their photosynthetic surface area. A review of temperate deciduous broadleaf and needle-leaf forests supports this notion with mean LAI's of $5.1m^2/m^2$ (±1.6) and $5.5m^2/m^2$ (±3.4) respectively (Asner, Scurlock et al. 2003). The concept of LAI regeneration at the CCZO has been framed as a "green blanket" which has perhaps masked enduring legacies of belowground agricultural degradation in the soil.

Soil biota and regenerating root networks in old-field forest soil ecosystems work to aerate soils and facilitate the movement of fluids into and out of soil (Krishnaswamy and Richter 2002, Callaham, Richter et al. 2006, Devine, Markewitz et al. 2014). The activity of regenerating roots and root-turnover serve to regenerate soil structure whereby roots and associated mycorrhizal hyphae grow and expand into and new soil volumes, opening soil pore spaces, then senesce and decompose leaving unoccupied soil pores and soil organic matter residues which promote soil cohesion and stability

(Krishnaswamy and Richter 2002, Bin and Xin-Hua 2006, Jackson 2010, Archer, Otten et al. 2016). As reforestation and old-field succession progresses, soil aggregate stability and the soil's resistance to slaking and erosion should increase. Root abundance and macroporosity should also increase driving a reduction in soil bulk density as micro-, meso-, and macropores are regenerated. Lastly, soil respiration in the production of CO_2 and consumption of O_2 should be enhanced where biota, including roots, are able to colonize more deeply into the soil environment (Richter and Billings 2015, Billings, Hirmas et al. 2018, Cherkinsky, Brecheisen et al. 2018).

5.1.5 Quantifying regeneration

In areas where perennially-rooted vegetation has been removed and soils were plowed consistently for decades, soil macropores and the root networks that form and occupy them can take decades or longer to regenerate if reforestation is allowed to progress, particularly deep in soil profiles (Billings 1938, Zimmermann and Elsenbeer 2008, Luo, Lin et al. 2010, Archer, Otten et al. 2016, Billings, Hirmas et al. 2018). Tracking the vertical propagation of rooting fronts into soils as secondary succession progresses is made difficult in two ways: a) root network reestablishment occurs slowly over decadal or centurial timescales (Billings 1938, Hoover 1950, Chazdon 2014, Sun, Dong et al. 2015, Billings, Hirmas et al. 2018) and b) direct measurement and quantification of highly spatially variable roots at depth is highly destructive and unlikely to accurately sample

the heterogenous rooting volume (Jose, Gillespie et al. 2001, Davey, Wigand et al. 2011, Maeght, Rewald et al. 2013, Fahey, Yanai et al. 2017).

The issue of the long temporal scale can be addressed using space-for-time substitution, i.e. a chronosequence design to study succession. The second issue is more difficult to address directly. While the surficial soil environment can be readily sampled and analyzed for structural and chemical characteristics, investigating the effects of old-field succession in deeper soils remains a challenge. Because of this, we present an approach using measurements of O_2 and CO_2 through time to quantify soil respiration at depth, driven by plant root and associated microbial activity, to enhance the study of ecological succession and deep rooting-network regeneration (Silver, Lugo et al. 1999, Liptzin, Silver et al. 2010, Rey, Pegoraro et al. 2011).

5.2 Methods

5.2.1 Chronosequence experimental design

In order to investigate the effects of 60-80 years of old-field succession in the SC Calhoun Critical Zone Observatory (CCZO) regarding soil biogeochemistry, chronosequence landuse history plots have been instrumented and studied. Chronosequence plots consist of n=3 reference hardwood forest (HW) plots, n=3 plowed agriculture (CF) plots, and n=3 old-field secondary pine forest (OF) plots for a total of 9 primary research plots. All of the reference hardwood forest and old-field secondary pine forest plot replicates are paired across research areas 1, 4, and 7 (Figure 1.2) such

that they are located within 200m of each other to minimize the effect of local landscape variability on observed soil properties allowing for direct comparison within replicates. Each of the paired forest replicates are >5km from one another in order to explore the consistency of observations across the broader CCZO landscape. In this framework, reference hardwood soil profiles are minimally impacted by historic agriculture in terms of soil structure and soil respiration while agricultural fields are maximally impacted. Old-field pine forests are expected to be intermediate in characteristics of soil structure and the dynamics of below ground respiration. The agricultural field treatment was pseudo-replicated three times within ~10ha field in the western portion of research area 1 (Figure 1.2). Because of this, linear mixed effect model analyses of soil gasses only consider the two forest treatments, reference hardwood forest (HW) and old-field forests (OF), though forest vs. cultivated field (CF) soil gas differences are explored graphically. Soil structural analyses were conducted via pairwise t-tests in R (R Core Team 2016) so that observed differences between all landuse treatments (HW, CF, and OF) can be easily evaluated and interpreted.

5.2.2 Forest vegetation data analyses

Each of the six soil gas-well forest plots were surveyed for woody vegetation with stems ≥6″ DBH within a 30m diameter area. Tree species were identified and their DBH and height were measured and recorded with forest vegetation survey data available for download and use (Cook, Brecheisen et al. 2018). The number of stems ≥6″

DBH and their basal area (BA) were calculated. Aboveground biomass was calculated using basal area and tree height for loblolly and shortleaf pine species (*P. taeda* and *P. echinata*) using the loblolly pine Allometric equation from Gonzalez et al. (2014) for both species. AGB for hardwood tree species and eastern red cedar (*Juniperus virginiana*) were calculated using DBH measurements and Allometric equations from Jenkins et al. (2003).

Leaf area index (LAI) was estimated for three paired reference hardwood and old-field forests in CCZO research areas 2, 4, and 5 (Figure 1.2) using two years of leaf litter fall collected in litter baskets totaling 2.05m^2 per plot from January 2016 to January 2018 published by Cook et al. (2018). Though leaf litter collection plots and aboveground vegetation plots were only coincident in one of three replicates (research area 4), LAI patterns observed are considered to be generally representative of reference hardwood and old-field forests. Leaf litter for each plot was sorted by species from October 2014 to January 2015 and projected Specific Leaf Area (SLA) was measured in cm^2/gram of leaf mass. A hemispherical SLA correction was applied by Cook et al. (2018) to all pine needle-leaf litter to increase the SLA estimate following the methodology used by Tissue et al. (1996). Plot-average SLA values were then estimated using the proportions of broadleaf and needle-leaves observed from October 2014 to January 2015.

Minimum LAI (LAI_{min}) is achieved during the winter months in temperate forests for deciduous broadleaf trees, which lose all of their leaves, as well as evergreen pine trees which shed their oldest cohort of needles (McCarthy, Oren et al. 2007, Liu, Chen et

al. 2015, Qi, Jin et al. 2017). Because of this, LAI_{min} in all plots is considered to be equal to the plots' minimum evergreen pine LAI. Evergreen needle-leaf LAI_{min} for each plot was calculated following the methodology of McCarthy et al. (2007) by aggregating the needle-leaf proportion of litter mass collected in autumn and early winter from August 2016 to January 2017 and August 2017 to January 2018 divided by 4.1 (2 autumns X 2.05m^2) to estimate average autumn needle-leaf litter fall in g/m^2. The proportion of litter mass by species in 2016-2018 was assumed to be equal to 2015 litter observations. The average litter mass was multiplied by the plot-average SLA to estimate LAI_{min} in each plot in m^2 of leaf area per m^2 of ground area. Plots with very little pine needle litter, like those in reference hardwood forests, will have LAI_{min} approximately equal to $0m^2/m^2$.

Because nearly all forested plots contain some proportion of mixed hardwood and pine tree vegetation, maximum LAI (LAI_{max}) for each plot must be estimated as the sum of deciduous hardwood broadleaf LAI_{max} and evergreen pine needle-leaf LAI_{max}. The deciduous hardwood component of LAI_{max} for each plot was estimated by aggregating the total mass of leaf litter collected from January 2016 to January 2018, multiplying it by the observed proportion of deciduous broadleaf litter in each plot, and multiplying it by the plots' average SLA. This value was added to the estimate of evergreen needle-leaf $LAI_{max} = LAI_{min}*1.73+0.1$ (McCarthy, Oren et al. 2007, Ward, Domec et al. 2015), and then again dividing by 4.1 to yield average annual total LAI_{max} in m^2/m^2.

Stem density, basal area, and aboveground biomass were compared between reference hardwood and old-field forests using paired t-tests and boxplots in R (R Core Team 2016). Differences in both LAI_{max} and LAI_{min} between the two forest types were tested simultaneously using linear mixed-effect models and general linear hypothesis tests in R with the nlme (Pinheiro, Bates et al. 2017) and multcomp (Hothorn, Bretz et al. 2008) packages in R.

5.2.3 Soil sampling for structural analyses

Three replicate soil cores were collected from each of the nine chronosequence plots of hardwood and old field forests and cultivated fields. For soil structural analyses, an additional three hardwood vs. old-field pine forest contrasts were added. A total of 15 plots were thus sampled for various soil structural analyses, six plots from each of the forest types and three plots from the cultivated treatment. Three replicate soil cores were collected from each of the 15 plots using a 6cm diameter slide hammer resulting in 45 total soil core samples. Soil core samples were 15cm deep starting from the mineral soil surface to 15cm depth in the soil and were extracted and stored in rigid polycarbonate sleeves. Soil cores in polycarbonate sleeves were capped on both ends in order to prevent loss of soil. Following field collection, soil cores were stored at 4°C until analyzed for X-ray Computed Tomography (X-ray CT) to minimize root and organic matter decomposition.

5.2.4 Soil X-ray Computed Tomography (CT) analyses

X-ray Computed Tomography was conducted in the Duke Shared Materials Instrument Facility. High Resolution X-ray CT was accomplished using a Nikon XTH 225 ST scanner with a 0.5mm copper filter with a 354ms exposure. Scans of 45 soil cores were conducted at 191-200kV from 246-263W. Along with each soil core, two standards were used to aid in subsequent image analysis: a quartz sample representative of the majority of rocky material found in soils at the CCZO and a 12mm dia. *P. taeda* tree core to aid in the identification of roots and coarse woody material in the soil (Figure 5.4). For each 15cm soil core, a z-stack of 1998 32bit images with an average x, y, z voxel resolution of 73.6μm on edge was produced.

Each of the 45 z-stacks were imported into imageJ/FIJI image analysis software (Schneider, Rasband et al. 2012) in order to determine appropriate upper and lower raster image threshold values for woody organic material. Voxels of lower density than organic matter are considered to be empty macropore voids and material that is of higher density than woody organic material is considered to be mineral soil or rocky material. The upper and lower organic matter voxel thresholds used in analyses were very consistent among the 45 soil core X-ray CT datasets, but were necessarily variable as the resulting CT image data was affected by the voltage and wattage used during the scan. Both voltage and wattage have to be adjusted depending on the number of scans

that have been run on the X-ray filament in the scanner and how recently the filament had been replaced. Voltage and wattage were increased slightly as the filament aged.

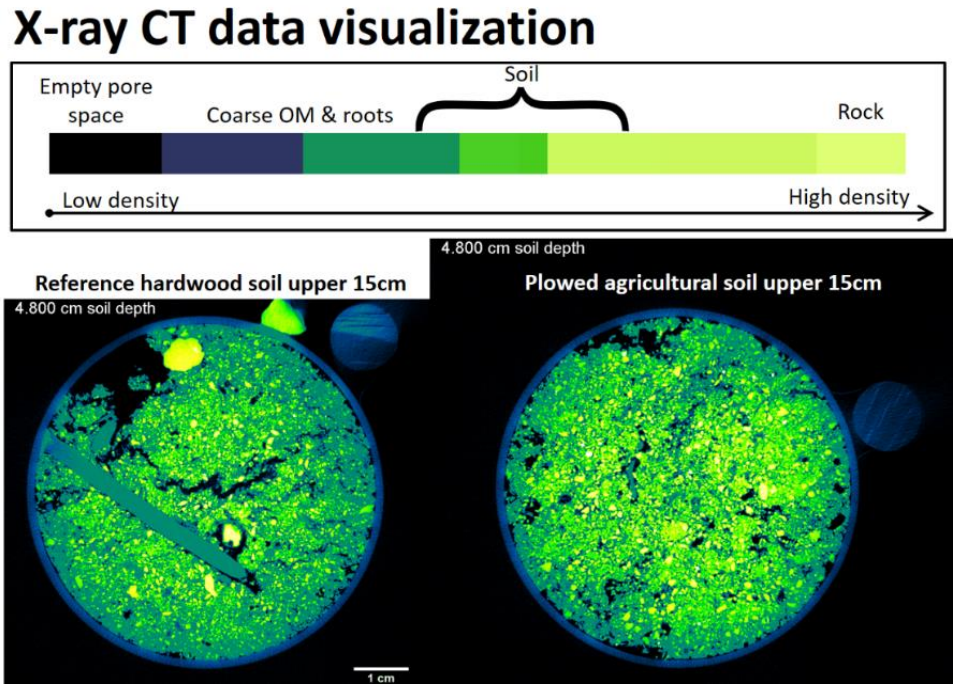

Figure 5.4: cross-sectional view of 6cm diameter soil cores scanned via X-ray CT contrasting reference hardwood (HW) (left) and agricultural (CF) (right) uppermost 15cm layers of mineral soil. Tree-core and quartz-chip standards are visible in the upper-right area of the reference HW image.

The upper 32-bit image raster threshold employed for organic matter ranged from 4000-5000 with a median value of 4500 and standard deviation of 330, the lower threshold for organic matter ranged from 1500-2500 with a median value of 2000 and standard deviation of 276. Image z-stacks were then imported to Avizo 9.1.1 analytical software and cropped in three dimensions using an adjustable cylindrical volume editing tool in order to crop out the outer ~1cm deep edge on all sides of the computed tomography volume for each soil core. This was done because a thin outer boundary of

the 6cm diameter soil cores were necessarily disturbed in the process of sampling and extraction. The inner portion of the X-ray CT soil core is minimally affected and thus is of higher analytical value. The porosity analysis wizard was run twice for each soil core: once including roots and coarse organic matter as part of the macropore volume using the upper threshold limit for organic matter and again using the lower threshold for organic matter in order to exclude roots from the macropore volume to identify unoccupied macropores. The porosity analysis wizard was run without adaptive thresholding and without disconnecting connected voids. An initial threshold for the detection of "strong voids," i.e. regions considered with high certainty to be void-space, was set to be equal to 90% of the upper and lower thresholds for root-inclusion and root exclusion respectively.

Data were exported from Avizo as .csv documents with each row corresponding to an individual macropore including its volume. These data were imported into R statistical software (R Core Team 2016). Within R, the total volume of the cylindrically-cropped CT voxel data was calculated and then the proportion of that soil core volume was estimated for: total macropore volume including roots, empty/unoccupied macropore volume, and root/coarse organic matter volume. Following the estimation of the three macropore fractions for each soil core, the three within-plot soil core replicate values were averaged and analyzed via one-tailed t-tests and box-plotting in base R (R Core Team 2016). Statistical comparisons of macroporosity among the three landuse

history treatments excluded one hardwood (HW) plot from analyses due to it being managed as a cattle pasture with its surface layers compacted by livestock. Comparisons between the two forest types and agricultural plots were conducted using one-tailed t-tests with the alternative hypothesis being that, since the reference hardwood forests were never cultivated or plowed, reference hardwood forests would have the highest proportions of all three macropore volumes: total macroporosity, unoccupied macropores, and root/coarse organic matter volume with agricultural fields having the lowest proportions for all three and old-field pine forests being intermediate.

5.2.5 Soil bulk density measurement

Upon completion of X-ray CT scanning of soil cores, the soils were removed from the 15cm X 6cm diameter polycarbonate sleeves and dried at 40°C in a drying oven for 10 days until consistent mass was achieved. Soils were oven dried at 40°C and not at higher temperature in order to minimize chemical alteration of organic compounds like fungal hyphae that function to promote soil aggregation and soil stability (Bin and Xin-Hua 2006, Duchicela, Sullivan et al. 2013, Devine, Markewitz et al. 2014). This drying temperature is also in agreement with summer temperature that bare soils experience in the field. Consistent mass indicated that all of the water had been removed from the soil samples in order to measure oven-dry soil mass for soil bulk density estimation. Soil bulk density is soil mass divided by soil volume. Soil volume for a 15cm deep core is approximately 424cm^3, though detailed measurements were taken and factored in two

instances when soil cores were slightly longer than 15cm. Bulk density statistical comparisons among the three landuse history treatments were conducted using one-tailed t-tests in R (R Core Team 2016) excluding the same pasture-managed hardwood (HW) plot from analyses. One-tailed t-tests assume that reference hardwoods should have the lowest bulk density and that agricultural soils should have the greatest bulk density with old-field pine forest bulk density being intermediate.

5.2.6 Soil aggregate stability analyses

Following drying and estimation of soil bulk density, all 45 soil samples (3 landuse history comparisons (HW, CF, OF), 6 HW plots + 3 CF plots + 6 OF plots, 3 soil core samples/plot) were gently sieved into four aggregate size classes: 6-4mm, 4-2mm, 2-1mm, and 1-0.5mm. For each of the 45 samples, approximately 8cm^3 of soil aggregates were subjected to wet-aggregate stability analysis (WSA). In WSA a known mass of soil aggregates is immersed in water and oscillated gently for a fixed period of time, dried, and weighed again to determine the proportion of stable soil aggregate mass that resisted disaggregation in water. WSA was conducted following the procedure outlined in Methods of Soil Analysis (Dane, Topp et al. 2002) with four modifications: 1) Sieve mesh sizes used were 4mm, 2mm, 1mm, and 0.251mm. 2) Soil aggregates were not premoistened prior to WSA in order to maximize the intensity of slaking and increase our ability to differentiate the two forest soils' stability. 3) Aggregates in soil sieves were oscillated at 38 cycles per minute for 1 hour. 4) Instead of immediate dispersion of

remaining aggregate material following WSA using sodium hexametaphosphate or sonic dispersion, aggregate samples were oven dried in their sieves after WSA in order to obtain the combined mass of stable-aggregate soil plus stone and coarse organic matter which was larger in size than the sieve mesh openings. After obtaining this aggregate-plus-coarse material mass, wet-sieving was conducted for the mechanical dispersion of remaining soil aggregate material.

After wet-sieving dispersion, the mass of gravels, coarse sand, and coarse organic matter in the samples was obtained and accounted for. Subtracting the mass of stones and coarse organic matter from the initial mass of aggregates, and from the post-WSA mass, allows for the estimation of the soil-only aggregate stability. Within-plot replicate samples for each aggregate size class (6-4mm, 4-2mm, 2-1mm, and 1-0.5mm) were averaged and pairwise one-tailed t-tests were performed in R for all soil cores, including the pastured hardwood forest (R Core Team 2016). T-tests contrasted hardwood forests to cultivated fields, hardwood forests to old-field pine forests, and cultivated fields to old-field pine forests. In t-tests it was hypothesized that for each aggregate size class, aggregate stability expressed as percent soil mass retained, would be greatest in reference hardwood forest soils and lowest in plowed cultivated field soils such that: $\%HW_{WSA} > \%OF_{WSA} > \%CF_{WSA}$.

5.2.7 Soil atmosphere monitoring framework and statistical analyses

As outlined in chapter 4, soil gas reservoirs were installed in each landuse chronosequence plot of HW (n=3), CF (n=3), and OF (n=3) for repeated long-term measurement. Four 750ml gas reservoirs were buried at 0.5m, 1.5m, 3m, and 5m depths with sampling ports at the surface for *in situ* FPGA CO_2 and O_2 analyses as well as soil gas collection for laboratory gas chromatography validation (Figure 4.3). Sampling and measurement was completed approximately every three weeks from 7/31/2015 to 12/19/2017 for a total of 43 observation dates. For each sample, Apparent Respiratory Quotient (ARQ) was calculated as outlined in chapter 4 (Figure 4.6) (Angert, Yakir et al. 2015). ARQ is formulated as the change in CO_2 concentration relative to aboveground ambient concentrations, a positive net accumulation in aerobic bulk soil, divided by the change in O_2 concentration, a negative net depletion in aerobic bulk soil, relative to aboveground ambient concentrations.

In order to structure the methods of statistical analysis, the probability density of ARQ values were plotted from all soil depths and landuse treatments (Figure 5.5). This plot indicates a bimodal distribution and an inconsistent, but apparently structured relationship between soil CO_2 and O_2. Angert et al. indicate that one factor that can lead to such apparent anomalies in ARQ can be linked to dissolution of CO_2 into water during high soil moisture conditions. It was observed that low ARQ values tended to be

associated with high precipitation events and moist soils and that mode 2 in the bimodal distribution might be associated with these time periods.

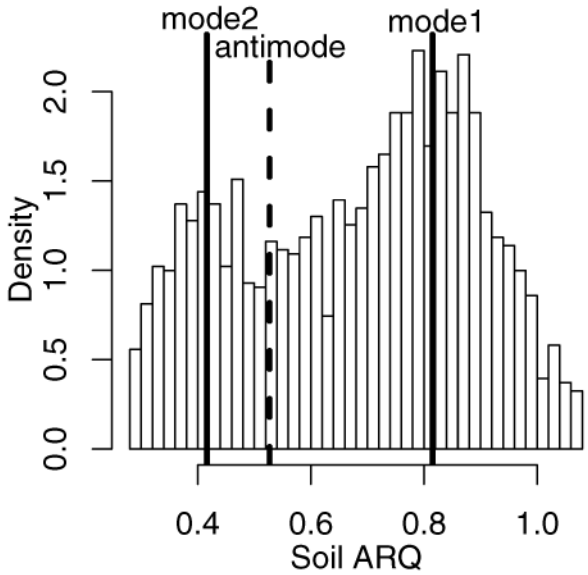

Figure 5.5: bimodal distribution of observed soil apparent respiratory quotient (ARQ) across landuse comparisons

Because of this, precipitation time series data generated and published via the CCZO (Mallard 2017) were analyzed. Precipitation was collected in a tipping bucket rain gauge with a 24.5 cm funnel (Campbell TE525MM) in a clearing within the first landuse history comparison replicate in research area 1 (Figure 1.2). The gauge was positioned to minimize canopy interception. The sensor was mounted approximately 1m above the ground and data were logged at 5 min resolution using a TruTrack GP-HR logger. Tipping bucket data were validated with a total catch gauge measured every 6-8 weeks. Precipitation data were aggregated into daily totals (mm) using the dplyr package and antecedent precipitation indices for 21 (API_{21}) and 90 (API_{90}) days (Figure 5.6) were

generated for each of the gas sampling observation days using the runsum function in the TTR package in R (Jiang, Woli et al. 2010, R Core Team 2016, Wickham and Francois 2016, Ulrich 2017).

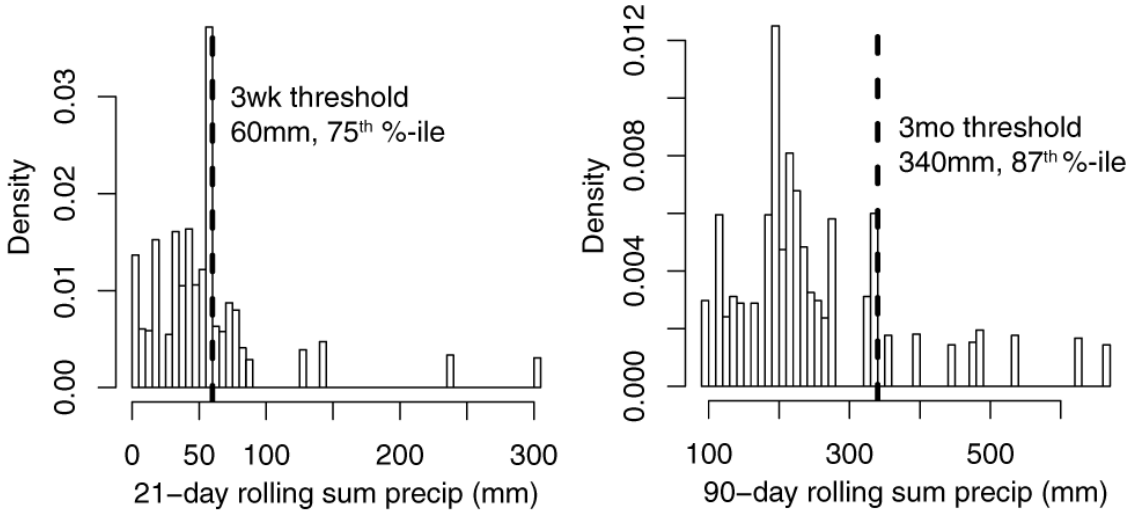

Figure 5.6: Accumulated precipitation index (API) distributions during soil gas observations consisting of 21 day (left) and 90 day (right) accumulated precipitation. Dashed line indicates thresholds used jointly to define "wet" vs. "dry" soil moisture periods in the interpretation of soil ARQ distributions.

API_{21} was employed as it was of the same frequency as the gas sampling observations and it performed better than API_7 or API_{14} in partitioning soil gas observations into "wet" vs. "dry" soil moisture time periods using a 60mm threshold when plotted against soil ARQ. API_{90} was employed out of a desire to capture longer-term deep seasonal soil moisture processes. A 90-day antecedent precipitation performed well in splitting soil gas ARQ into wet vs. dry time periods when plotted against soil ARQ using a 340mm threshold. The bimodal distribution of observed ARQ

values partitioned into "wet" vs. "dry" antecedent precipitation periods indicated that there are two overlapping soil gas ARQ distributions (Figure 5.7). Soil ARQ thus appears to be an integrative critical zone variable incorporating the effects of weather and soil moisture on gas dynamics. As such, soil ARQ was included in linear mixed-effect (LME) model analyses of repeated measurements of CO_2 and O_2.

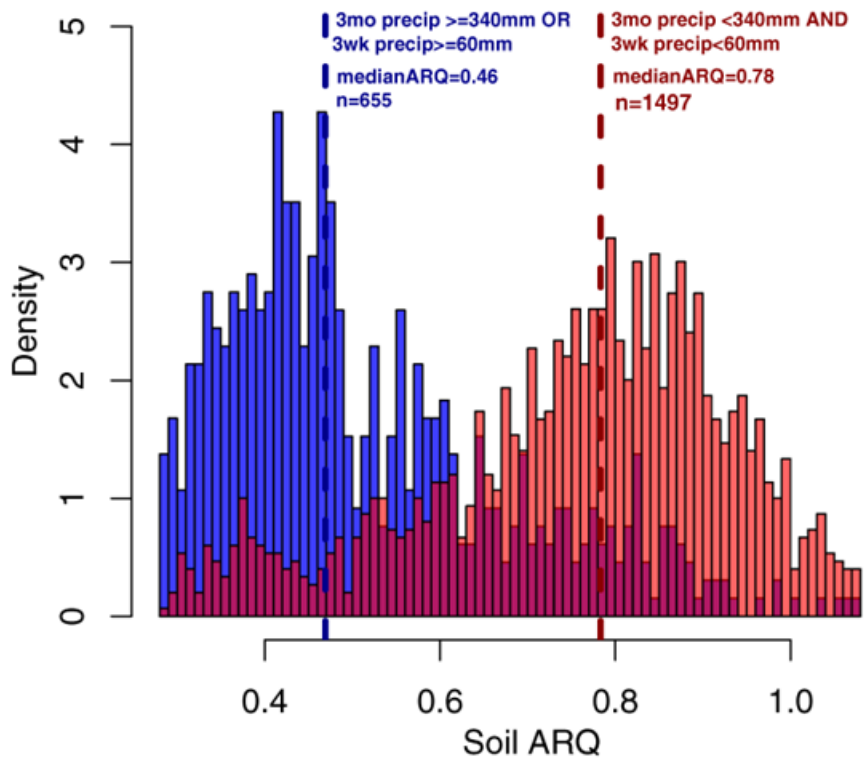

Figure 5.7: observed soil gas ARQ values partitioned into wet (blue) vs. dry (red) periods indicate the underlying mechanism of variation is related to soil moisture being generated by high precipitation periods and low evapotranspiration conditions. Purple areas indicate overlap of the two ARQ probability distributions.

Time series heatmap plots of soil CO_2, O_2, ARQ, and a semi-quantitative soil moisture index (Austin, Brecheisen et al. 2018) averaged across landuse history

replicates were generated using the fields package in R (Nychka, Furrer et al. 2016, R Core Team 2016). Because long-term soil profile moisture data are currently uncalibrated, they are presented for visual representation only. Additionally, in order to illustrate contrasts between the three landuse history treatments (HW, CF, and OF), the relative difference of averaged O_2 and CO_2 time series datasets between landuse treatments were calculated via subtraction and plotted as heat maps. Daily temperature observations and precipitation were also plotted beneath time series heatmaps.

LME models were used to evaluate the effect of forest landuse history (HW vs. OF), soil depth, and seasonality on gas concentrations. ARQ was added as an explanatory variable in order to account for abiotic effects of storms on the dissolution of soil gasses and sealing of B-horizons by perched water tables. The plot replicates and repeated measurement dates were considered as nested random effects using the lme function in the nlme package in R (Pinheiro, Bates et al. 2017). Seasonality was incorporated into the explanatory models by adding sine and cosine functions of the sampling observation Julian date (JD) formulated as the sine or cosine of:

$\sin(2*\pi*JD/365)$ and $\cos(2*\pi*JD/365)$ as described by Stolwijk et al. (1999).

In order to contrast soil gas concentrations under both reference hardwood and old-field pine forests at specific soil depths of 0.5, 1.5, 3, and 5m, LME explanatory models were also generated with factors of combined treatment+depth (e.g. HW1.5m vs. OF1.5m) for sequential multiple comparison using the general linear hypothesis testing (glht)

function with Hochberg adjustment in the multcomp package in R (Hothorn, Bretz et al. 2008, R Core Team 2016, Pinheiro, Bates et al. 2017).

5.3 Results and conclusions

5.3.1 Reference hardwood vs. old-field forest vegetation

Analyses of aboveground forest vegetation contrasting reference hardwood and old-field forests indicate that there are significantly more stems ≥6″ DBH per unit area in old-field forests (t=-3.28, df=2, p=0.04) (Figure 5.8a). In spite of having nearly 50% more stems in observed old-field forest plots, there is no significant difference in observed BA between the two forest types (t=0.69, df=3.17, p=0.27) (Figure 5.8b). Though it doesn't quite surpass a 95% confidence threshold, AGB tends to be higher in reference hardwood plots than old-field forests (t=-2.19, df=2, p=0.08) (Figure 5.8c). Leaf Area Index (LAI) analyses of LAI_{max} and LAI_{min} via linear mixed effect modeling indicates significant differences between the two treatments (F=207.97, df=3, p<0.05) and sequential hypothesis testing in R indicates that reference hardwood forest plots have lower maximum LAI (z=-5.82, p<0.05) and lower minimum LAI (z=-9.18, p<0.05) than the old-field forests in the study (Figure 5.8d). This surprising result for LAI_{max} is attributed to the presence of both a mature emergent evergreen pine needle-leaf canopy plus an incipient hardwood understory canopy in OF plots whereas HW plots studied at the CCZO tend to only have a single emergent hardwood canopy. Minimum LAI being greater under OF forests, though not surprising due to the high proportion of evergreen

pine trees in the plots studied (30-75% of litter by mass), it is important to recognize that the persisting metabolically-active evergreen leaf vegetation requires the pine trees to maintain a more active (i.e. non-dormant) metabolism relative to hardwood tree phenology and physiology which allows them to go dormant during leaf-off periods in the fall and winter.

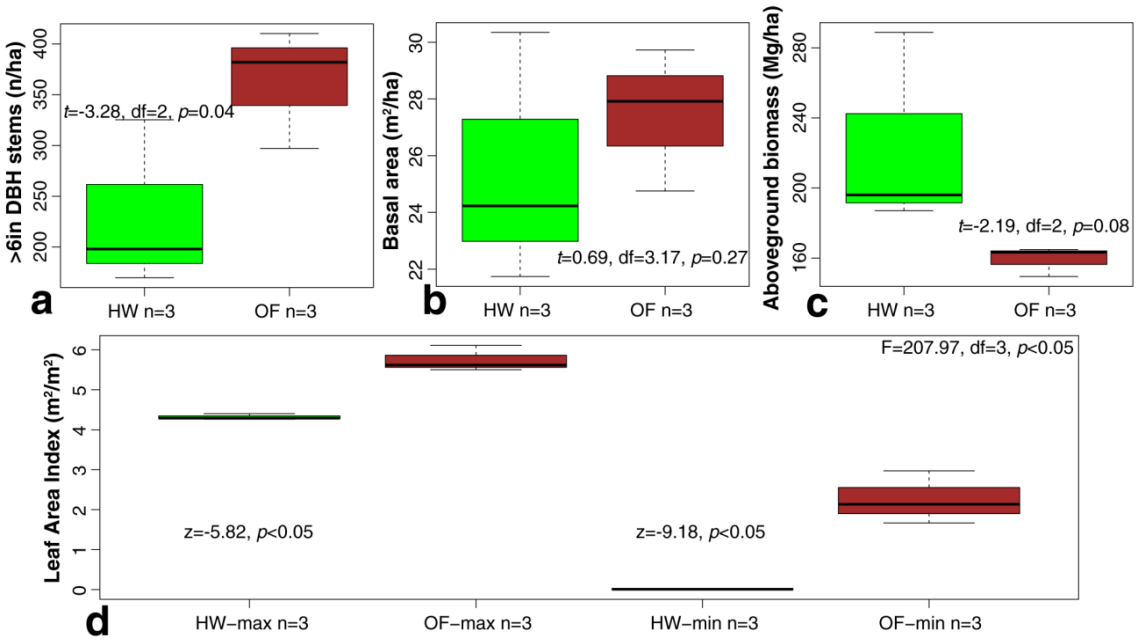

Figure 5.8: Aboveground reference hardwood (HW) vs. old-field (OF) forest comparison results for a) stem density, b) basal area, c) biomass, and d) leaf area index results.

5.3.2 Soil ecoporosity regeneration through old-field succession

Soil structure regeneration in the top 0-15cm of soil was evaluated among five metrics contrasting reference hardwood forests (HW), cultivated agricultural fields (CF), and old-field pine forests (OF) in chronosequence: 1) bulk density, 2) percent soil volume of total macropores, 3) percent soil volume of vacant macropores, 4) percent soil

volume of roots and coarse organic matter, and 5) soil aggregate water stability (Figure 5.8), see Table 5.1 for detailed statistical results.

5.3.2.1 Bulk density

Bulk density results (Figure 5.9a, Table 5.1) indicate that all three landuse histories have unique bulk density distributions but do show the beginnings of a reduction in bulk density (BD) within OF pine forest soils. Hardwood soils have much lower BD than CF (t = -5.96, df = 6.75, $p < 0.05$). Relative to CF soil bulk densities (median = 1.45g/cm^3), OF pine forest soils appear to have greatly reduced historic compaction (t = 2.32, df = 6.19, $p < 0.05$). Though reference HW soils and OF pine forest soils have equal median bulk densities (1.29g/cm^3), indicating some recovery of OF forest surface soils, OF soils still remain compacted (t = -1.87, df = 7.80, p = 0.0496).

5.3.2.2 Macroporosity

The proportions of soil volume that consisting of total macroporosity indicate that all three landuse histories are significantly different from each other with results in agreement with expected patterns of high total macroporosity in HW forest soils (median ~26% of total soil volume), very low macroporosity in CF agricultural soils (~12%), and partially regenerated, though highly variable, total macroporosity in OF pine forest soils (median ~17%) (Figrue 5.8b, Table 5.1). Though total macroporosity is significantly higher under OF than CF indicating a partial regeneration of macroporosity, the proportion of the soil volume that consists of empty macropores is

not significantly different between agricultural CF soils (~7%) and OF pine forest soils (~6%) (Figure 5.9c) indicating a persisting legacy of agricultural degradation. Contrary to the initial hypothesis, OF pine forests frequently have lower unoccupied macropore volume than CF soils. Reference HW forests have the highest proportion of empty macropore volume (~11%). Comparisons of root and coarse organic matter (OM) volume agree with the intermediate and incomplete regeneration hypothesis as reference HW soils have the highest root volume (~14%), CF soils have the least root volume (~4%) and OF soils have ~11% of their upper 15cm soil volume occupied by roots or coarse OM (Figure 5.9d).

5.3.2.3 Aggregate stability

For the three smallest aggregate size classes, reference HW soils have the highest aggregate stability (median value 72%-60%) and CF soils have the lowest aggregate stability (39%-24%) with OF soils having partially regenerated aggregate stability ranging from 58%-55%. Old-field soil aggregate stability appears to have regenerated considerably as it is not statistically different from hardwood soils for either 1-2mm or 2-4mm aggregate size classes and is only barely significant for the 0.5-1mm size class via one-tailed t-test (t=1.85, df=9.91, p=0.047). Nonetheless, 4-6cm large aggregate stability remains diminished in OF forests relative HW (t=1.96, df=10.30, p=0.039).

Aggregate stability contrasts of the three landuse histories indicate a general decline in percent soil mass retained (i.e. “stability”) across landuse histories as soil

aggregate size class increases from 0.5-1mm up to 2-4mm diameter aggregates, but then increases for 4-6mm diameter aggregates in all landuse history treatments (Figure 5.9e). This pattern is so pronounced in the CF agricultural soil that, in spite of every other CF aggregate size class having the lowest aggregate stability compared to the forested treatments, 4-6mm CF aggregate stability is indistinguishable from either reference HW or OF pine forest soils. The unexpected spike in 4-6mm aggregate stability in cultivated fields is likely due to those soils having higher clay content in the topsoil (Figure 5.3) than the two forest soils with clay particles helping to promote aggregation in the largest aggregate size class. The general trend of higher aggregate stability in this size class across landuse history treatments may be related to the surface-area:volume ratio of the aggregates crossing a stability threshold specific to the WSA procedure used here.

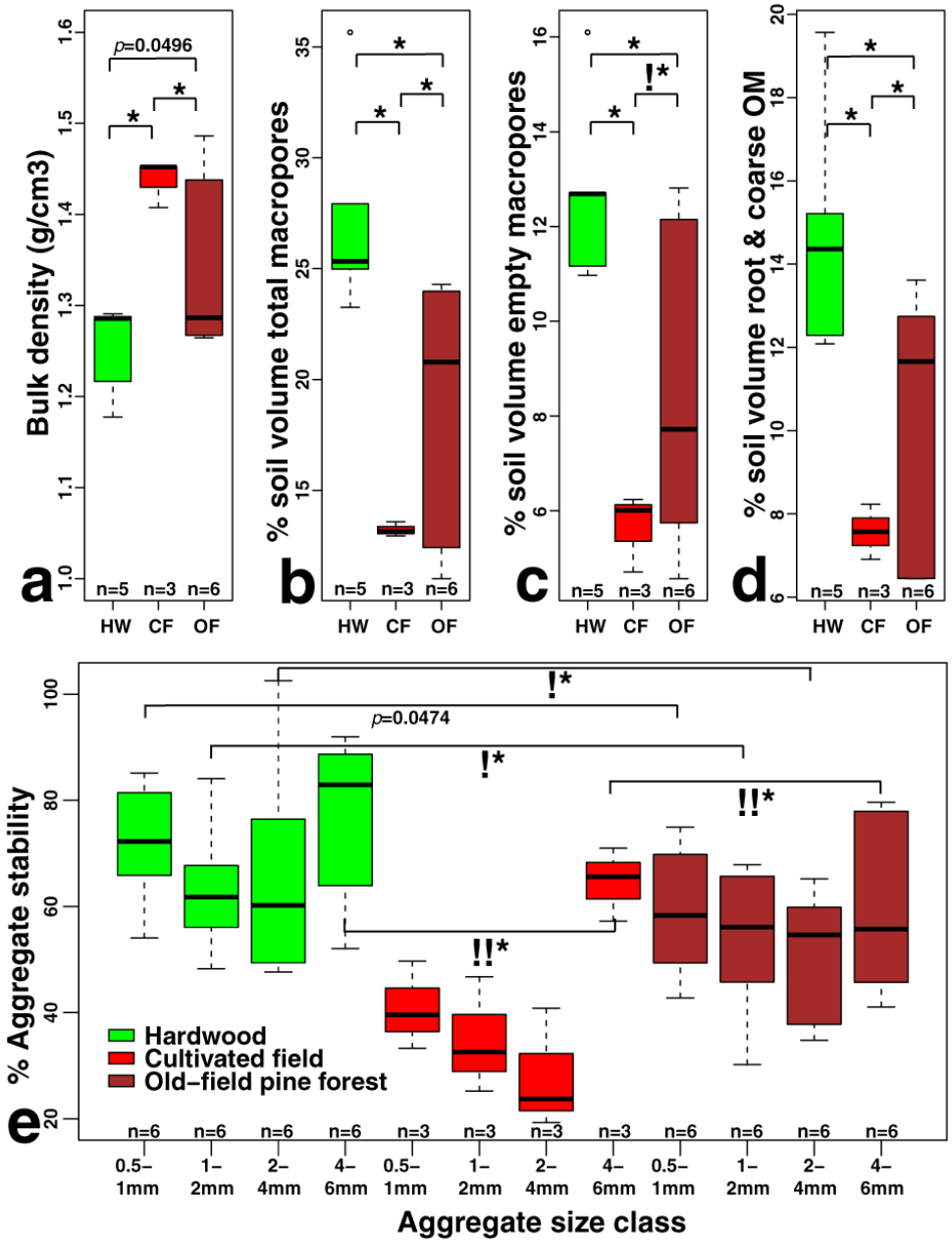

Figure 5.9: landuse comparisons of a) soil bulk density, b) total soil macropore volume proportion c) empty soil macropore proportion, d) soil root and coarse organic matter (OM) volume proportion, e) soil aggregate stability results. Statistically significant t-test differences are indicated by "*", non-significant results are indicated by "!*", non-significant results linked to experimental anomaly are indicated by "!!*". Significant results with *p*-values close to a 0.05 significance threshold are reported numerically.

Table 5.1: Detailed soil structure statistical results

Comparison	Variable	t-stat	df	p-value
HW-CF	BD	-6.75	5.96	0.0003
HW-CF	% tot. macropore	6.46	4.06	0.0014
HW-CF	% empy macropore	6.83	5.63	0.0003
HW-CF	% coarse root & OM	5.07	4.60	0.0024
HW-CF	%0.5-1mm agg. stab.	4.62	5.64	0.0021
HW-CF	%1-2mm agg. stab.	3.79	3.65	0.0114
HW-CF	%2-4mm agg. stab.	3.97	6.40	0.0032
HW-CF	%4-6mm agg. stab.	1.79	8.33	0.0546
HW-OF	BD	-1.87	7.80	0.0496
HW-OF	% tot. macropore	2.61	9.00	0.0140
HW-OF	% empy macropore	2.50	8.20	0.0181
HW-OF	% coarse root & OM	2.28	8.78	0.0246
HW-OF	%0.5-1mm agg. stab.	1.85	9.91	0.0474
HW-OF	%1-2mm agg. stab.	1.35	9.30	0.1045
HW-OF	%2-4mm agg. stab.	1.69	11.80	0.0590
HW-OF	%4-6mm agg. stab.	1.96	10.30	0.0390
CF-OF	BD	2.32	6.19	0.0290
CF-OF	% tot. macropore	-2.32	5.06	0.0336
CF-OF	% empy macropore	-1.84	5.97	0.0575
CF-OF	% coarse root & OM	-2.12	5.80	0.0401
CF-OF	%0.5-1mm agg. stab.	-2.57	6.09	0.0210
CF-OF	%1-2mm agg. stab.	-2.21	5.21	0.0381
CF-OF	%2-4mm agg. stab.	-2.82	4.38	0.0216
CF-OF	%4-6mm agg. stab.	0.65	6.94	0.7330

5.3.3 Characteristics of soil atmosphere dynamics across landuse histories

Heatmap plotting of soil gas timeseries of soil CO_2 and O_2 indicate that the deep soil environment is highly variable in the concentrations of both gasses through time across all three landuse history comparisons (Figure 5.10). Under both forest types (HW and OF), gasses beneath the B-horizon (>~2m depth) display an equal and possibly

greater range of variation in CO_2 (~2.5-5.5%) and O_2 (~17-12%) than soils within or above the B-horizon (<2m depth) on average (~0.5-3% and ~20.5-16% respectively). The cultivated agricultural field (CF) treatment, in contrast, had the greatest variation in CO_2 and O_2 concentrations within the upper 2m of soil (Figure 5.10, rows 1 and 2) due to lower production of CO_2 and consumption of O_2 at depth in agricultural soils. Consistently higher CO_2 concentrations and reduced O_2 concentrations are evident below the B-horizon under reference HW forests than either CF agricultural plots or OF pine forests.

The period from 2015 fall into 2016 spring had large amounts of precipitation, and consequently high infiltrating soil moisture, associated with Hurricane Joaquin and other storms (Figure 5.10, bottom row). This coincided with a rapid reduction in soil CO_2 concentrations under both forest treatments and an increase in CF CO_2 in the upper meter of soil. Analyzed via calculation and timeseries plotting of soil Apparent Respiratory Quotient (ARQ), it is clear that CO_2 concentrations were disproportionately reduced relative to the observed O_2 concentrations during this period of intense and repeated storms across all land use treatments (Figure 5.10, row 3). Though the remainder of the observation period generally had low precipitation, an intense storm in the summer of 2017 coincided with another reduction in observed soil ARQ which is matched by increased qualitative soil moisture observations under both forest treatments (Figure 5.10). The associated wetting front and ARQ reduction zone appears

to be restricted to the upper 2-3m of soil (Austin, Brecheisen et al. 2018) (Figure 5.10, row 4) in the OF treatment. In the CF treatment, soil moisture appears to remain high and ARQ relatively low compared to the forested treatments throughout the observational period.

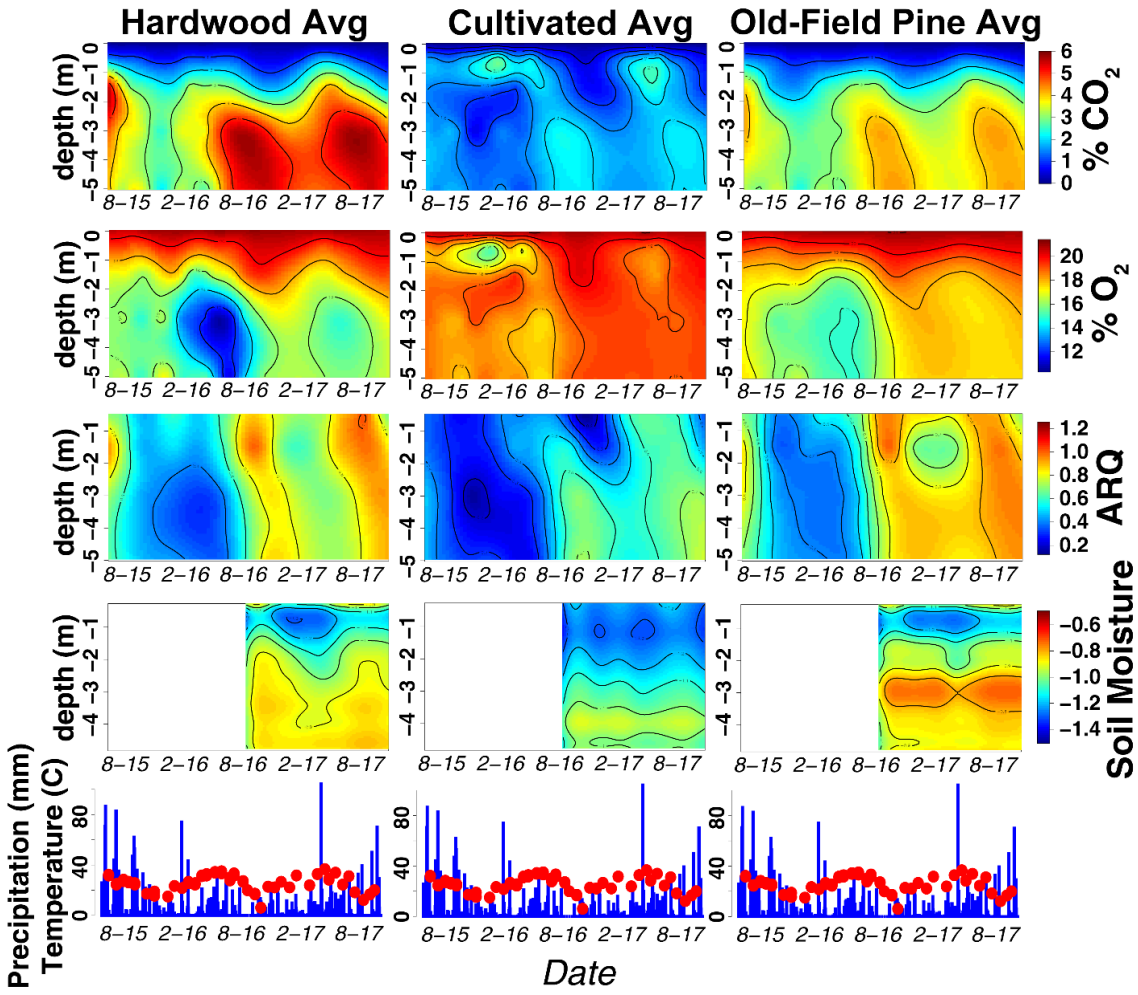

Figure 5.10: Heatmap plotting of bulk gas concentrations of soil CO2 (top row) and O2 (second row), soil gas ARQ timeseries (third row), and relative soil moisture index is plotted in the bottom heatmap with cooler colors corresponding to more moist conditions. Y-axis is soil depth and the x-axis corresponds to time with color intensity corresponding to the variable of interest on all heatmaps. Precipitation (blue) and temperature (red) are plotted for reference in the bottom row.

Mixed linear effect models of forest soil CO_2 and O_2 concentrations through time as functions of landuse history treatment, soil depth, ARQ, and seasonality across 43 sampling periods with 925 measurements of soil gasses indicate that all of the explanatory variables are highly significant for both gasses. The general effect of forest treatment type indicates significant reductions in O_2 (-0.60%±0.10%) concentrations in reference hardwood soil O_2 (F=63.55, df=1, p<0.0001) and higher CO_2 (0.52%±0.07%) concentrations than in old-field pine forest soils (F=50.56, df=1, p<0.0001). Soil depth was the strongest explanatory variable for both gasses (CO_2: F=1034.69, df=1, p<0.0001; O_2: F=758.65, df=1, p<0.0001) with CO_2 accumulation and O_2 depletion generally increasing with depth, though 3m and 5m depths were not statistically different within forested treatments (p=0.72). In fact, the 5m depth values for CO_2 and O_2 were frequently slightly lower and higher respectively than 3m suggesting higher root activity at 3m.

The soil gas apparent respiratory quotient (ARQ) was employed in this analysis to account for the abiotic processes of CO_2 dissolution into soil water and the sealing of clay-rich B-horizons during wet periods which appears to enhance O_2 depletion by inhibiting the resupply of O_2 to deep soils. Surprisingly, ARQ appears to have a stronger effect on soil O_2 (F=267.83, df=1, p<0.0001) than CO_2 (F=11.96, df=1, p=0.0006), though it is difficult to isolate the physical and chemical ARQ effects of precipitation on soil gasses from seasonal effects because the majority of storms during the observation period occurred during fall and winter months when soil respiration activity is lowest.

Seasonality, incorporated in LME models via sine and cosine functions, was similarly significant for both gasses (Sine - CO_2: F=30.82, df=1, p<0.0001; O_2: F=27.01, df=1, p<0.0001) (Cosine - CO_2: F=34.65, df=1, p<0.0001; O_2: F=43.06, df=1, p<0.0001) and appears to accurately capture the seasonal dynamics in both gasses (Figure 5.11).

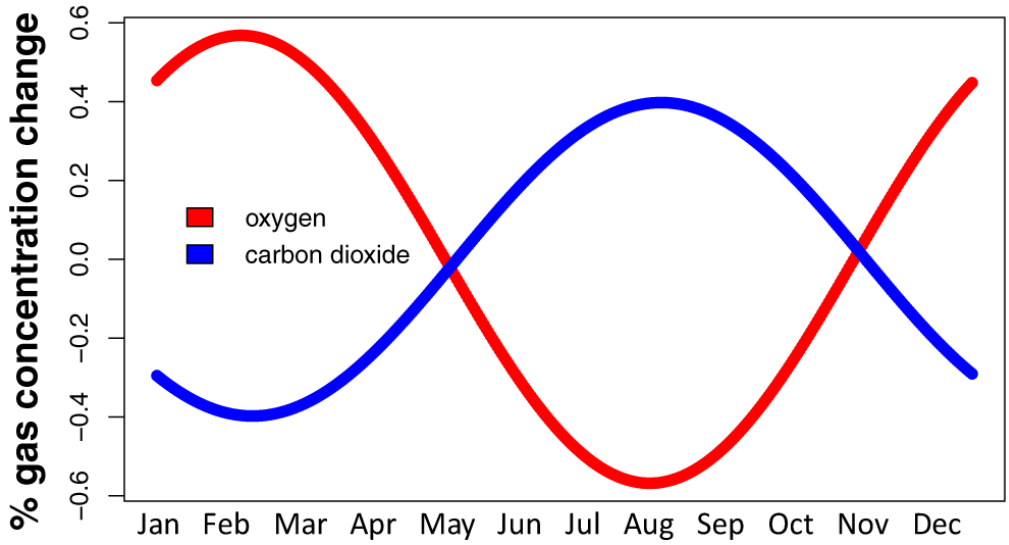

Figure 5.11: Seasonality patterns as fit to the observed concentrations of soil oxygen (red) and carbon dioxide (blue) via sine and cosine functions in linear mixed-effect models.

5.3.4 Soil atmosphere landuse history contrasts

Though pseudo-replication of agricultural CF treatments hinders formal statistical analyses of that landuse treatment, simple graphical comparison of longitudinal soil gas concentrations is possible. This was accomplished via pairwise subtraction of soil gas timeseries (TS) datasets between landuse contrasts for CO_2 and O_2. This subtractive contrast takes the general form of:

$$TS.treatment1_{gas1} - TS.treatment2_{gas1}$$

and is plotted via heatmaps in the same manner as bulk gas concentrations. In this graphical approach, colored z-values correspond to the difference between the landuse average gas concentration values for each time period (Figure 5.12). Plotted this way, regions of the heatmaps with values equal to or less than 0 reflect depths and time periods when treatment 2 had a greater concentration of either CO_2 (Figure 5.12, left column) or O_2 (Figure 5.12 right column) than treatment 1.

This comparison highlights both depth- and time-dependent differences between the three ecosystems which can be attributed to the rooting depth and phenology of vegetation. In contrasting reference HW forests and CF agricultural treatments, the shallow rooting depth and associated aerobic metabolism of cultivated fields appear highly constrained to the upper 1m of soil as indicated by difference plots of CO_2 and O_2 (Figure 5.12, row 1). Contrasting reference HW forests against OF pine forests (Figure 5.12, row 2) highlights four key processes at work between these forest soils: 1) Through old-field succession the rooting depth of OF pine forests has deepened to the point that it has enabled pine forests to reach and penetrate into at least the top of the B-C horizon transition with OF pine forest CO_2 accumulation and O_2 depletion frequently equal to or slightly greater in magnitude than reference HW forests up to 2m depth. 2) The time periods in which apparent OF respiration activity is greater than reference HW are seasonal. They appear to be directly linked to the differing phenologies of deciduous hardwood vs. evergreen coniferous forests as they occur only during fall and winter

months when HW forests have shed their leaves and gone dormant. 3) Though there is much greater accumulation of CO_2 and depletion of O_2 under OF forests than under CF agricultural plots, beneath the B-horizon at depths >~2m, reference HW forests have consistently higher CO_2 accumulation and O_2 depletion than OF forests (Appendices C, D, and E). The only exception of this trend was during the time period of Hurricane Joaquin in 2016 and it indicates that reference HW forests have greater root activity through and past the B-horizon into the C-horizon than OF forests. 4) Intense precipitation events that infiltrate and drain through the soil can be seen to "flush" or "scrub" CO_2 from the deep soil environment, dissolving and transporting it into groundwater. This process effectively "resets" the deep soil environment beneath forests such that both OF pine and reference HW forests are approximately equal in CO_2 and O_2 concentrations during these periods. The final subtraction comparison of OF pine forests vs CF agricultural plots (Figure 5.12, row 3) shows that there is much greater root respiration activity below 1m in OF pine forests than the agricultural fields. This indicates that OF forest rooting re-establishment has progressed considerably following agricultural abandonment, though it has not yet returned to the pre-disturbance reference HW state.

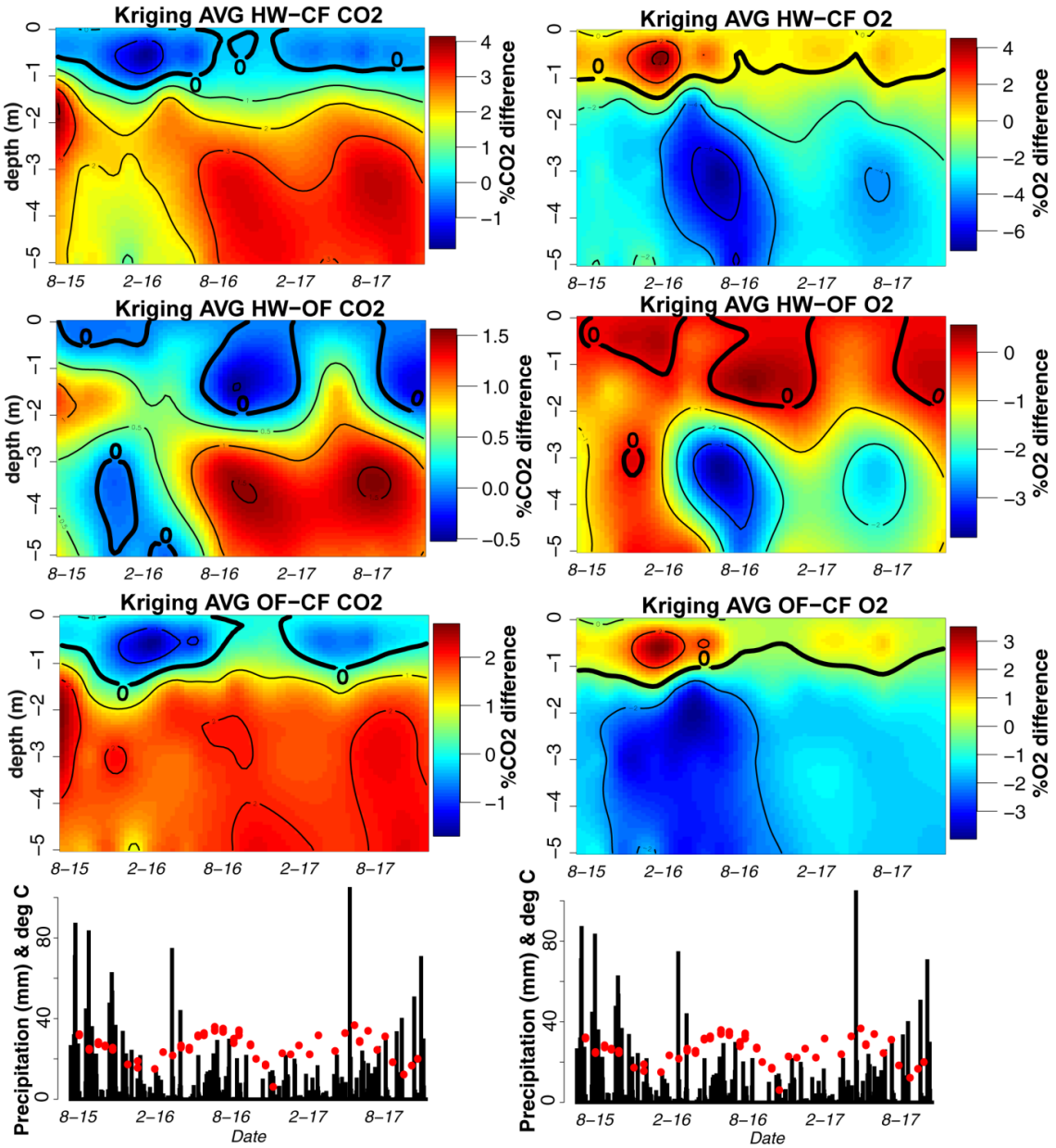

Figure 5.12: subtraction difference plots contrasting averaged timeseries observations of soil CO2 (left) and O2 (right). Bolded contours indicate the zero-difference transition between two landuse treatments. Precipitation (black) and temperature (red) are plotted in the bottom row for reference.

Linear mixed effect models targeting the combined effect of landuse history and soil depth on forest soil gas concentrations indicate that significant differences between

treatments exist for both CO_2 (F=315.79, df=7, p<0.0001) and O_2 (F=240.20, df=7, p<0.0001) with the remaining explanatory variables of ARQ (CO_2: F=26.05, df=1, p<0.0001; O_2: F=369.68, df=1, p<0.0001) and seasonality (Sine - CO_2: F=46.27, df=1, p<0.0001; O_2: F=35.89, df=1, p<0.0001) (Cosine - CO_2: F=65.13, df=1, p<0.0001; O_2: F=70.81, df=1, p<0.0001) still statistically significant. Sequential generalized linear hypothesis testing indicates that there is no statistically significant difference between soil gas concentrations at 0.5m (CO_2: z=-1.31, df=7, p=0.20; O_2: z=-1.04, df=1, p=0.30) or 1.5m (CO_2: z=-1.88, df=7, p=0.12; O_2: z=1.69, df=7, p=0.23) between reference HW and OF pine forests. Deeper in the soil profile however, 60-80-year-old OF pine forest CO_2 is 0.90%±0.1% lower at 3m (z=-8.91, df=7, p<0.0001) and 0.78%±0.1% lower at 5m (z=-7.53, df=7, p<0.0001) than in reference HW forest soils. Oxygen, being the terminal electron acceptor for aerobic respiration, displays a reversed trend whereby deep sub B-horizon soils under OF pine forests have 1.19%±0.15% more O_2 at 3m and 1.01%±0.15% more O_2 at 5m depth (z=-8.91, df=7, p<0.0001) than reference HW soils. These inferences of more intense and rapid cycling of CO_2 and O_2 at depth in reference hardwood soils are supported by preliminary isotopic analyses of ^{18}O in soil O_2 and ^{13}C and ^{14}C in soil CO_2 currently in review by Cherkinsky et al. (2018) (Figure 5.13). Pronounced ^{18}O enrichment in deep reference hardwood soil O_2 suggests far greater respiratory oxygen demand by roots relative to agricultural soils which has only been partially regenerated in deep old-field forest soils. Further, high depletion of heavy ^{13}C and ^{14}C isotopes in deep HW soil CO_2 suggests that soil gasses at

depth have shorter residence time than in CF or OF soils. This is a clear indication that there are production and cycling rate differences with HW soils being higher than OF as OF forest soils appear to have a lingering deficit in rooting depth and associated respiratory activity as reported by Billings et al. (2018) (Figure 5.14).

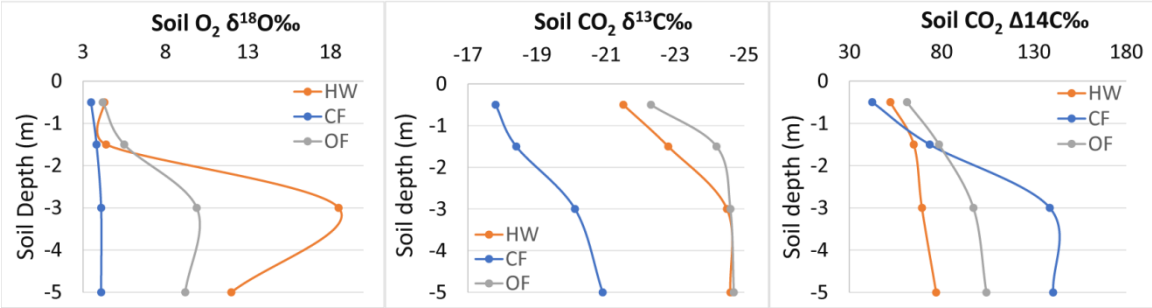

Figure 5.13, adapted from Cherkinsky et al (2018): Preliminary analyses of oxygen and carbon isotopes from one set of 2016-summer soil gas samples analyzed by Cherkinsky at el.

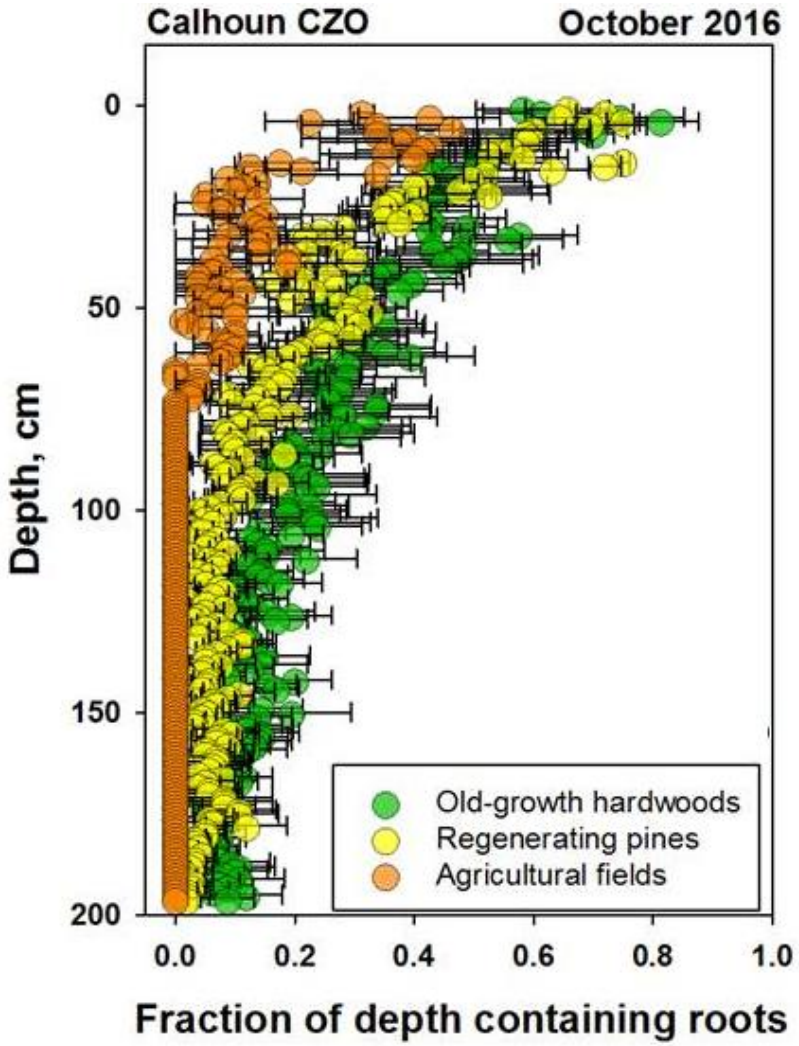

Figure 5.14: Root density across landuse history comparisons to 2m depth, figure from Billings et al. (2018).

5.4 Discussion

Considered together, soil structure and soil atmosphere analyses indicate that despite significant soil regeneration in the upper 2m of soil under old-field pine forests over 60-80 years of secondary forest growth following agricultural abandonment, there remain detectable legacies of agricultural degradation. Surface soil bulk density has been

reduced to near reference-condition levels in many cases as tree rooting has created, occupied, and stabilized macropores, but remains higher than reference hardwood surface soil bulk density (Figure 5.15). A component of this persistent post-agricultural legacy in soil structure is revealed by macroporosity analyses. All three macropore categories remain diminished in OF surface soils compared to reference HW soils. Additionally, OF surface soils continue to have significantly lower aggregate stability than reference HW in two out of four soil aggregate size classes.

This is not to say there has been no regeneration or recovery in the upper 2m of soil in OF forest plots as BD has been reduced, aggregate stability enhanced, and macroporosity generally regained relative to CF agricultural fields. Looking a little deeper into the soil profile through time series measurements of soil CO_2 and O_2 at 50cm and 1.5m depths, the effects of old-field regeneration are similarly apparent in the concentrations of the two gasses. Oxygen and CO_2 do not differ by more than 0.5% on average in the upper 2m from one forest type to the other and are statistically indistinguishable from each other to this depth. The timing of and fluctuation of the ~0.5% difference between the two forest types whereby HW forests tend to be higher in spring and summer seasons while OF forests are higher in fall and winter periods reflects differing natural histories and phenologies of the deciduous vs. mixed-evergreen forest communities. These soil gas dynamics paired with observational root and isotopic

data further highlight what appears to be the limit of the rooting-depth regeneration front within the clay-rich B-horizon (Figure 5.15).

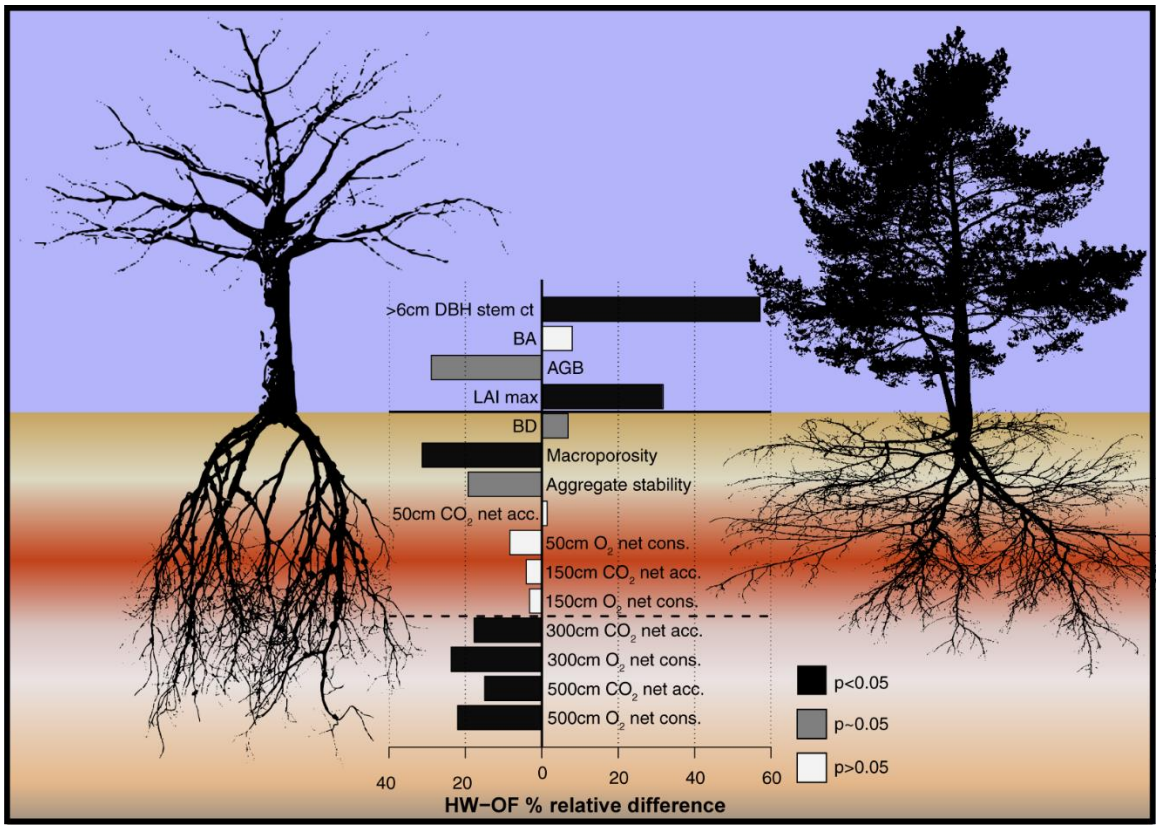

Figure 5.15: Synthesis of observed old-field regeneration and persistent legacies of degradation at the Calhoun CZO. Bar lengths are equal to the percent relative difference for each variable measured. Bars extending to the left indicate that reference hardwood (HW) forests have greater observed values than old-field (OF) forests with the converse being true for bars extending to the right. Significance of the result is indicated by the color of the bar with white being non-significant, grey is bordering on significance, and black indicating significant differences at a 95% confidence threshold.

Beneath ~2m soil depth, a strong and enduring legacy of agricultural degradation is evident in old-field forests. Reference HW soils have significantly higher CO_2 and depleted O_2 concentrations indicating greater rooting penetration and activity

through and beneath the B-horizon. One mechanism for the persistent lag in rooting depth regeneration between the two forest types could be directly linked to the erosive landuse history of OF secondary forests. With clay-rich agricultural CF soils having as low as 30% observed aggregate stability and very high slaking potential, there is reasonable potential for deep soil macropores to have been filled or sedimented by vertically transported clay and silt soil particles. Laboratory experiments on intact soil cores, with and without the addition of micron- to sub-micron particles, have shown that the size distribution of particles transported vertically through soil columns decreases even over periods of hours.

One explanatory mechanism put forward for this observation is the physical entrapment and sieving of larger particles lodging in macropores (Jacobsen, Moldrup et al. 1997, Rousseau, Pietro et al. 2004, Bin, Cao et al. 2011). This is the essential mechanism underlying the fundamental soil-formation process of lessivage and the development of Bt-horizons in advanced-stage soils like Ultisols (Quénard, Samouëlian et al. 2011). Sedimentation and clogging of macropores is another mechanism, beyond the physical compaction of soils during plowing and cultivation, by which total macroporosity can be reduced, particularly at depth. In this case the clogging of deep macropores would present a persistent barrier to the reestablishment of deep rooting that old-field secondary forests seem to have only partially overcome.

There is photographic evidence of the infilling of macropores at the Calhoun CZO thought to have occurred over long geologic time scales where fine textured clays have completely filled fractures in saprolite (Figure 5.16, top), as well as evidence of what appears to be coarser-texture and differently-colored vertically transported soils within the B-horizon in the CF agricultural fields (Figure 5.16, middle and bottom). These inferences are supported by the apparent reduction in the wetting front propagation below ~2m depth on average in the OF field treatment during the intense 2017 summer storm (Figure 5.10, row 3, column 3). This reduced moisture front propagation and reduction in ARQ are highly concentrated in the upper 3m whereas the reference HW treatment experienced a reduction in ARQ throughout the entire 5m monitored soil profile and a clear observed wetting front propagation down to 4m.

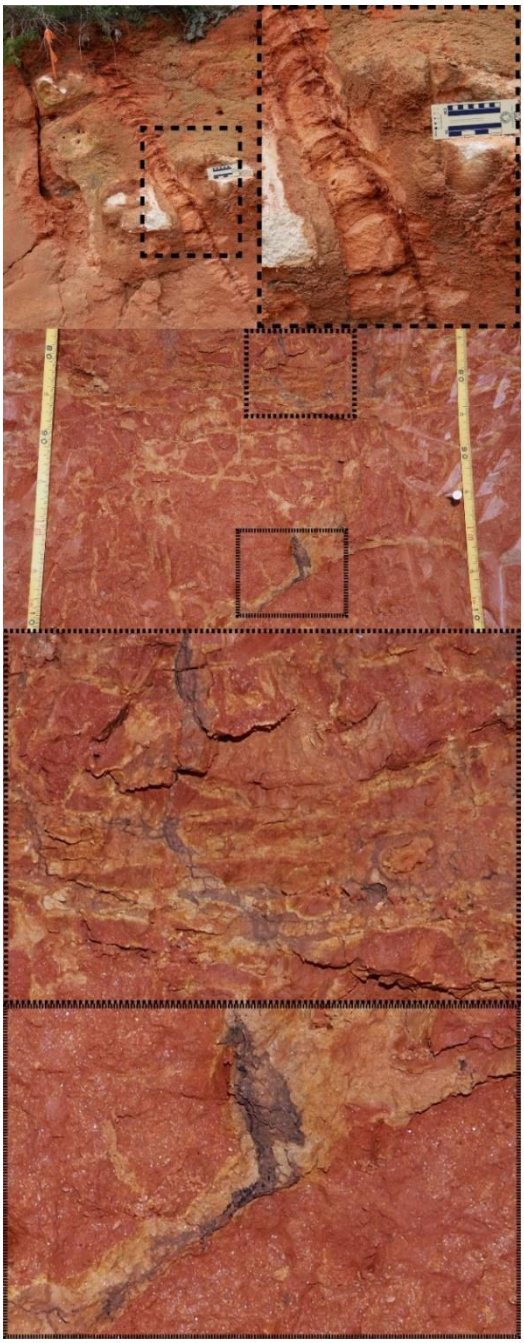

Figure 5.16: soil profiles with evidence macropores filled by eluviated soil material in: Top) road cut with red clay-filled pore off of HWY-49 near Union, SC, photo credit: Terry Ferguson. Second to bottom) cultivated agricultural field R1C3 from ~75-110cm depth with evidence of foreign soil in corresponding panels indicated by dashed lines, photo credit: Charles Cook.

The thick low conductivity B-horizon seems to function as a barrier to new root penetration in OF forests, but also functions as a cap helping to retain and slow the diffusion of deeply respired CO_2 such that it accumulates to concentrations which are two orders of magnitude greater than aboveground ambient air. Though this enhanced accumulation and build-up of CO_2 does not result in complete retention of deep soil CO_2 (evidenced by a seasonal ebb and flow even below 2m depth), the enhanced retention of deep soil CO_2 allows for what must be a large proportion of terrestrially-derived CO_2 export to groundwater and streams (Mayorga, Aufdenkampe et al. 2005, Johnson, Lehmann et al. 2008, Angert, Yakir et al. 2015). The timing and significance of storm events in this process as well as the ramifications for mineral weathering and soil formation are exciting frontiers for research. These observations were made possible via the tandem monitoring of soil O_2 and CO_2 and the calculation and monitoring of soil ARQ. ARQ appears to integrate the effects of changes in the diffusivity and permeability of saturated soils to deep soil oxygen resupply and the preferential dissolution of CO_2 into soil moisture. Ongoing work aims to quantify the magnitude of these deep critical zone processes and the change in transport of CO_2 into streams across a landscape which, like rest of the Southeastern US, is dominated by intermediately-regenerated secondary-succession old-field pine forests.

6. Conclusions

6.1 Summary of research findings

In Chapter 2 a new geomorphic analytical perspective was developed at the Calhoun Critical Zone Observatory (CCZO) in SC which hierarchically ranks interfluves or ridges and their corresponding "hillsheds" the same way as streams and their watersheds according to Hortonian methodology. First-order interfluves lead to 2nd, 3rd, 4th, or 5th order interfluves. In addition to the order of a particular feature, further information on the local geomorphic neighborhood is captured in the uphill junction orders for ordered interfluves. In the Southern Piedmont, interfluve orders capture landscape patterns in the abundance of interfluves within each order, their areas, elevations, and slopes. Low-order interfluves are abundant, small, low elevation, and steep while high-order interfluves are rare, large, high elevation, and flatter. Practical applications of interfluve ordering indicate that historic and contemporary agriculture has been concentrated and persisted on high-order interfluves largely in private ownership. Low-order interfluves are predominantly public lands that have generally been reforested in areas of agricultural abandonment. These patterns are linked to slope through the process of soil erosion. Soil erosion potential was modeled under theoretical uniform forest in pre-colonial conditions with 1st order interfluves having the highest erosion potential and decreasing as order increases. Agricultural landcover in 1933 and contemporary erosion-prone agricultural landcover was and still is concentrated on

high-order interfluves with low-order interfluves having the highest potential for erosive loss. The third application regarding bedrock weathering depth indicates that narrow and steep 1st order interfluves have the deepest and most variable weathering front depths with both the variation and depth decreasing as order increases.

Chapter 3 honed in on a finer-scale spatial perspective and described the methodology developed and implemented at the Calhoun Critical Zone Observatory in South Carolina to isolate minimally eroded hillslopes and 1st order catchments. Nearly all of the Southern Piedmont in the southeastern US was subjected to agricultural erosion due to plantation agriculture for ~200 years. These lands were abandonded for plowed agricultural production by the 1930's largely succeeding to loblolly pine dominated forests. High resolution LiDAR Digital Elevation Model (DEM) micro-topographic roughness analyses were employed in conjunction with historic 1933 aerial photographs and contemporary satellite imagery. The 1933 imagery captures the CCZO landscape prior to much of the agricultural abandonment that took place throughout the southeastern US as highly erosive tobacco and cotton plantation agriculture failed and was abandoned. High resolution LiDAR raster elevation data was used to generate a slope-map for the CCZO which lies in the broader Enoree district of the Sumter National Forest in SC. Spatial variation in the steepness of slopes was interpreted to be a highly sensitive indicator of historic erosion at the CCZO. This inference has been employed through “microtopographic roughness analysis” (MTRA) and was implemented by

calculating the standard deviation of slope within a 7.5m X 7.5m moving window across the slope map for every pixel across the CCZO. From here, mean and variance values of microtopographic roughness (MTRA) were calculated for 37 1st-order watersheds including 13 watersheds determined to minimally eroded via MTRA and 26 other random 1st-order catchments. The resulting watershed roughness surface data were interpreted to reflect the degree of degradation. Lower mean watershed roughness values and lower variation in roughness within watersheds reflect smoother and less eroded surfaces than those which were previously cleared and cultivated. These results were supported by remote sensing of contemporary and historic landcover which indicated that areas determined to have very low microtopographic roughness generally had high forest cover in 1933 and were characterized in modern times as having tall deciduous forest canopies. Because microtopographic erosion features are things like rills and gullies on the spatial scale of meters, often with many meters of uneroded terrain in between, this makes watershed-scale variation in roughness directly and strongly proportional to mean watershed roughness and a practical and simple technique for evaluating the erosion history of terrain.

Having located rare and informative reference hardwood plots with minimally disturbed soils, the next step was to prepare for intensive long-term soil studies of these and other locations in the field. To this end, Chapter 4 outlines the construction and use of the Field Portable Gas Analyzer (FPGA). The FPGA integrates off-the-shelf Vaisala™

non-dispersive infrared (NDIR) CO_2 probes and electro-chemical Apogee™ O_2 probes for flow-through gas analyses using a Cole-Parmer™ vacuum-pressure pump. Four prototypes of the ultra-portable gas analyzer have been constructed over the last three years and field-tested to monitor soil respiration. This is accomplished via the sampling and analysis of gasses in buried soil gas reservoirs in a variety of remote field settings including agricultural fields, managed timber pine forests, natural hardwood forests, and vineyards at depths as much as 10m below the soil surface in some locations. In addition to on-site gas analysis, the FPGA can also be used to collect gas samples in the field for laboratory analyses and FPGA's have further been developed for bench-top laboratory applications for soil incubation experiments. The FPGA platform lends itself well to the calculation of respiratory quotients and shows great promise to enrich soil respiration studies (Jenkins and Adams 2011, Mamilov and Dilly 2011, Angert, Yakir et al. 2015).

The final investigation in Chapter 5 digs deeply into the belowground effects of old-field succession using tools like the FPGA, X-ray CT, aggregate stability analyses, and others. The below-ground effects of old-field forest succession in the US, South Carolina, Calhoun Critical Zone Observatory were explored by contrasting reference hardwood forest stands, plowed agricultural fields, and old-field secondary pine forest stands. Hardwood forest soils have higher CO_2 concentrations and lower O_2 below the B-horizon, than either agricultural plots or old-field pine forests. Though surficial soil

regeneration in old-field secondary forests seems to have progressed substantially in terms of rooting, respiration dynamics, and soil structure, deep CZ respiration and apparent rooting patterns remain significantly altered under old-field pine forests. This seems to indicate a lag in below-ground regeneration. This regeneration of deep rooting and macropore formation seems to occur within the low permeability, clay-rich B-horizon which is acting as a barrier. Interestingly, abiotic CZ processes like storms appear to play an important role in the deep system dynamics of all of the landuse treatments which experienced deep "flushing" of CO_2 presumably transported into groundwater.

6.2 Integration of research findings

The landscape geomorphology work in Chapter 2 has spectacular potential for adoption and utility within academic and management circles. This is because it adapts well-known hydrologic Hortonian stream-network concepts and applies them in an entirely new context to terrestrial landforms, i.e., hillsheds, and environmental processes. Thanks to Horton and Strahler, stream orders and watersheds are common parlance within the Earth and environmental science and management communities. As we have presented our approach herein applying this same ordering to terrestrial geomorphology with hillshed and interfluve ordering, our colleagues appear to intuitively and immediately understand and appreciate the geomorphic approach

presented in this article, and to be very excited by its implications, applications, and ease of utility.

Fields such as geomorphology and land management are currently lacking methodologies to describe networks of connected topographic areas (i.e. the hillsheds of interfluve networks) that are analogous to ordered streams and watersheds. By applying a Horton-Strahler framework to terrestrial geomorphology, we have developed a conceptual, analytical, statistical, and possibly management-oriented framework for quantitative landscape geomorphology. This approach has a special ability to inform land management and help us to understand environmental processes throughout the terrestrial world.

The work of Chapter 3 is intended to have similar potential for utility in the identification of minimally eroded terrain for conservation and research. While many researchers are using LiDAR technology to identify irregular structures across landscapes, we took a different perspective. Irregular, roughened, terrain features predominate the Southeastern US where historic agriculture gullied eroded the majority of the landscape. Instead of searching for means to characterize this irregularity, the goal here was to find watersheds where such irregularity was absent in order to identify and target reference areas for intensive study. This work aims to help solve an important problem in environmental and ecological sciences: how to define the reference condition in an area known to have been degraded or otherwise impacted by human activity. This

effort has played a very influential role within the NSF-sponsored Calhoun Critical Zone Observatory and for the last several years the reference hardwood watersheds identified in this manuscript have been enthusiastically utilized by researchers from many universities and disciplines and has clear potential for adoption and use elsewhere. There are often similar needs for the identification of these sort of reference areas in many fields and applications. Whether for ecological conservation and study, analyzing the effects of land management practices, or to aiding in the reconstruction of environmental histories, this approach has a special ability to inform land management and help us to understand environmental processes throughout the terrestrial world.

The work of Chapter 4 of the development and use of analytical for field work is perhaps not common outside of engineering-based research but may have the greatest potential for widespread adoption of the entire dissertation. While there is currently one product on the market offered by Los Gatos Inc. which measures both CO_2 and O_2 through high-flow aspirated analysis, they are prohibitively expensive for many researchers costing $37,000 or more, are very heavy precluding actual field portability at over 37lbs, and do not have internal battery power. Existing products also do not offer the ability to collect field gas samples for laboratory analyses. The field-portable gas sampler and analyzer (FPGA) is incredibly light at ~18lbs including internal 12V battery power and is a fraction of the cost of existing products at <$2,000 in materials (Appendix B) that can be purchased by almost any researcher. The dissertation work presented here

focused on using FPGAs in forest and agricultural systems, but they could be used to study the deep metabolism of grasslands, deserts, shrub-lands, savannahs, and other ecosystems around the world.

The final research Chapter 5 illustrates the tremendous ecological value of "old-growth" forests beyond being mere vessels for storing and holding large quantities of carbon. Old-growth forests in the Southeastern Piedmont seem to be fundamentally different in terms of how and where they cycle their carbon. It appears that reference hardwood forests send more CO_2 into deeper soils where it is held beneath a low permeability clay layer until much of it is dissolved and flushed into deep groundwater systems. This appears to contrast with younger secondary pine forests in two ways 1) During low intensity or isolated storm events, low conductivity B-horizons whose macropores may have been sedimented and clogged macropores due to historic agriculture prevent the deep flushing and infiltration of water into soils. 2) Secondary forests seem to release less CO_2 into the deep soil environment beneath the B-horizon and hence have reduced potential for groundwater CO_2 loading. These results highlight an amazing opportunity to advance our fundamental understanding of the linkages between aboveground land management, aerobic respiration, and deep critical zone processes like mineral weathering and the export of terrestrially-derived CO_2 to streams.

Appendix A BCCZO interfluve network

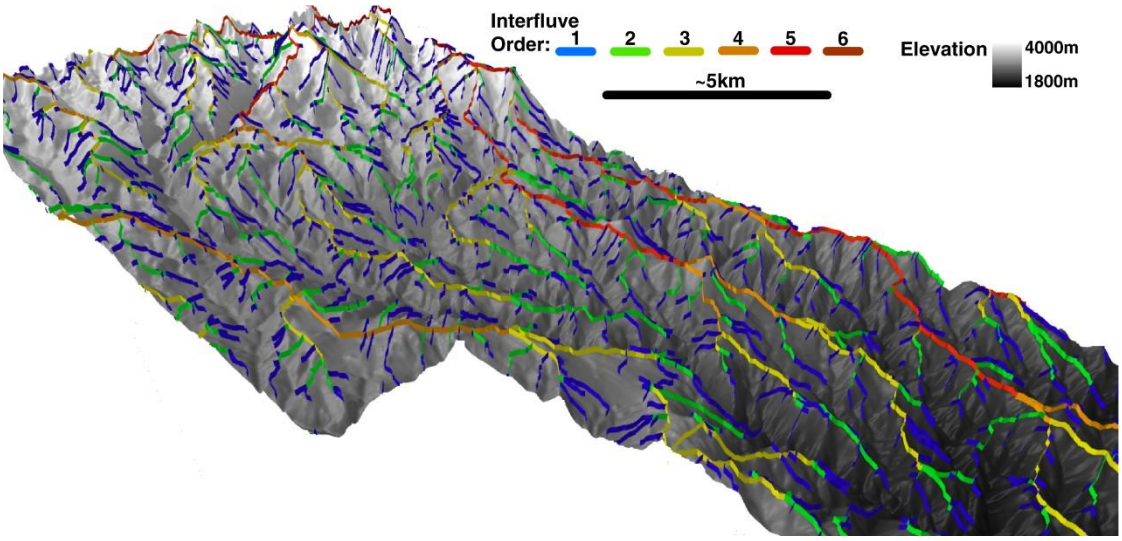

Figure A.1: 3D representation of the Boulder Creek CZO mountain terrain at 3X vertical exaggeration with an ordered interfluve network.

Appendix B Itemized FPGA parts list

Table B.1: Itemized parts list required for FPGA construction

Supplier	*Part #*	*Desc*	*quantity*	*unit price*	*Website*
FPGA materials					
Amazon (various)	1270	12V 7ah battery	1	20	http://www.amazon.com/gp/product/B002BJU8YQ
Apogee	MO-200	O2 meter w flow-thru head, 2m cable	1	365	http://www.apogeeinstruments.com/oxygen-sensor-with-handheld-meter-mo-200/
Bjerg Instruments		timer (optional)	1	18.99	https://www.amazon.com/gp/product/B01BUCOG60/
Cole-Parmer	EW-07532-25	Air cadet pump	1	299.99	https://www.coleparmer.com/i/mn/0753225
Cole-Parmer	EW-30600-23	Large-bore 3-way, male-lock, stopcocks	1	33.5	https://www.coleparmer.com/i/cole-parmer-large-bore-3-way-male-lock-stopcocks-10-pack-non-sterile/3060023?searchterm=EW-30600-23
Cole-Parmer	EW-30800-06	Female Luer to 1/4" J Barb Adapter, 25pk	1	10.5	https://www.coleparmer.com/i/cole-parmer-adcf-female-luer-to-1-4-j-barb-adapter-pp-25-pk/3080006?searchterm=EW-30800-06
Cole-Parmer	EW-30800-22	Male Luer to 1/4" J Barb Adapter, 25pk	1	16.25	https://www.coleparmer.com/i/cole-parmer-adcf-male-luer-to-1-4-j-barb-adapter-pp-25-pk/3080022?searchterm=EW-30800-22
Extech	MN26T	Extech MN26T Multimeter	1	40.49	https://www.amazon.com/gp/product/B0000WU1AM/
Grainger	2GUL4	female branch tee	1	7.34	https://www.grainger.com/product/PARKER-Barbed-Female-Branch-Tee-2GUL4?searchBar=true&searchQuery=2GUL4
Grainger	4FLZ2	vacuum gauge	1	12.37	https://www.grainger.com/product/GRAINGER-APPROVED-1-1-2-Test-Vacuum-Gauge-4FLZ2
Pelican	1400	Pelican 1400 Case	1	71.66	https://www.amazon.com/Pelican-1400-Case-Camera-Black/dp/B00009XVKY/
Pilot Automotive	PL-SW26	toggle switch	1	6.5	https://www.amazon.com/gp/product/B000GTMUUI/
US Plastic Corporation	61057	Jaco 1/4" nylon bulk-head union	1	1.37	https://www.usplastic.com/catalog/item.aspx?itemid=29652
Vaisala	GMM221L0N0A4A2E2A	GMM221 - CO2 probe	1	812	http://www.vaisala.com/en/products/carbondioxide/Pages/GMm220.aspx
Masterflex	L/S 24, 25 ft	platinum-cured silicone tubing,	1	127	https://www.masterflex.com/i/masterflex-platinum-cured-silicone-tubing-l-s-24-25-ft/9641024?pubid=SI
			Total:	1842.96	
Gas well connections and tubing					
US Plastic Corporation	56285	Tubing .170" ID x 1/4" OD	TBD	0.6	https://www.usplastic.com/catalog/item.aspx?itemid=35641
US Plastic Corporation	61005	Jaco 1/4" nylon union	TBD	0.92	https://www.usplastic.com/catalog/item.aspx?itemid=25575

Appendix C Soil atmosphere monitoring replicate 1

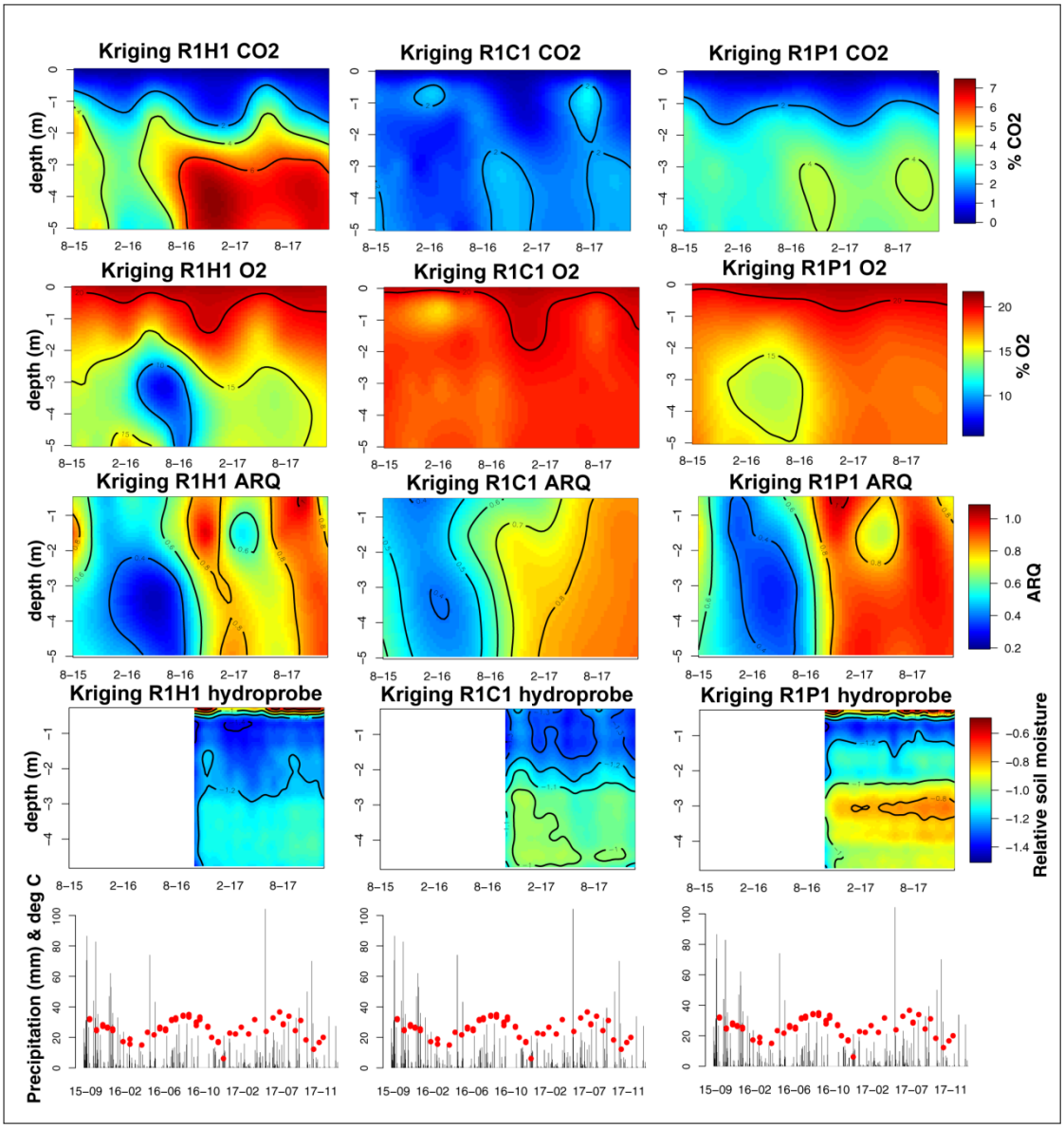

Figure C.1: Heatmap plotting of bulk gas concentrations of soil CO2 (top row) and O2 (second row), soil gas ARQ timeseries (third row), and relative soil moisture index is plotted in the bottom heatmap with cooler colors corresponding to more moist conditions. Y-axis is soil depth and the x-axis corresponds to time with color intensity corresponding to the variable of interest on all heatmaps. Precipitation (grey bars) and temperature (red) are plotted for reference in the bottom row.

Appendix D Soil atmosphere monitoring replicate 2

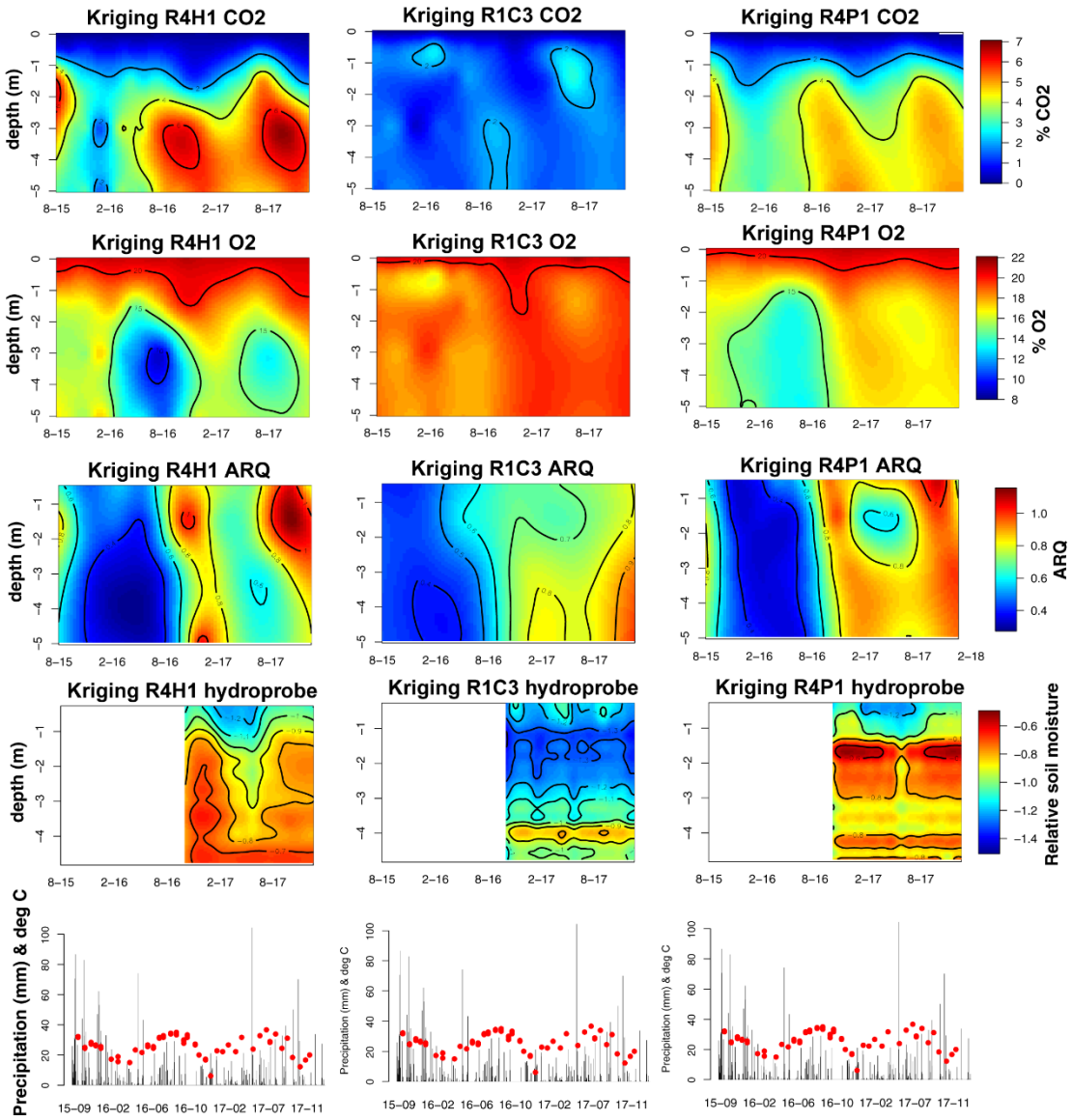

Figure D.1: Heatmap plotting of bulk gas concentrations of soil CO2 (top row) and O2 (second row), soil gas ARQ timeseries (third row), and relative soil moisture index is plotted in the bottom heatmap with cooler colors corresponding to more moist conditions. Y-axis is soil depth and the x-axis corresponds to time with color intensity corresponding to the variable of interest on all heatmaps. Precipitation (grey bars) and temperature (red) are plotted for reference in the bottom row.

Appendix E Soil atmosphere monitoring replicate 3

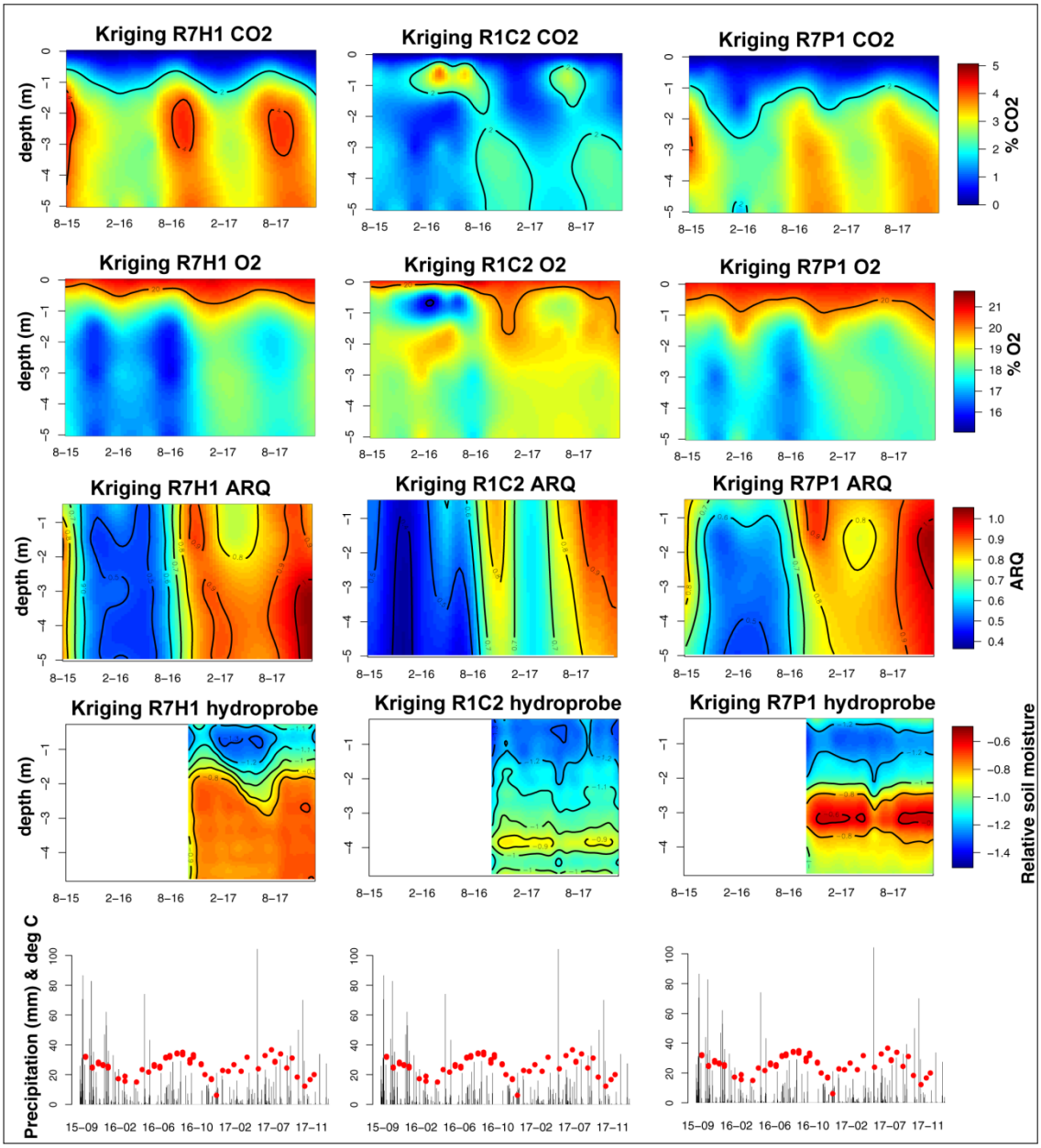

Figure E.1: Heatmap plotting of bulk gas concentrations of soil CO2 (top row) and O2 (second row), soil gas ARQ timeseries (third row), and relative soil moisture index is plotted in the bottom heatmap with cooler colors corresponding to more moist conditions. Y-axis is soil depth and the x-axis corresponds to time with color intensity corresponding to the variable of interest on all heatmaps. Precipitation (grey bars) and temperature (red) are plotted for reference in the bottom row.

References

Akagi, M. (2015). "Qgis2threejs." Quantum GIS Python Plugins.

Anderson, R. S. (2015). "Pinched topography initiates the critical zone: Geophysical imaging provides a clearer picture of how rock turns into soil." GEOPHYSICS.

Anderson, S. P., et al. (2012). "Landscape scale linkages in critical zone evolution." Comptes Rendus Geoscience **344**(11-12): 586-596.

Angert, A., et al. (2015). "Using O2 to study the relationships between soil CO2 efflux and soil respiration." Biogeosciences **12**(7): 2089-2099.

Archer, N. A. L., et al. (2016). "Rainfall infiltration and soil hydrological characteristics below ancient forest, planted forest and grassland in a temperate northern climate." Ecohydrology **9**(4): 585-600.

Asner, G., et al. (2003). "Global synthesis of leaf area index observations: implications for ecological and remote sensing studies." Global Ecology & Biogeography **12**: 191-205.

Austin, J. C., et al. (2018). Calhoun CZO - Hydroprobe Data 2016-2018. C. CZO.

Bacon, A. R., et al. (2012). "Coupling meteoric ^{10}Be with pedogenic losses of ^{9}Be to improve soil residence time estimates on an ancient North American interfluve." Geology **40**(9): 847-850.

Barbosa, J. M., et al. (2014). "Remotely sensed biomass over steep slopes: An evaluation among successional stands of the Atlantic Forest, Brazil." ISPRS Journal of Photogrammetry and Remote Sensing **88**: 91-100.

BCCZO (2010). "Boulder Creek (Snow off - filtered - Last stop) - 1m Filtered Lidar DEM ".

Billings, S., et al. (2018). "Loss of deep roots limits biogenic agents of soil development only partially restored by 80y of forest regeneration." In Review - Elementa: Science of the Anthropocene.

Billings, W. D. (1938). "The Structure and Development of Old Field Shortleaf Pine Stands and Certain Associated Physical Properties of the Soil." Ecological Monographs **8**(3): 437-500.

Bin, G., et al. (2011). "Colloid Deposition and Release in Soils and Their Association With Heavy Metals." Critical Reviews in Environmental Science and Technology **41**(4): 336-372.

Bin, Z. and P. Xin-Hua (2006). "Organic Matter Enrichment and Aggregate Stabilization in a Severely Degraded Ultisol After Reforestation." Pedosphere **16**(6): 699-706.

Bos, R. H. G. (1971). Quaternary evolution of a mountainous area in N.W. Tunisia; a geomorphological and pedological analysis, [Amsterdam], [publisher not identified], 1971. 167 pages : illustrations ; 24 cm

Brantley, S., et al. (2014). "Relating weathering fronts for acid neutralization and oxidation to pCO 2 and pO 2."

Brantley, S. L., et al. (2016). "Designing a suite of measurements to understand the critical zone." Earth Surface Dynamics **4**(1): 211-235.

Brantley, S. L., et al. (2007). "Crossing Disciplines and Scales to Understand the Critical Zone." Elements **3**(5): 307-314.

Brecheisen, Z., et al. (2015). "Calhoun Experimental Forest, Union County, SC - 1933 aerial imagery composite ".

Brecheisen, Z. S., et al. (2018). "Quantitative analysis of hillshed geomorphology and critical zone function." In Prep.

Brubaker, K. M., et al. (2013). "The Use of LiDAR Terrain Data in Characterizing Surface Roughness and Microtopography." Applied and Environmental Soil Science **2013**: 1-13.

Callaham, M. A., et al. (2006). "Long-term land-use effects on soil invertebrate communities in Southern Piedmont soils, USA." European Journal of Soil Biology **42**: S150-S156.

Callow, J., et al. (2007). "How does modifying a DEM to reflect known hydrology affect subsequent terrain analysis?" Journal of Hydrology **332**: 30-39.

Chang, T. J., et al. (2016). "Applications of erosion hotspots for watershed investigation in the Appalachian Hills of the United States." Journal of Irrigation and Drainage Engineering **142**(3): 04015057.

Chazdon, R. L. (2014). Second growth : the promise of tropical forest regeneration in an age of deforestation. Chicago, The University of Chicago Press.

Cherkinsky, A., et al. (2018). "Carbon and oxygen isotope composition in soil carbon dioxide within deep Ultisols at the Calhoun CZO, South Carolina, USA." In Review - Radiocarbon.

Christensen, N. L. (2014). "An historical perspective on forest succession and its relevance to ecosystem restoration and conservation practice in North America." Forest Ecology and Management **330**: 312-322.

Cook, C. W., et al. (2018). Calhoun CZO - Vegetation - Tree Survey (2014-2017). Calhoun-CZO.

Cook, C. W., et al. (2018). Calhoun CZO - Vegetation - Litterfall (2014-2017). Calhoun-CZO.

Coughlan, M., et al. (2017). "Historical land use dynamics in the highly degraded landscape of the Calhoun Critical Zone Observatory." Land **6**(2): 32.

Dane, J. H., et al. (2002). Methods of soil analysis. Part 4, Physical methods. Madison, Wis., Soil Science Society of America.

Davey, E., et al. (2011). "Use of computed tomography imaging for quantifying coarse roots, rhizomes, peat, and particle densities in marsh soils." Ecological Applications **21**(6): 2156–2171.

Davidson, E. and S. Trumbore (1995). "Gas diffusivity and production of CO2 in deep soils of the eastern Amazon." Tellus **47B**.

Devine, S., et al. (2014). "Soil aggregates and associated organic matter under conventional tillage, no-tillage, and forest succession after three decades." PLoS One **9**(1): e84988.

Dialynas, Y., et al. (2016). "Topographic variability and the influence of soil erosion on the carbon cycle." In Review.

Dietrich, W. E., et al. (1992). "Erosion thresholds and land surface morphology." Geology **20**(8): 675.

Dikau, R. (1990). Geomorphic landform modelling based on hierarchy theory. Proceedings of the 4th International Symposium on Spatial Data Handling, Department of Geography, University of Zürich.

Duchicela, J., et al. (2013). "Soil aggregate stability increase is strongly related to fungal community succession along an abandoned agricultural field chronosequence in the Bolivian Altiplano." Journal of Applied Ecology: n/a-n/a.

ESRI (2014). "ArcGIS Desktop: Release 10.2.2."

ESRI (2014, 10/18/2016). "SSURGO Downloader 2014." Retrieved 10/29/2016, 2016, from http://landscapeteam.maps.arcgis.com/apps/SimpleViewer/index.html?appid=4dbfecc52f1442eeb368c435251591ec.

Evans, I. S. (2012). "Geomorphometry and landform mapping: What is a landform?" Geomorphology **137**(1): 94-106.

Evans, J. S. (2016). spatialEco.

Fahey, T. J., et al. (2017). "Sampling and processing roots from rocky forest soils." Ecosphere **8**(6).

Fernandes, N. F. and W. E. Dietrich (1997). "Hillslope evolution by diffusive processes: The timescale for equilibrium adjustments." Water Resources Research **33**(6): 1307-1318.

Franzmeier, D., et al. (2009). Indiana soils: evaluation and conservation online manual. West Latayette, Indiana, Purdue University.

Gilbert, G. K. (1887). Geology of the Henry Mountains. Washington, D.C., Government Printing Office.

Gonzalez-Benecke, C. A., et al. (2014). "Local and general above-stump biomass functions for loblolly pine and slash pine trees." Forest Ecology and Management **334**: 254-276.

Hall, S. J., et al. (2012). "When Wet Gets Wetter: Decoupling of Moisture, Redox Biogeochemistry, and Greenhouse Gas Fluxes in a Humid Tropical Forest Soil." Ecosystems **16**(4): 576-589.

Han, M., et al. (2016). "An Extreme Learning Machine based on Cellular Automata of edge detection for remote sensing images." Neurocomputing **198**: 27-34.

Hansen, W. F. (1991). " Land Rehabilitation on the Sumter National Forest." Proceedings of the Fifth International Sedimentation Conference.

Hasenmueller, E. A., et al. (2015). "Topographic controls on the depth distribution of soil CO 2 in a small temperate watershed." Applied Geochemistry **63**: 58-69.

Heine, P. (2018). Calhoun CZO - Gas Wells Soil Texture Analysis. CCZO.

Hightower, J., et al. (2014). "Quantifying Ancient Maya Land Use Legacy Effects on Contemporary Rainforest Canopy Structure." Remote Sensing **6**(11): 10716-10732.

Hijmans, R. J. (2015). "raster: Geographic data analysis and modeling.".

Hoover, M. (1950). "Hydrologic Characteristics of South Carolina Piedmont Forest Soils." Soil Science Society of America Proceedings **49**(14): 353-358.

Horton, R. E. (1945). "Erosional development of streams and their drainage basins; hydrophysical approach to quantitative morphology." Geological Society of America Bulletin **56**(3): 275.

Hothorn, T., et al. (2008). "Simultaneous Inference in General Parametric Models." Biometrical Journal **50**(3): 346-363.

Jackson, J. A. (2010). Dissertation: Molecular Approaches to Estimating Soil Fungal Diversity and Community Shifts in Response to Land-Use Change. University Program in Ecology. Durham, NC, Duke University.

Jacobsen, O. H., et al. (1997). "Particle transport in macropores of undisturbed soil columns." Journal of Hydrology **196**: 185–203.

James, L. A. (2013). "Legacy sediment: Definitions and processes of episodically produced anthropogenic sediment." Anthropocene **2**: 16-26.

James, L. A., et al. (2007). "Using LiDAR data to map gullies and headwater streams under forest canopy: South Carolina, USA." Catena **71**(1): 132-144.

Jenkins, M. E. and M. A. Adams (2011). "Respiratory quotients and Q10 of soil respiration in sub-alpine Australia reflect influences of vegetation types." Soil Biology and Biochemistry **43**(6): 1266-1274.

Jennifer C. Jenkins, D. C. C., Linda S. Heath, Richard A. Birdsey (2003). "National-Scale Biomass Estimators for United States Tree Species." Forest Science **49**(1).

Jenny, H. (1994). Factors of Soil Formation: A System of Quantitative Pedology, Dover.

Jiang, R., et al. (2010). "Hydrological process controls on nitrogen export during storm events in an agricultural watershed." Soil Science and Plant Nutrition **56**(1): 72-85.

Johnson, M. S., et al. (2008). "CO2efflux from Amazonian headwater streams represents a significant fate for deep soil respiration." Geophysical Research Letters **35**(17).

Jose, S., et al. (2001). "Comparison of minirhizotron and soil core methods for quantifying root biomass in a temperate alley cropping system." Agroforestry Systems **52**: 161-168.

Kim, H., et al. (2017). "Feedbacks among O 2 and CO 2 in deep soil gas, oxidation of ferrous minerals, and fractures: A hypothesis for steady-state regolith thickness." Earth and Planetary Science Letters **460**: 29-40.

Krishnaswamy, J. and D. D. Richter (2002). "Properties of Advanced Weathering-Stage Soils in Tropical Forests and Pastures." Soil Science Society of America Journal **66**(1): 244-253.

Lindsay, J. (2014). "The Whitebox Geospatial Analysis Tools project and open-access GIS."

Liptzin, D., et al. (2010). "Temporal Dynamics in Soil Oxygen and Greenhouse Gases in Two Humid Tropical Forests." Ecosystems **14**(2): 171-182.

Listopad, C. M. C. S., et al. (2011). "Portable and Airborne Small Footprint LiDAR: Forest Canopy Structure Estimation of Fire Managed Plots." Remote Sensing **3**(12): 1284-1307.

Liu, Z., et al. (2015). "Estimating seasonal variations of leaf area index using litterfall collection and optical methods in four mixed evergreen–deciduous forests." Agricultural and Forest Meteorology **209-210**: 36-48.

Londoño, A. C. (2008). "Pattern and rate of erosion inferred from Inca agricultural terraces in arid southern Peru." Geomorphology **99**(1-4): 13-25.

Luo, L., et al. (2010). "Quantification of 3-D soil macropore networks in different soil types and land uses using computed tomography." Journal of Hydrology **393**(1-2): 53-64.

MacMillan, R. A. and P. A. Shary (2009). Chapter 9 Landforms and Landform Elements in Geomorphometry. Developments in Soil Science. T. Hengl and H. I. Reuter, Elsevier. **33:** 227-254.

Maeght, J. L., et al. (2013). "How to study deep roots-and why it matters." Front Plant Sci **4**: 299.

Mallard, J. (2017). "Calhoun CZO Precipitation, Water Years 2015-2016." HydroShare.

Mamilov, A. and O. Dilly (2011). "Shifts in Respiratory Quotient and δ13C Isotopic Signature of CO2Produced by Soils under Long-Term Agricultural Use in Arid Steppe Ecosystems." Geomicrobiology Journal **28**(7): 625-631.

Masiello, C. A., et al. (2008). "Evaluating two experimental approaches for measuring ecosystem carbon oxidation state and oxidative ratio." Journal of Geophysical Research **113**(G3).

Maxwell, A. E. and M. P. Strager (2013). "Assessing landform alterations induced by mountaintop mining." Natural Science **05**(02): 229-237.

Maxwell, J. C. (1870). " On hills and dales." Philosophical Magazine **4**: 421-427.

Mayorga, E., et al. (2005). "Young organic matter as a source of carbon dioxide outgassing from Amazonian rivers." Nature **436**(7050): 538-541.

McCarthy, H. R., et al. (2007). "Temporal dynamics and spatial variability in the enhancement of canopy leaf area under elevated atmospheric CO2." Global Change Biology **13**(12): 2479-2497.

Meerveld, I. T.-v. and M. Weiler (2008). "Hillslope dynamics modeled with increasing complexity." Journal of Hydrology **361**(1-2): 24-40.

Metz, L. J. (1958). The Calhoun Experimental Forest. Asheville, NC, USDA Forest Service Southeastern Forest Experiment Station.

Mitasova, H., et al. (2013). GIS-based soil erosion modeling. Treatise on Geomorphology. J. Schroder, San Diego Academic Press. **3:** 228-258.

Mitasova, H., et al. (2014). "Soil erosion and deposition modeling: ArcGIS workflow." Retrieved 5-01, 2017, from http://ncsu-geoforall-lab.github.io/erosion-modeling-tutorial/arcgis.html.

Montgomery, D. R. and W. E. Dietrich (1992). "Channel Initiation and the Problem of Landscape Scale." Science **255**(5046): 826-830.

Moon, S., et al. (2017). "A model of three-dimensional topographic stresses with implications for bedrock fractures, surface processes, and landscape evolution." Journal of Geophysical Research: Earth Surface **122**(4): 823-846.

NCALM (2014). "Calhoun CZO - LiDAR - Hyperspectral and LiDAR Survey ".

Nychka, D., et al. (2016). "fields: Tools for Spatial Data. R package version 8.3-6."

Peet, R. K. and N. L. Christensen (1980). "Succession: a Population Process." Vegetatio **43**: 131-140.

Perron, J. T., et al. (2009). "Formation of evenly spaced ridges and valleys." Nature **460**(7254): 502-505.

Pike, A., et al. (2012). "Terrain Analysis for Locating Erosion Channels: Assessing LiDAR Data and Flow Direction Algorithm." Plant and Soil Sciences Faculty Publications.

Pinheiro, J., et al. (2017). "nlme: Linear and Nonlinear Mixed Effects Models." **Version: 3.1-131**.

QGIS Development Team (2016). "QGIS Geographic Information System."

Qi, Y., et al. (2017). "Optical and litter collection methods for measuring leaf area index in an old-growth temperate forest in northeastern China." Journal of Forest Research **18**(5): 430-439.

Quénard, L., et al. (2011). "Lessivage as a major process of soil formation: A revisitation of existing data." Geoderma **167-168**: 135-147.

R Core Team (2016). "R: A language and environment for statistical computing."

Rempe, D. M. and W. E. Dietrich (2014). "A bottom-up control on fresh-bedrock topography under landscapes." PNAS **111**(18): 6576-6581.

Rey, A., et al. (2011). "Impact of land degradation on soil respiration in a steppe (Stipa tenacissima L.) semi-arid ecosystem in the SE of Spain." Soil Biology and Biochemistry **43**(2): 393-403.

Richter, D. and S. A. Billings (2015). "'One physical system': Tansley's ecosystem as Earth's critical zone." New Phytol **206**(3): 900-912.

Richter, D. D. and D. Markewitz (1995). "How Deep Is Soil?" BioScience **45**(9): 600-609.

Richter, D. d. and D. Markewitz (2001). Understanding soil change: soil sustainability over millennia, centuries, and decades. Cambridge;New York;, Cambridge University Press.

Rousseau, M., et al. (2004). "Preferential Transport of Soil Colloidal Particles: Physicochemical Effects on Particle Mobilization." Vadose Zone Journal **3**: 247–261.

Ruhe, R., et al. (1967). Landscape evolution and soil formation in southwestern Iowa. USDA, Soil Conservation Service.

Schaetzl, R. J. and S. Anderson (2005). Soils : genesis and geomorphology. Cambridge ; New York, Cambridge University Press.

Schneider, B. (2005). "Extraction of hierarchical surface networks from bilinear surface patches." Geographical Analysis **37**.

Schneider, C. A., et al. (2012). "NIH Image to ImageJ: 25 years of image analysis." Nature methods **9**(7): 671-675.

Silver, W., et al. (1999). "Soil oxygen availability and biogeochemistry along rainfall and topographic gradients in upland wet tropical forest soils." Biogeochemistry **44**.

Slik, J. W. F., et al. (2013). "Large trees drive forest aboveground biomass variation in moist lowland forests across the tropics." Global Ecology and Biogeography **22**(12): 1261-1271.

St Clair, J., et al. (2015). "Geophysical imaging reveals topographic stress control of bedrock weathering." Science **350**(6260): 534-538.

Stahl, P. W. (2015). "Interpreting interfluvial landscape transformations in the pre-Columbian Amazon." The Holocene **25**(10): 1598-1603.

Stenberg, L., et al. (2016). "Evaluation of erosion and surface roughness in peatland forest ditches using pin meter measurements and terrestrial laser scanning." Earth Surface Processes and Landforms **41**(10): 1299-1311.

Stolwijk, A., et al. (1999). "Studying seasonality by using sine and cosine functions in regression analysis." J Epidemiol Community Health **53**: 235-238.

Strahler, A. N. (1957). "Quantitative analysis of watershed geomorphology." Eos, Transactions American Geophysical Union **38**(6): 913-920.

Strickland, M. S., et al. (2010). "Rates of in situ carbon mineralization in relation to land-use, microbial community and edaphic characteristics." Soil Biology and Biochemistry **42**(2): 260-269.

Sun, T., et al. (2015). "Fine root dynamics of trees and understorey vegetation in a chronosequence of Betula platyphylla stands." Forest Ecology and Management **346**: 1-9.

Tarboton, D. G. (1996). "Fractal river networks, Horton's laws and Tokunaga cyclicity." Journal of Hydrology **187**.

Thomas, A. L. (1993). Poly3D: A Three-Dimensional, Polygonal Element, Displacement Discontinuity Boundary Element Computer Program with Applications to Fractures, Faults, and Cavities in the Earth's Crust. Stanford, CA, Stanford University.

Tissue, D. T., et al. (1996). "Growth and photosynthesis of loblolly pine (Pinus taeda) after exposure to elevated CO2 for 19 months in the field." Tree Physiology **16**: 49-59.

Trimble, S. (2008). Man induced soil erosion on the Southern Pidemont, Soil/Water Conserv. Soc.

Tucker, G. and R. Bras (1998). "Hillslope processes, drainage density, and landscape morphology." Water Resources Research **34**(10): 2751-2764.

Ulrich, J. (2017). "TTR: Technical Trading Rules." CRAN.R-project.org **R package version 0.23-2**.

USDA (1972). USDA-soil conservation service - national engineering handbook Washington, D.C.

USFS (2016). "Southern USA basic ownership boundaries." http://data.fs.usda.gov/geodata/edw/datasets.php.

USGS (2016). "EarthExplorer." Retrieved 09/05/2015, 2016, from http://earthexplorer.usgs.gov/.

Vaglio Laurin, G., et al. (2014). "Above ground biomass estimation in an African tropical forest with lidar and hyperspectral data." ISPRS Journal of Photogrammetry and Remote Sensing **89**: 49-58.

VanDerWal, J., et al. (2014). "SDMTools: Species Distribution Modelling Tools: Tools for processing data associated with species distribution modelling exercises."

Ward, E. J., et al. (2015). "Fertilization intensifies drought stress: Water use and stomatal conductance of Pinus taeda in a midrotation fertilization and throughfall reduction experiment." Forest Ecology and Management **355**: 72-82.

Warntz, W. (1975). "Stream ordering and contour mapping." Journal of Hydrology, **25**.

Warren, S. D., et al. (2005). "Validation of a 3-D enhancement of the Universal Soil Loss Equation for prediction of soil erosion and sediment deposition." Catena **64**(2-3): 281-296.

Werner, C. (1972). "Patterns of drainage areas with random topology." Geographical Analysis **4**(2): 119-133.

Werner, C. (1988). "Formal analysis of ridge and channel patterns in maturely eroded terrain." Annals of the Association of American Geographers **78**(2): 253-270.
Wickham, H. and R. Francois (2016). dplyr: A Grammar of Data Manipulation.

Wilcox, D. and H. Moellering (1995). "Pass location to facilitate the direct extraction or Warntz networks from grid digital elevation models." Proceedings on Computer Assisted Cartography **12**.

Wilson, J. P. and J. C. Gallant (2000). Primary topographic attributes. Terrain Analysis: Principles and Applications. New York, Wiley**:** 51–85.

Xi, W. and R. Peet (2011). The Complexity of Catastrophic Wind Impacts on Temperate Forests. Recent Hurricane Research - Climate, Dynamics, and Societal Impacts.

Zimmermann, B. and H. Elsenbeer (2008). "Spatial and temporal variability of soil saturated hydraulic conductivity in gradients of disturbance." Journal of Hydrology **361**(1-2): 78-95.

Biography

Zachary Scott Brecheisen was born in Albuquerque, New Mexico on November, 29th 1988 and grew up climbing trees and cliffs in wild and rural NM. He earned Bachelor of Arts Degrees in Biology and Anthropology with a supplemental major in Sustainable Development from New Mexico State University in Las Cruces, NM graduating with Distinction in University Honors in December of 2012. His undergraduate honors thesis, "Tidak hutan, tidak hujan: globalization and the deforestation, degradation, and development of rural Indonesia" was carried out under the supervision of Dr. Constance Falk, professor of Agricultural Ecoonmics. He then pursued a PhD in Environmental Science and Policy with Dr. Daniel Richter.

Brecheisen was an adjunct instructor of environmental biology at Durham Technical College and completed certificate programs at Duke in College Teaching and Geospatial Analysis. His dissertation research was supported by: NSF IGERT WISeNet Fellowship, the Forest History Society's F. K. Weyerhaeuser Fellowship, and a Duke Incubation Fund Grant. Brecheisen's peer-reviewed publications to date include:

Brecheisen, et al. (2014). "Ordering Interfluves: A Simple Proposal for Understanding Critical Zone Evolution," Procedia Earth and Planetary Science **10**

Brecheisen, et al. (2015) "Dataset: Calhoun Experimental Forest-Union County, SC 1933 aerial imagery composite," Calhoun Critical Zone Observatory and USFS

Billings, et al. (2018). "Loss of deep roots limits biogenic agents of soil development that are only partially restored by decades of forest regeneration," Elementa: Science of the Anthropocene **In press.**